ABSTRACT

Title of Dissertation: THE EFFECTS OF ELASTICITY AND GEOMETRY ON CELL MIGRATION AND POLARIZATION

Katrina Adlerz, Doctor of Philosophy, 2017

Dissertation directed by: Associate Professor Dr. Helim Aranda-Espinoza, Fischell Department of Bioengineering

Cell migration is a crucial process in the development and maintenance of the human body. Migration is also involved in a number of pathologies. In atherosclerosis, for example, immune cells migrate to the site of inflammation and contribute to the progression of the disease. In cancer, cells migrate out of the primary tumor through the body to metastasize at distant sites creating deadly secondary tumors. In all of these examples, cells confront and must adapt to a broad range of extracellular environments. Two important properties that cells encounter in the body are the elasticity of the environment and confinement. A better understanding of how a cell responds to these parameters would offer insights into the progression of diseases like cancer and atherosclerosis. Much cell migration research, however, has focused on cells moving on flat stiff substrates, like a glass culture dish. Therefore, in this dissertation, we investigated the effects of substrate elasticity and confinement on cell polarization and migration.

First, macrophage behavior was studied on substrates of different stiffness. We found that macrophages are mechanosensitive and respond with changes in area, proliferation, and migration. To further investigate cell migration in response to stiffness we focused on polarization, the first step in directed cell migration, and found that the position of the centrosome, an organelle indicating polarity, was dependent on substrate elasticity. Micropatterned one-dimensional lines and a microfluidic device were used to study the effect of confinement on cell polarization and migration. We discovered that the centrosome position for cells migrating on lines is different than in two-dimensional migration and we also show the importance of microtubule polymerization forces in maintaining centrosome position. We used a microfluidic device to mimic the three-dimensional confinement cells encounter in the body. Under increased confinement, the centrosome position is more similar to migration on lines than on flat surfaces and is maintained even when cells change directions. These results demonstrate how the elasticity and confinement of a cell's microenvironment affect cell polarization and migration. These results are important to further understand the role of these parameters in the progression of diseases like atherosclerosis and cancer.

THE EFFECTS OF ELASTICITY AND GEOMETRY ON CELL MIGRATION AND POLARIZATION

by

Katrina Marguerite Adlerz

Dissertation submitted to the Faculty of the Graduate School of the
University of Maryland, College Park, in partial fulfillment
of the requirements for the degree of
Doctor of Philosophy
2017

Advisory Committee:
Professor Helim Aranda-Espinoza, Chair
Professor Norma Andrews
Professor Giuliano Scarcelli
Professor Kimberly Stroka
Professor Ian White

Dedication

I would like to dedicate this work to my family, thank you for your continued support and belief in me.

Acknowledgements

First, I would like to thank my advisor Professor Helim Aranda-Espinoza for his mentorship, continuous support and encouragement, and the many opportunities he has provided me with. His guidance was essential in all of the research in this thesis.

Thank you to the rest of my thesis committee for their insight and comments. I would also like to thank Professor Heather Hayenga for her training and guidance in the macrophage project. My sincere thanks goes to Professor Kimberly Stroka who gave me access to her laboratory and to her student Marina Shumakovich for teaching me how to set up the microfluidic device used in the migration through three-dimensional confinement project.

Table of Contents

Dedication ii
Acknowledgements iii
Table of Contents iv
List of Tables vii
List of Figures viii
Chapter 1: Introduction 1
Chapter 2: Background 3
2.1 Significance of Cell Migration in Disease 3
2.2 Substrate Stiffness and Cell Behavior 4
2.3 Cell Polarization and Migration on Two-Dimensional Surfaces 5
2.4 Current Models for Confined Migration 6
2.4.1 One-Dimensional Migration 7
2.4.2 Migration through Three-Dimensional Confinement 8
2.5 Cell Polarization and Centrosome Position 9
2.6 Tools for Investigating Individual Aspects of Cell Migration 10
2.6.1 Polyacrylamide Gels 10
2.6.2 Micropatterns 11
2.6.3 Microfluidic Devices 11
Chapter 3: Substrate Elasticity Regulates the Behavior of Human Monocyte-derived Macrophages 13
3.1 Introduction 13
3.2 Materials and Methods 15
3.2.1 Polyacrylamide Gel Preparation 15
3.2.2 Migration Assay 16
3.2.3 Phagocytosis Assay 17
3.2.4 Immunostaining 17
3.2.5 Proliferation Assay 18
3.2.6 Statistical Analysis 18
3.3 Results 19
3.3.1 Cell Area Increases with Increasing Stiffness 19
3.3.2 Macrophage Migration Depends on Elasticity 20
3.3.3 Actin Arrangement in Macrophages 21
3.3.4 Phagocytosis Does Not Depend on Stiffness 23
3.3.5 Doubling Time Faster on Stiff Substrates 24
3.4 Discussion 25
Chapter 4: Centrosome Positioning During One-Dimensional Cell Migration 31
4.1 Introduction 31
4.2 Materials and Methods 33
4.2.1 3T3 Fibroblast Cell Culture 33
4.2.2 Polyacrylamide Gel Preparation 33
4.2.3 Micropatterning Lines 34
4.2.4 Live-Cell Imaging and Analysis 34

4.2.5 2D Migration Analysis 35
4.2.6 1D Migration Analysis 35
4.2.7 Statistical Analysis 36
4.3 Results 37
4.3.1 Nucleofection Does Not Affect Cell Migration on Lines 37
4.3.2 Centrosome Position on Different Stiffnesses 37
4.3.3 Centrosome Position in 1D Migration 39
4.3.4 Centrosome Position Does Not Affect Cell Migration 40
4.3.5 Centrosome Position is Maintained During Change of Directions 41
4.3.6 Centrosome after Cell Division 43
4.3.7 Microtubules Exhibit Polarity 43
4.3.8 Microtubules Needed for Migration and Persistence 43
4.3.9 Blebbistatin-Treated Cells Do Not Migrate Persistently on Lines 45
4.3.10 Dynein Inhibition has Small Impact on Centrosome Position 46
4.3.11 Microtubules and Centrosome Dynamics 46
4.4 Discussion 48
Chapter 5: Centrosome and Nucleus Positioning During Migration Under Three-Dimensional Confinement 56
5.1 Introduction 56
5.2 Methods 58
5.2.1 Cell Culture and Reagents 58
5.2.2 Microfluidic Device 59
5.2.3 Cell Seeding into Device and Imaging 59
5.2.4 Switching the Chemoattractant 60
5.2.5 Migration and Position Analysis 60
5.2.6 Statistical Analysis 60
5.3 Results 61
5.3.1 Microfluidic Device for 3D Confinement 61
5.3.2 Migration Speed Depends on Degree of Confinement 61
5.3.3 3D Confinement Affects Centrosome and Nucleus Position 63
5.3.4 Centrosome Position Entering Channel 65
5.3.5 Centrosome Position During Changes of Direction 66
Discussion 67
Chapter 6: Conclusions and Future Work 73
6.1 Monocotye-derived Macrophages are Mechanosensitive 73
6.2 Cell Polarization is Affected by Substrate Elasticity 75
6.3 Future Work with Substrate Stiffness Gradients 75
6.4 Centrosome Position is Maintained by Microtubule Pushing Forces in 1D Migration 76
6.5 Centrosome is Polarized in Microchannels 77
6.6 Changing Directions in Confinement 77
6.7 Future Work Investigating Cancer Cells 78
6.8 Conclusions 79
Appendices 80
Appendix A: MATLAB Program for Analyzing Migration and Centrosome Position on Gels and Glass 80

Appendix B: MATLAB Program to Analyze Cell Migration and Centrosome Position on 1D Lines or in Channels 84
Appendix C: Analysis of Salmonella Motility..... 89
Bibliography 113

List of Tables

Table C.1 Molecular functions and primer sequences of target genes used in qRT-PCR analysis for S. Tymphimurium. 96

Table C.2 Antibacterial effect of blackberry and blueberry pomace extracts on S. Tymphimurium. 99

Table C.3 Physiochemical properties and mechanical behaviors of S. Tymphimurium treated with blackberry (Blk), blueberry (Blb) pomace extracts and 1:1 combination (BPE)..... 99

Table C.4 Analysis of motility pattern in ST treated with SLC_{2LOG} of BPE. 101

List of Figures

Figure 2.1 Illustration of different confinement conditions in cell migration. In 1D confinement cells adhere to a narrow strip of matrix, in 2D cells spread and migrate, in 3D confinement cells are unable to send out actin-based lamellipodia. Image adapted by permission from Macmillan Publishers Ltd: Nature Reviews Molecular Cell Biology [4], copyright 2014. 7

Figure 3.1 The surface area of macrophages is dependent on substrate stiffness. Initially all macrophages have the same area. After 1 hour, the cells have nearly reached their maximum area on each substrate stiffness. **A** Phase contrast images of cells on 1 kPa and glass substrates at 0 hr, 1 hr, and 18 hr. Scale bar 25 μm **B** The maximum area is statistically different for the soft (1-5 kPa) substrates compared to the stiff (280 kPa, glass). Statistically different groups at 18 hours determined by ANOVA followed by multiple comparison tests and indicated by different symbols ($n \geq 20$ cells in 3 independent experiments for each stiffness, $p < 1e\text{-}4$) 19

Figure 3.2 Macrophage migration paths were random, with minimal dependency on substrate stiffness. **A** Directionality is determined by dividing the cell's contour path by the net translocation displacement. A ratio less than 0.5 suggests the motion of the macrophages is not directed. **B** Although macrophages on the 3 kPa substrate had a slightly higher ratio, it was still under 0.5 ($n \geq 20$ cells, * $p < 0.05$). **C** Plots of the cell tracks, with each cell starting at the origin, illustrates the random motion of the macrophages ($n = 10$). 20

Figure 3.3 The speed of macrophages was fastest on the 280 kPa gel (12.0 ± 0.5 μm/h) and slowest on the 3 kPa gel (5.0 ± 0.4 μm/h). The other substrates had an average speed of 7.4 ± 0.5 μm/h. Statistically different groups determined by multiple comparison test and indicated by different symbols ($n \geq 20$ cells, $p < 0.05$). 21

Figure 3.4 F-actin content as determined by fluorescent intensity per macrophage. **A** The total F-actin content on the basal surface of each macrophage is fairly consistent, regardless of substrate stiffness. However, the F-actin per macrophage area is greatest on the 1 kPa gel and least on the 280 kPa gel ($n \geq 9$ cells). **B** This difference is perhaps due to actin fibers in macrophages becoming more organized and forming longer stress fibers on stiffer substrates. Scale bar 25 μm. 22

Figure 3.5 Macrophage phagocytosis of 1 μm particles does not depend on substrate stiffness. **A,B** On average, macrophages phagocytosed 2.0 ± 0.3 beads after 1 hour and 35.0 ± 1.3 beads after 3 hours. **C** Regardless of substrate stiffness, after 1 hour, on average, about 38.0 ± 2.4%, 43.0 ± 1.1%, and 19.0 ± 1.7% of

macrophages had consumed no beads, 1-3 beads, and over three beads, respectively. 23

Figure 3.6 Macrophages proliferate in less time on stiffer substrates. Initially, the same number of cells were plated on gels with fibronectin-stamped circles. **A** Cells on stiff substrates (280 kPa) had a significantly smaller doubling time than cells on the substrate of intermediate stiffness (13 kPa). **B** The number of cells in each 400 μm circle was not statistically different at 1, 24, or 70 hours, but at 45 hours, the stiff substrate (280 kPa) had significantly more cells (student's t-test, $p<0.05$). **C** Images captured during timelapse microscopy show cells proliferating to fill in patterned circles at 0, 18, 36, and 54 hours. Representative of at least 20 images taken for each stiffness at each timepoint. 25

Figure 4.1 Percentage of cells migrating persistently on 1 kPa, 280 kPa, or glass substrate with the centrosome (red) in front of or behind the nucleus (blue, in the sketches above). ($n \geq 13$ cells for each condition, 3 experiments). **A** The centrosome position is defined as in front or back of the nucleus (90° angle). The majority of cells on stiff substrate and glass have the centrosome in front of the nucleus, while a majority have it in the back on the soft substrate. **B** Centrosome position is defined as in the front, back or side. The proportion of cells with the centrosome in front and back is similar to as with the previous definition. 38

Figure 4.2 Centrosome position depends on geometrical constraints. **A** Phase images merged with fluorescent images of centrosome (red) and nucleus (blue) of 3T3 fibroblasts migrating on 1D micropatterned lines show a cell migrating with the centrosome in front of the nucleus (left), behind the nucleus (middle), and a cell migrating with the centrosome in front during 2D migration on glass (right). **B** Comparison of centrosome position in front of or behind the nucleus for 3T3 fibroblasts during 1D and 2D migration. (1D migration n=19 cells, 7 experiments. 2D migration n=14 cells, 4 experiments. Two proportion z-test, *p=0.016). 39

Figure 4.3 Biophysical parameters of migration do not depend on centrosome position. **A** Depiction of cells moving on 1D micropatterned lines and the definitions of the distance between centrosome (red) and back and front of a cell (nucleus in blue). **B** The distance between the centrosome and the back of the cell is shorter when the centrosome is behind the nucleus compared to when it is in front. **C-E** The mean cell width, speed as measured by tracking the centrosome, and distance travelled persistently of 3T3 fibroblasts migrating on 1D micropatterned lines do not depend on the position of the centrosome in front of or behind the nucleus. Mean + s.e.m. is shown, centrosome in back n=12, centrosome in front n=7, 7 experiments, all non-significant student's t-test. 40

Figure 4.4 Centrosome position is maintained as evidenced when cells change directions on lines. **A** Fluorescent images from timelapse of nucleus (blue) and centrosome (red) during a change of directions on lines. **B** Outline of the cell changing direction. The centrosome (red x) changes positions to remain behind the nucleus (blue outline) as the cell switches from migrating down to migrating up. **C** The speeds of the centrosome and nucleus during the change of directions suggests the centrosome has a faster speed than the nucleus..... 42

Figure 4.5 Microtubule polymerization depends on centrosome position. **A** Fibroblast transfected with EB3-gfp migrating on a 1D line. **B** When the centrosome is in back, a higher percentage of cells have greater EB3 intensity at the front of the cell. (Back: n=8 cells, Front: n=6 cells, 3 experiments, two proportion z-test, p=0.059). **C** The percent difference in fluorescent intensity of EB3 between the front and back of the cell is higher for cells with the centrosome in back, meaning that they have more EB3 towards the front. (Student's t-test p=0.029). **D** Schematic of microtubule polarization with microtubules in green, nucleus in blue, and centrosome in red. When the centrosome is in back of the nucleus more microtubules push against the front of the cell (left)..... 44

Figure 4.6 Disruption of actin and microtubule polymerization affects fibroblast migration on lines. **A** Cell speed as measured by tracking the cell center, centrosome, and nucleus is affected by drugs to dynein, myosin II, microtubule polymerization, and microtubule dynamics. Mean + s.e.m. is shown, control n=19 cells, 7 experiments, cytoplasmic dynein inhibitor n=24, 6 experiments, blebbistatin n=9, 2 experiments, nocodazole n=7, 3 experiments, taxol n=10, 3 experiments. Student's t-test for mean cell speed for each drug treatment compared to control * $p<0.05$. **B** Percentage of 3T3 cells migrating on 1D lines with the centrosome in back comparing control cells and cells treated with blebbistatin or cytoplasmic dynein inhibitor. (Two-proportion z-test p=0.153, 0.116). **C** Trajectory plots of cell centroids for cells observed migrating on 1D lines show the cytoskeleton's role in cell migration. **D** Representative phase images of a blebbistatin-treated cell moving along the micropatterned line. Time stamp (h:min). 45

Figure 4.7 Actin and microtubule polymerization disruption affects centrosome dynamics. **A** Definition of the angle between the centrosome and center of the nucleus. **B** Average deviation from 90 degrees of the angle between the centrosome and nucleus shows the centrosome is displaced from directly in front of or behind the nucleus in nocodazole and taxol treated cells. Mean + s.e.m. is shown, control n=19 cells, 7 experiments, cytoplasmic dynein inhibitor n=24, 6 experiments, nocodazole n=7, 3 experiments, taxol n=10, 3 experiments. Student's t-test nocodazole compared to control p=0.005, taxol compared to control p=0.002. **C** Average standard deviation of the angle between the centrosome and nucleus shows increased dynamics of the

centrosome for nocdazole-treated cells. Student's t-test nocodazole compared to control p=0.005. **D** Representative plots of the angle between the centrosome and nucleus over the time course of an experiment, with time=0 starting at the origin for control and drug-treated cells. **E** The distance between the center of the cell and the centrosome for all cells (left). The distance depends on the position of the centrosome in front of the nucleus (middle) or in back of the nucleus (right). 47

Figure 5.1 Microfluidic device to study 3D migration. **A** Schematic of the microfluidic device, image based on one from [119]. **B** Phase image of the channels portion of the microfluidic device with cells moving from the cell seeding channel towards the chemoattractant. **C** 3T3 fibroblasts migrating in 3 μm channels (cells are significantly deformed and hard to see in a single frame from the timelapse, they are indicated by arrows), 6 μm channels, on micropatterned 1D fibronectin lines, and on a fibronectin-coated 2D glass substrate. Scale bars as indicated. 62

Figure 5.2 Centrosome position depends on confinement. **A** Average nucleus width for cells migrating in the 3 μm channels (n=25 cells, 4 independent experiments), 6 μm channels (n=34 cells, 7 experiments), on 1D lines (n=19 cells, 7 experiments), or on a 2D glass substrate (n=14 cells, 4 experiments). Mean + s.e.m. is shown, ANOVA p=9.7e-19 followed by multicomparison tests p < 1e-8 between groups with different symbols. The same symbol indicates the groups are not statistically different. **B** Cell speed as measured by tracking the nucleus center. The symbols represent statistical significance. Mean + s.e.m. is shown, ANOVA p=1.7e-9 followed by multicomparison tests p < 1e-4. **C** Plots of the distances between the centrosome and closest edge of the nucleus. **D** Two cells in 3 μm channels. Cell on left has small distance between the nucleus (blue) and centrosome (red), cell on right has increased distance, scale bar 5 μm. **E** Percentage of cells with the centrosome positioned in front of the nucleus (black) or in back (white)..... 64

Figure 5.3 Centrosome and nucleus entering the channels. **A** Cell entering the 3 μm channel with centrosome (red) behind the nucleus (blue), scale bar 5 μm, time stamp (hrs:mins). **B** Cell entering the 3 μm channel with centrosome initially leading the nucleus then switching to the back, scale bar 5μm, time stamp (hrs:mins). **C** Scatter plot of the time it takes for the nucleus to enter the channel when the centrosome is in front or behind the nucleus, each tick represents one cell, mean entry time depicted as bold tick. Entry time for 3 μm channels is on the left (n=20, 4 experiments), 6 μm channels is on the right (n=21 cells, 7 experiments), difference between means is non-significant by student's t-test. 65

Figure 5.4 Cells repolarize during change of directions in the microchannels. **A** Schematic of how cells were induced to reverse directions by changing which channel contains the media+serum that acts as a chemoattractant. **B**

Representative cell after the chemoattractant was switched in a 3μm channel. The centrosome (red) is repositioned towards the new back of the cell, behind the nucleus (blue), scale bar 5 μm, time stamp is the time after the switch (hrs:mins). The channel is shown in brightfield to the left. The image is representative of 7 cells in 3 experiments in the 3μm channel. 67

Figure 6.1 A Characterization of gels with a stiffness gradient shows that over a length of 1.5 mm there is a gradual increase in stiffness. Characterization done with Brillouin microscopy by Milos Nikolic in Dr. Giuliano Scarcelli's lab. **B** Fibroblast cells plated on a gel with a stiffness gradient. The dark line indicates where the transition from soft to stiff takes place as indicated by fluorescent micobeads mixed into the stiff gel. Cells are more rounded at first on the soft gel and more elongated on the stiff side of the gel. Scale bar 50 μm. 76

Figure C.1 Adhesion and invasiveness of ST to INT407 (Pre-treatment: **A** & Post-treatment: **B**), HD11 (Pre-treatment: **C** & Post-treatment: **D**) and DF1 (Pre-treatment: **E** & Post-treatment: **F**) respectively in the presence of blackberry (blk), blueberry (Blb) pomace extracts and their 1:1 combination. 101

Figure C.2 Relative expression of virulence genes of ST treated with SLC_{2LOG} of blackberry (Blk), blueberry (Blb) pomace extracts and their 1:1 combination. 103

Figure C.3 ST planktonic cell growth (**A**) and biofilm formation (**B**) on glass slides in the presence of SLC_{2LOG} of BPE. 104

Figure C.4 Natural colonization of Salmonella in chick cecum after three weeks (**A**) and seven weeks (**B**). Each dot indicates Salmonella CFU per g of cecum content from one chick and the horizontal bars indicate median value in each group. 105

Chapter 1: Introduction

Cell polarization and migration are essential to a healthy, functioning body. Cell polarization is the first step in cell migration and involves the cell organizing a distinct front and rear, which allows for migration in a directed manner. These processes are crucial in many development and maintenance processes. Cell polarization and migration also play a role in the progression of diseases like atherosclerosis and cancer. During the course of these diseases, cells encounter a wide range of chemical and mechanical environments that they must respond to. Two important parameters migrating cells encounter in both of these diseases are changes to the elasticity of their environment and confinement in tight spaces. Much research has focused on understanding the mechanisms cells use to move on stiff, two-dimensional substrates like glass or tissue culture plastic. It has recently been understood that the cell's environment, such as its stiffness and confinement, influences cellular behavior. Much work needs to be done to fully understand the effect of these parameters on migration.

Therefore, **the overall objective of this research was to investigate the effects of substrate elasticity and confinement on cell polarization and migration**. The overall objective was achieved by studying two different hypotheses:

First, we hypothesized that the changing elasticity of the blood vessel during the progression of atherosclerosis influences macrophage behavior, a key immune cell involved in the progression of the disease. An in vitro model was used to isolate the effects of substrate stiffness and we showed that macrophage behavior including cell area, cytoskeletal arrangement, proliferation, and migration is influenced by the

stiffness of the environment (Chapter 3). To further investigate the effects of substrate stiffness on cell migration, we looked at its effects on cell polarization, the first step in migration. We found that the position of the centrosome, an organelle involved in cell polarization, was affected by the stiffness of the substrate (Chapter 4).

Our second hypothesis was that cell polarization would be influenced by confinement. This hypothesis was investigated in two different studies. First, we studied cells migrating on micropatterned, one-dimensional lines. We found that the position of the centrosome is influenced by confinement and maintained by microtubule pushing forces (Chapter 4). In the next study, we found that three-dimensional confinement of cells in microfluidic devices also influences centrosome positioning, cell polarity, and therefore cell migration (Chapter 5).

The research presented here advances the understanding of cell migration in response to the cell's environment, specifically in response to substrate stiffness. The results also show that centrosome positioning, a key player in cell polarity, which precedes cell migration, is affected by both stiffness and geometrical confinement.

Chapter 2: Background

2.1 Significance of Cell Migration in Disease

Cell migration is indispensable in the development and maintenance of all multicellular organisms [1]–[3]. For example, it plays a critical role in wound healing and the immune response. In wound healing, fibroblast cells must migrate into a wound to deposit new extracellular matrix and rebuild the connective tissue. In the immune response, circulating leukocytes migrate from the bloodstream and through tissue in order to reach the site of inflammation. Moving cells must be able to respond to and handle the variety of chemical and topology cues that they encounter in vivo [1], [4].

Cell migration is also an important aspect in many diseases. For instance, in cancer metastasis tumor cells must detach from the primary tumor, intravasate into the bloodstream, extravasate into tissue, then colonize in a secondary organ [5], [6]. During this process the cells encounter a variety of environments that they must navigate to successfully form a secondary tumor. Geometric constraints include pores in the extracellular matrix, narrow capillaries, and endothelial cell-cell junctions [5], [7], [8]. One approach to better understand metastasis has been to gain a better understanding of how healthy cells and cancer cells migrate through these spaces.

Changes in tissue stiffness often accompany the onset of cancer. In fact, oncologists often detect primary tumors after detecting a stiffening of the tissue by palpation. This elasticity change is due to changes in the extracellular matrix in the cancer cell's environment [9]. It has been shown that cancer cells do in fact respond

to stiffer substrates. For example, one studied response is increased integrin activation which leads to increased Rho signaling and tissue growth [10].

In the normal immune response, circulating leukocytes also have to migrate through confined spaces from the bloodstream to the site of inflammation in tissue [11]. This is a normal response to foreign entities in the body but it also contributes to diseases like cardiovascular disease [12]. In atherosclerosis, cholesterol-rich lipoproteins accumulate in the vascular wall. These molecules are pro-inflammatory and induce activation of the endothelium which recruits monocytes to the site [12], [13]. The monocytes differentiate into macrophages that proliferate and phagocytose the low-density lipoproteins. These macrophages, called foam cells, have a diminished capacity for migration and accumulate in the atherosclerotic plaque, resulting in a very soft necrotic core [14]. If the stiff fibrotic cap over the necrotic core ruptures, it could result in a myocardial infarction or stroke [15]

While plaques and tumors are complex environments, investigating cell migration and behavior in response to the specific parameters of substrate stiffness and confinement offers insight into the overall process and the importance of these parameters in the disease.

2.2 Substrate Stiffness and Cell Behavior

In the body, tissues vary over a wide range of stiffnesses. For example, bone is extremely stiff with a Young's elastic modulus on the order of 2 to 4 GPa while endothelial tissue is typically much softer with a modulus of around 10 kPa [16]. In an atherosclerotic plaque, the stiffness can range from around 1 kPa for lipids up to around 250 kPa in calcified areas. It has been demonstrated that cells are able to sense

and respond to these different underlying substrate stiffnesses. For instance, cell adhesion, proliferation, migration, and cytoskeleton arrangement are some parameters that may be influenced by substrate stiffness [17]. To more fully understand the effects of stiffness on cells, it is important to investigate the response of specific cell types. For example, fibroblasts will migrate towards regions of increasing stiffness [18], stem cells will differentiate down different lineages depending on substrate stiffness [19], and neutrophil speed and transmigration through endothelial layers depends on the underlying elasticity of the substrate [20], [21].

While the response of monocyte-derived macrophages to varying stiffness has not been studied, there is some evidence that other types of macrophages are mechanosensitive. For instance, alveolar macrophages that reside in the lung responded to different substrates with varying elasticities with an increase in cell area on stiffer surfaces of glass (70 MPa) compared to when plated on soft polyacrylamide gels (40 kPa) or on layers of epithelial cells (~0.1 kPa) [22]. Chapter 3 describes our study that used polyacrylamide gels to isolate the effect of stiffness on monocyte-derived macrophages. We showed that monocyte-derived macrophages are in fact mechanosensitive.

2.3 Cell Polarization and Migration on Two-Dimensional Surfaces

Traditional migration studies focus on cells moving on two-dimensional (2D) surfaces (Figure 2.1), this serves as a model for cells moving in to close wounds or on the surface of blood vessels [1]. In a typical motile cell, the steps of cell migration are: cell polarization, protrusion and adhesion formation, cell body translocation, and finally rear retraction [3], [23].

Briefly, in the first step, polarity proteins like Cdc42 and Par proteins are involved in generating a clear front and rear of the cell with different processes at each end [3]. Microtubules are organized, then the Golgi apparatus and the centrosome, also known as the microtubule organizing center, are localized towards the front of the cell [24]. In fact, the centrosome and nucleus define the axis of polarity with the centrosome near the center of the cell, between the nucleus and the leading edge [24]. Modeling and in vitro experiments have shown that dynein, microtubules, and actin flow could all play a role in centrosome positioning [25]–[27].

After polarization, Rac signaling targets WASP/ WAVE proteins that regulate the formation of actin branches allowing the cell to extend a lamellipodium, a broad actin-based protrusion, in the direction of migration [3]. The lamellipodium adheres to the substrate with the support of various integrin molecules. To move, the adhesions at the cell rear disassemble first, then the cell rear retracts in a process mediated by myosin II, and the cell body displaces [2], [3].

2.4 Current Models for Confined Migration

Cell migration in different environments is a new emphasis of study in the field. Many researchers are interested in how cells move in confined environments, where cells do not have the freedom to send out broad lamellipodia like in migration on two-dimensional surfaces [4], [8]. These environments are prevalent in the body and can include long singular collagen fibers or collagen bundles (20-50 μm diameter) [28], [29], pores and holes in the extracellular matrix (2-10 μm diameter)

[28], capillaries (5-10 µm diameter) [30], gaps in the endothelium (4-6 µm) [31], and recently suggested microtracks through extracellular matrix (3-30 µm wide) [32].

2.4.1 One-Dimensional Migration

In comparison with migration on 2D surfaces, migration along things like collagen fibers has been termed one-dimensional (1D) migration (Figure 2.1) [1], [4], [33]. In this case cells adhere to a narrow fiber, align along it, and rapidly migrate with greater persistence than in 2D [1], [33].

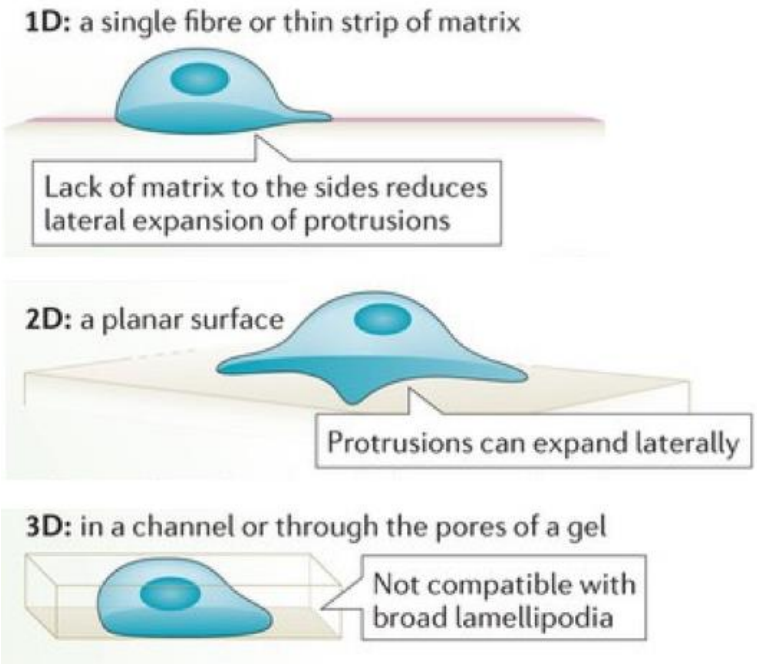

Figure 2.1 Illustration of different confinement conditions in cell migration. In 1D confinement cells adhere to a narrow strip of matrix, in 2D cells spread and migrate, in 3D confinement cells are unable to send out actin-based lamellipodia. Image adapted by permission from Macmillan Publishers Ltd: Nature Reviews Molecular Cell Biology [4], copyright 2014.

Yamada et al. compared cell migration between 1D and 2D environments and found that migration on narrow 1D lines is dependent on actomyosin and microtubule networks. And in comparison to 2D, cell migration is not dependent on ECM ligand density and has a decreased dependence on adhesion [33]. This type of rapid

migration was also observed for cells moving through three-dimensional fibrillar extracellular matrices where they may follow a single fiber for long lengths [33].

2.4.2 Migration through Three-Dimensional Confinement

Cells also must move in three-dimensional (3D) confinement in the body (Figure 2.1). It has been suggested that the nucleus, as the largest and stiffest organelle in the cell, may be the limiting factor as cells move through tight spaces [34], [35]. For comparison, the elasticity of an endothelial cell nuclei is 8 kPa while the cytoplasm is significantly softer, only 0.5 kPa [36]. One study by Wolf and colleagues showed that cell migration through nondegradable 3D matrix was stopped when cells reached a pore size at 10% of nuclear cross section [37]. Another experiment used a chromatin decondensation drug and found that cell transit time through microchannels was greatly increased after decondensation, suggesting that the bigger nucleus somehow impaired cell migration through the small channels [38]. Nuclear lamina, the filaments in the nucleoplasm that connect to transmembrane proteins in the nuclear envelope, have been a focus of recent research as well. It was found that lamin over- or under- expression can lead to changes in the nuclear viscosity [39]. Furthermore, downregulating lamin-A increased cell migration through microchannels [35] and migration through small pores [40], again suggesting that the nucleus and its mechanical properties play a role in confined migration.

While the nucleus may be important in cell migration, it does not act alone. The cytoskeletal elements are physically linked to lamina in the nucleoplasm through transmembrane proteins in the nuclear envelope called linkers of nucleoskeleton to cytoskeleton (LINC complexes) [41], [42]. Therefore, the nucleus must move with

the cell's cytoskeletal elements, which also must deform as a cell moves through tight spaces [43]. For example, it has been shown that cancer cells moving through very small channels require microtubule dynamics but were able to continue migration with disrupted F-actin [44]. Cells are able to change the volume of the nucleus and cytoplasm in response to confinement [1], and cancer cells are also able to move with this mechanism by the polarized distribution of aquaporins [45].

2.5 Cell Polarization and Centrosome Position

As discussed above, polarization and centrosome positioning are a key aspect to cell migration in two-dimensions. A number of approaches have been used to understand the mechanisms of centrosome positioning in the cell. For example, in vitro experiments have shown that the centrosome can be centered in a chamber by both pushing forces due to microtubule polymerization and pulling forces generated from the microtubule motor dynein [46]–[48]. The results of modeling experiments have also suggested that dynein contributes to centrosome positioning in cells [48], [49].

A number of studies investigated centrosome positioning using wounded monolayers of fibroblast cells moving on 2D glass surfaces. These studies showed that dynein inhibition prevented centrosome reorientation towards the front of the cell in cells at the wound edge [50], [51]. A number of parameters, however, have been shown to affect centrosome positioning in cells. For example, the centrosome and nucleus were pulled toward cell-cell contacts of adjacent, neighboring cells [6]. Cell confluence and cell shape have also been shown to affect centrosome position relative to the center of the cell [7]. Therefore, centrosome positioning in single cells, not just

in cell monolayers, needs to be studied. In fact, experiments with single cells and modeling suggested that microtubule pushing forces, pulling forces, and actin flow all contribute to centrosome positioning for cells migrating on 2D surfaces [26], [27].

Furthermore, there have been studies that observed that centrosome positioning may be altered when cells are confined. Pouthas et al. seeded cells on micropatterned lines and saw that the Golgi apparatus and centrosome were behind the nucleus compared to cells migrating in 2D, where the Golgi is found at the leading edge of cells [52]. Yamada et al. saw similar behavior with fibroblasts migrating on lines [33]. The centrosome position for cells under three-dimensional confinement has not previously been studied nor have the mechanisms underlying these observations in 1D migration and the implications for nucleus migration. Therefore, we investigate these, with our results described in Chapters 4 and 5.

2.6 Tools for Investigating Individual Aspects of Cell Migration

We used a number of different tools to capture certain parameters of the cell's microenvironment and study them in vitro. A few of these are described below.

2.6.1 Polyacrylamide Gels

Polyacrylamide gels have been characterized and used extensively to study the effects of substrate stiffness on a variety of cell behaviors including: cell differentiation [19], migration [18], [20], [53], [54], cytoskeletal arrangement [55], and transmigration [21], [56], [57]. These gels are useful because they are easily tunable to physiologically-relevant stiffnesses, can be coated with fibronectin for uniform cell adhesion, and cells plated on them are easily imaged with microscopy.

More details on the methods and our results in studies with macrophage behavior and centrosome positioning are described in Chapters 3 and 4.

2.6.2 Micropatterns

In vivo, cells are sensitive to geometrical or mechanical constraints, and respond by adapting their cytoskeleton, which can lead to further changes in cell division, differentiation, cell polarity, and cell migration [1], [2]. Micropatterns provide a technique to investigate geometrical constraints in vitro [58], [59]. To create the micropatterns, a silicon wafer is etched using photolithography techniques. This wafer acts as a mold for polydimethylsiloxane (PDMS). The patterned PDMS is cut out and used as a stamp. For cellular applications, the stamp is then inked with a protein that promotes cellular adhesion, such as fibronectin. Then cells are plated and adhere preferentially to the protein [58]. With this technique it was found that controlling the cellular geometry influenced the axis of division [60]. Micropatterns have also been used to stamp asymmetric teardrops to manipulate cell shape into a migratory phenotype. In these shapes the centrosome did in fact polarize towards the wider part of the cell in front of the nucleus and when the cells were released from the patterns the cells migrated in the direction of polarization [61]. We used large circular micropatterns to confine cells to study macrophage proliferation (results in Chapter 3) and to investigate 1D cell migration on narrow stamped lines (results in Chapter 4).

2.6.3 Microfluidic Devices

While micropatterns are useful for confining the cellular adhesion and area, microfluidic devices offer the opportunity to clearly image cells as they move through

precisely defined three-dimensional geometric constraints [62]. Microfluidic devices with a wide variety of geometries have been used to study cell migration. Straight and tapered channels are a popular geometry for cell migration studies [44], [63], [64]. They mimic tracks through the extracellular matrix [44] and if the channels are narrow enough, cells entering the channels must deform the nucleus to squeeze through, like cells do as they move through small pores (Figure 2.1) [65]. Centrosome position relative to the nucleus had not been studied previously, and our results, that the centrosome is more likely to be found behind the nucleus in small channels, adds to the knowledge of cells migrating in channels and through small spaces in the body.

Chapter 3: Substrate Elasticity Regulates the Behavior of Human Monocyte-derived Macrophages[†]

3.1 Introduction

The mechanical environment of a cell may influence the properties and behavior of that cell. In general, an artery seeks to return to homeostasis, the mechanical state before a perturbation. For example, a vascular smooth muscle cell exposed to greater cyclic stretch than normal will synthesize platelet-derived growth factor (PDGF) and proliferate [66]. This cellular response is what causes, in part, arterial wall thickening in the case of hypertension. In turn, wall thickening returns the circumferential stress closer to the value before the increase in arterial pressure and cyclic stretch. This relationship can be appreciated through the simple hoop stress equation: $\sigma_\theta = \frac{Pa}{h}$. Where the mean homeostatic circumferential stress, σ_θ, is around 100 kPa in a large artery, *P* is the transmural pressure, *a* is the radius, and *h* is the wall thickness. Whereby if the pressure increases, either the radius needs to decrease or the wall thickness needs to increase in order to restore the circumferential stress. In addition to arterial remodeling, perturbations to the mechanical properties can lead to sudden catastrophic events. The material properties of constituents in an atherosclerotic plaque can range in stiffness from 1 to 250 kPa; ranging approximately from lipid (1 kPa), cellular fibrotic (10 kPa), hypocellular fibrotic (60 kPa), elastic (80 kPa), to calcified (250 kPa) areas. Mechanical discontinuities in the

[†]Republished with permission of Springer Science, from: Substrate elasticity regulates the behavior of human monocyte-derived macrophages K. M. Adlerz, H. Aranda-Espinoza, and H. N. Hayenga, *European Biophysical Journal*, vol. 45, no. 4, pp. 301–309, 2016; permission conveyed through Copyright Clearance Center, Inc.

material properties of a plaque, particularly microcalcifications near the cap, result in local stress concentrations and often lead to fissures [67], [68]. Yet, it is still unclear how the mechanical perturbations in arterial tissue, as in the case of an advanced atherosclerotic plaque, affect the properties of residing macrophages.

Other types of vascular cells (i.e., endothelial, smooth muscle, and fibroblast) have been shown to respond to the mechanical cues of their environment. Endothelial cells will increase proliferation [69], cell–cell junction width [70], and leukocyte transmigration [21], [56] on substrates more stiff than the healthy range (i.e. >5 kPa) [71]. Endothelial cells will also increase cell–cell conductivity, cell alignment in the direction of flow, and inhibit smooth muscle cell proliferation, platelet and leukocyte adhesion, and arterial narrowing under physiologic, undisturbed flows [72]. Vascular smooth muscle cells display polarization and durotaxis in response to substrate stiffness gradients [53]. The third primary cell type in arteries, fibroblast cells, have been reported to increase their surface area and form actin stress fibers on substrates above 3 kPa [55]. However, not all vascular cells are mechanosensitive. In fact, the spreading area of chemically activated neutrophils does not depend on substrate stiffness. Neutrophils are able to extend an actin filled protrusion on soft substrates without generating traction forces on the substrate [55], [73]. While limited results have been reported on the mechanosensitivity of murine alveolar [22] and murine tumor (RAW 264.7, U937) macrophages [74], [75], the mechanosensitive behavior of macrophages derived from a monocyte, a type of leukocyte in the blood, has not been shown.

Indeed, discovering how macrophages are affected by their mechanical environment may shed light on mechanical cues that either ameliorate or worsen the progression of atherosclerotic plaques. Studies suggest local proliferation of macrophages residing in a plaque, rather than monocyte recruitment from the blood stream, dominates the progression of atherosclerotic plaques [76]–[81]. Macrophages are important to the progression of an atherosclerotic plaque forming fatty streaks in early lesions and the necrotic core in late, unstable plaques. Since macrophages are mechanosensitive, and cells seek to return the environment towards that at homeostasis, we hypothesize the proliferation, migration, phagocytosis, and cytoskeleton of monocyte-derived macrophages will be affected by altered substrate stiffness. Identifying how macrophages are influenced by their mechanical cues will provide insight into how a plaque may progress as well as guide the development of treatment and therapeutic options for atherosclerosis.

3.2 Materials and Methods

3.2.1 Polyacrylamide Gel Preparation

Fibronectin (0.1 mg/ml) (Sigma, St. Louis, MO, USA) was coated onto polyacrylamide gels of varying stiffnesses. Stiffnesses of the polyacrylamide gels were based on the following concentrations of acrylamide (acyl) and bis: 280 kPa—15% acryl and 1.2% bis, 13 kPa—8% acryl and 0.2% bis, 5 kPa—8% acryl and 0.07% bis, 3 kPa—5% acryl and 0.05% bis, 1 kPa—3% acryl and 0.1% bis (Bio-Rad laboratories, Hercules, CA, USA) as previously quantified [20], [82]. Gel substrates of ~80 μm thickness were made by dispensing 30 μl of polyacrylamide onto an

amine-activated glass coverslip (22x22 mm, No.1.5, Fisher Scientific, Pittsburg, PA, USA), and then placing a UV-sterilized coverslip on top. The resulting gels were cured for 30 minutes at room temperature before prying the top coverslip off using the edge of a sterile razor blade. The uniformity and final concentration of fibronectin on the gels was determined using antibodies targeted to fibronectin (Sigma, St. Louis, MO, USA). A fibronectin coating was chosen because it has been reported to be optimal over collagen-1 and fibrinogen for 2D timelapse random migration assays of macrophages [83].

3.2.2 Migration Assay

Forty-thousand human, monocyte-derived macrophages (Celprogen, Torrance, CA, USA) cultured in macrophage media (Celprogen), were plated onto a fibronectin-coated gel. Timelapse microscopy was completed at 37 °C and 5% carbon dioxide with an Olympus IX71 microscope and QImaging camera. Phase-contrast images were captured every 5 minutes for 20 hours. Cell area was found using ImageJ software by manually circling the outline of each macrophage. The center of the cell was manually tracked in ImageJ as well, and this data was used to find cell trajectories and speeds. Speed is defined as the displacement of the center of the cell for each 20 minute time interval divided by the time interval. The speed was found for each cell then averaged for each stiffness. The trajectory data was used to find the ratio between net translocation and contour length where net translocation is defined as the difference between the coordinates of the cell at 0 and 18 hours while contour path is the total distance traveled (Figure 3.2A). The ratio gives information about whether a cell is moving randomly; it was found for each cell and then averaged over

each stiffness. The cell trajectories were also plotted with each cell beginning at coordinate (0,0).

3.2.3 Phagocytosis Assay

Macrophages were plated onto various substrate stiffnesses ($2.5x10^5$ cells per 45x50 mm gel per 35-mm Petri dish) and incubated for 43 hours. Prior to confluency, the macrophages were exposed to 7 ml media with 87.5 μl of 1 μm Nile red fluorescent beads (Life Technologies, Grand Island, NY, USA) for up to 4 hours. Afterwards, macrophages were washed with warmed PBS to remove excess beads. Macrophages were then removed from the gels with 1 ml Trypsin–EDTA (Sigma, St. Louis, MO, USA) and fixed with 4% paraformaldehyde. After centrifugation, macrophages from each condition were counted and resuspended at the same density. Fluorescent flow cytometry (Becton–Dickinson FACScan) was used to count the number of beads internalized by each macrophage. Quantification was confirmed by visualization of the macrophages with optical microscopy (Olympus IX71).

3.2.4 Immunostaining

Single macrophages plated on gels were fixed, permeabilized, and blocked for nonspecific binding. Cells were then stained with phalloidin–tetramethylrhodamine isothiocyanate (Sigma, St. Louis, MO, USA) to label F-actin and 2 μg/ml Hoechst stain (Sigma) to label nuclei. Fluorescence microscopy was done with an Olympus IX71 microscope with consistent exposure times. ImageJ software was used to determine the fluorescence intensity of each cell.

3.2.5 Proliferation Assay

Microcontact printing was used to pattern the surface of the substrates [84]. PDMS stamps with 400-μm-diameter circles were cast from a silicon wafer that was etched 40 μm deep with standard photolithography. These stamps were inked in a 0.1% rhodamine fibronectin solution (Cytoskeleton, Denver, CO, USA) for 30 min, then pressed into a dehydrated gel and allowed to sit for 2 hours in order for the fibronectin to transfer to the gel. Then, the gel was rehydrated in PBS for at least 2 hours before $4x10^4$ cells were plated in macrophage media. Images were captured at 1, 24, 48, and 72 hours after plating and cells in each circle were counted using the Cell Counter Plug-in in ImageJ Software. Doubling time (DT) between each of the time points was found according to the following equation: $DT = \frac{T \ln(2)}{\ln(\frac{X_e}{X_b})}$ where T is the incubation time, X_b is the cell number at the start of the incubation time, and X_e is the cell number after the incubation time. The calculated doubling time was then averaged to find a doubling time for each stiffness. At least 20 stamped circles were imaged for each stiffness at each time point.

3.2.6 Statistical Analysis

Statistical tests were done among groups of data using ANOVA, followed by multiple comparison tests in MATLAB or between pairs using Student's t-test. Statistical significance is considered for $p < 0.05$ and results are reported as mean ± standard error mean (SEM).

3.3 Results

3.3.1 Cell Area Increases with Increasing Stiffness

Cell spreading area is dependent on substrate stiffness and time. First, we found that fibronectin density and uniformity on the gel surface is independent of gel stiffness. The fluorescent intensity of fibronectin antibodies to the 100 μg/ml fibronectin-coated gels was not statistically significant. This result is consistent with those reported by others [55], [85]. Macrophages plated on substrates of each stiffness initially began as a round sphere (Figure 3.1A) with an average area of 155 ± 11 μm^2. By 1 hour, macrophages plated on the stiffer substrate (280 kPa) were already significantly larger than cells plated on soft gels (1, 3, and 5 kPa) (Figure 3.1B).

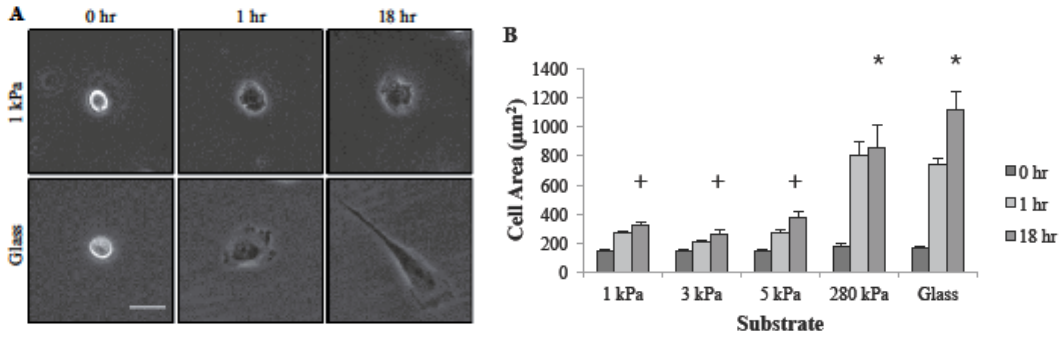

Figure 3.1 The surface area of macrophages is dependent on substrate stiffness. Initially all macrophages have the same area. After 1 hour, the cells have nearly reached their maximum area on each substrate stiffness. **A** Phase contrast images of cells on 1 kPa and glass substrates at 0 hr, 1 hr, and 18 hr. Scale bar 25 μm. **B** The maximum area is statistically different for the soft (1-5 kPa) substrates compared to the stiff (280 kPa, glass). Statistically different groups at 18 hours determined by ANOVA followed by multiple comparison tests and indicated by different symbols ($n \geq 20$ cells in 3 independent experiments for each stiffness, $p < 1e\text{-}4$).

This result suggests that macrophages began sensing and responding to the substrate stiffness in less than 1 hour after plating. The increased area on stiff substrates was also seen up to 18 hours after plating, when cells on the softer

substrates had an average area of 318 ± 31 μm^2, and macrophages plated on the stiff substrate had a significantly larger area of 988 ± 136 μm^2.

3.3.2 Macrophage Migration Depends on Elasticity

To understand the migration of single macrophages, the trajectories of their migration were plotted (Figure 3.2C).

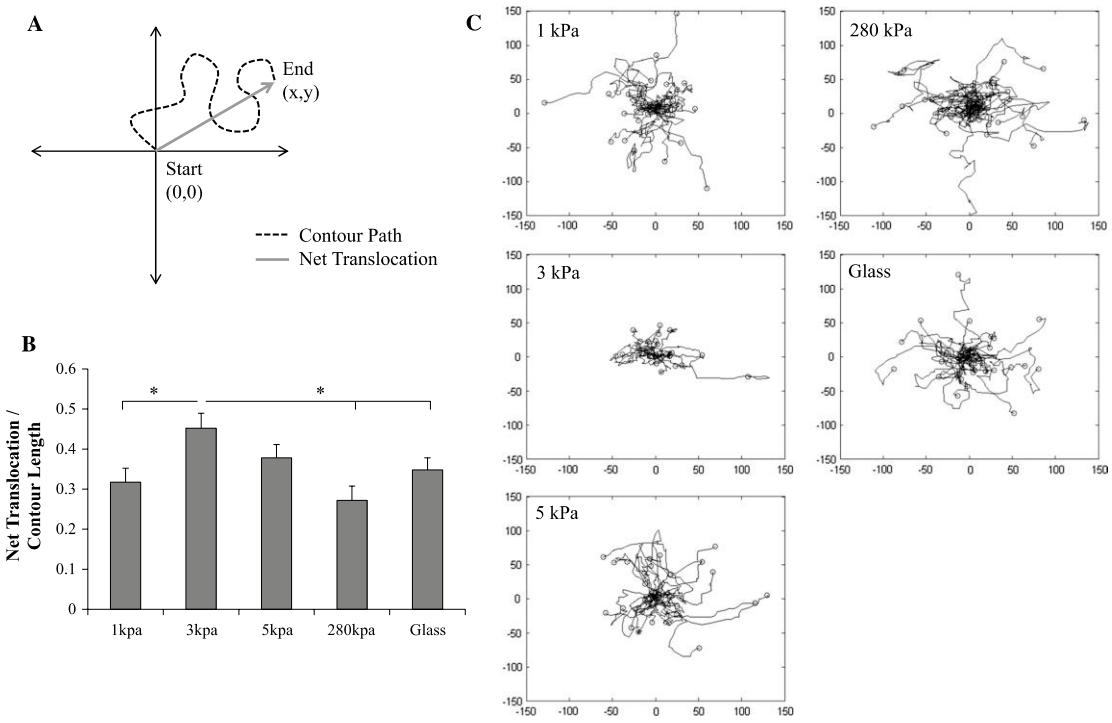

Figure 3.2 Macrophage migration paths were random, with minimal dependency on substrate stiffness. **A** Directionality is determined by dividing the cell's contour path by the net translocation displacement. A ratio less than 0.5 suggests the motion of the macrophages is not directed. **B** Although macrophages on the 3 kPa substrate had a slightly higher ratio, it was still under 0.5 ($n \geq 20$ cells, * $p<0.05$). **C** Plots of the cell tracks, with each cell starting at the origin, illustrates the random motion of the macrophages (n=10).

While most cells seemed to cluster around the origin, some cells on substrates of each stiffness displayed more directed migration to locations further out. To more quantitatively analyze whether directed migration was occurring on substrates of a particular stiffness, the ratio of net translocation to contour length was found for each

cell. The averages for each stiffness were all under 0.5, suggesting migration is random on all stiffnesses (Figure 3.2B). Although migration was random on all stiffnesses, macrophage migration speed was affected by substrate stiffness. The speed was found for each cell, then averaged for each stiffness.

Cells were found to move significantly faster on the 280 kPa substrate 12.0 ± 0.5 μm/h, and significantly slower on the 3 kPa substrate, 5.0 ± 0.4 μm/h (Figure 3.3). Moreover, on the most soft (1 kPa), intermediate (5 kPa), and most stiff (glass) substrates the speed was around 7.4 μm/h with speeds of 7.3 ± 0.6 μm/h on 1 kPa, 7.4 ± 0.6 μm/h on 5 kPa and 7.5 ± 0.2 μm/h on glass. These differences were not significant if the time interval over which the speed was determined was greater than 20 minutes.

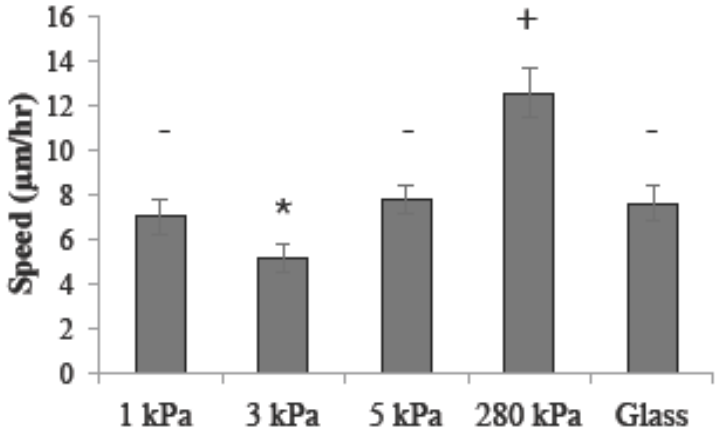

Figure 3.3 The speed of macrophages was fastest on the 280 kPa gel (12.0 ± 0.5 μm/h) and slowest on the 3 kPa gel (5.0 ± 0.4 μm/h). The other substrates had an average speed of 7.4 ± 0.5 μm/h. Statistically different groups determined by ANOVA followed by multiple comparison test and indicated by different symbols ($n \geq 20$ cells, $p < 0.05$).

3.3.3 Actin Arrangement in Macrophages

The total amount of F-actin appears to be a function of substrate stiffness (Figure 3.4). Macrophages spread out to a greater extent on stiff substrates (Figure

3.1). Therefore, quantifying F-actin per area reveals that the F-actin/area ratio is greatest in macrophages on soft substrates (1 and 3 kPa), slightly less on intermediate substrates (5 and 13 kPa), and the least on the stiff substrate (280 kPa). Moreover, the total F-actin per macrophage did not significantly change on soft and intermediate substrates but was significantly lower on the stiff substrate. In cells, actin moves between pools of monomeric (G-actin) and double helical filaments (F-actin). On soft substrates, actin may be mostly in the monomeric form, as opposed to macrophages on stiff substrates where the actin is primarily organized into filaments (Figure 3.4B). Thus, the total F-actin content in macrophages appears lower on stiff substrates due to the actin reorganization into F-actin stress fibers.

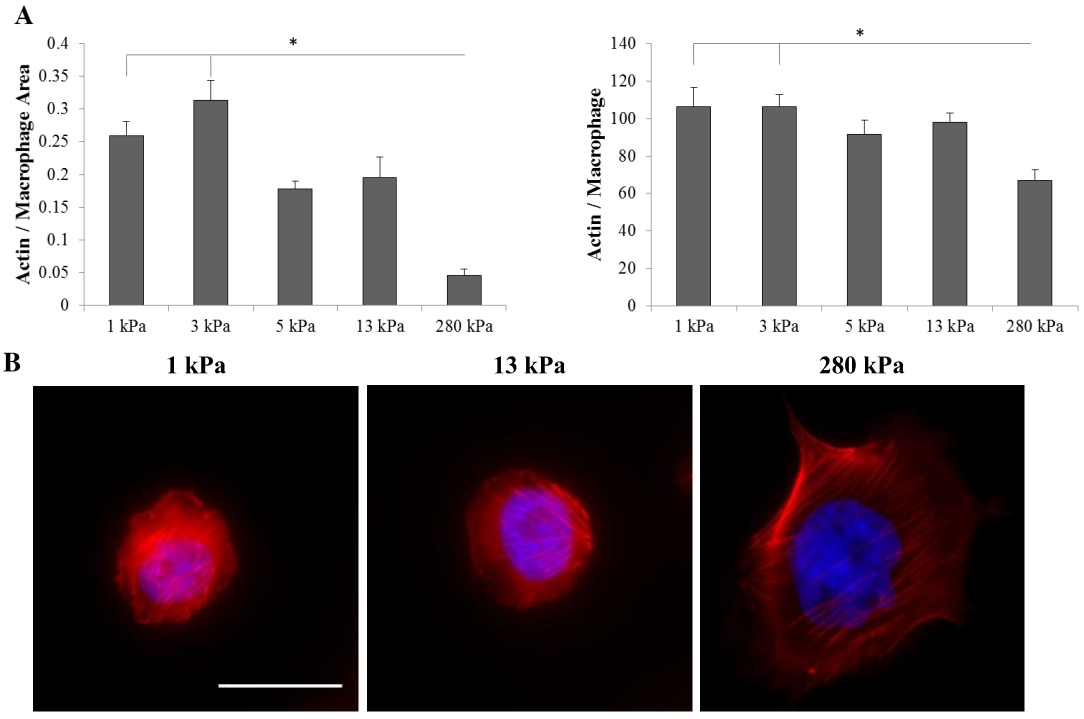

Figure 3.4 F-actin content as determined by fluorescent intensity per macrophage. **A** The total F-actin content on the basal surface of each macrophage is fairly consistent, regardless of substrate stiffness (right graph). However, the F-actin per macrophage area is greatest on the 3 kPa gel and least on the 280 kPa gel (n≥9 cells). **B** This difference is perhaps due to actin fibers in macrophages becoming more organized and forming longer stress fibers on stiffer substrates. Scale bar 25 μm.

3.3.4 Phagocytosis Does Not Depend on Stiffness

The ability of macrophages to phagocytose particles does not depend on substrate stiffness (Figure 3.5). Based on results from flow cytometry, macrophages internalized, on average, two 1 µm fluorosphere beads after 1 hour. After 3 hours, an average of 35 beads were internalized. The number of beads per cell was identified based on mean fluorescence. That is, the mean fluorescence of a single fluorosphere bead was about 4000 a.u., for two beads 8000 a.u., three beads 12,000 a.u., and so on. Bead distribution was also determined for cells incubated with beads for 1 hour. Macrophages only took up an average of two beads and there was no difference between different stiffnesses (Figure 3.5C).

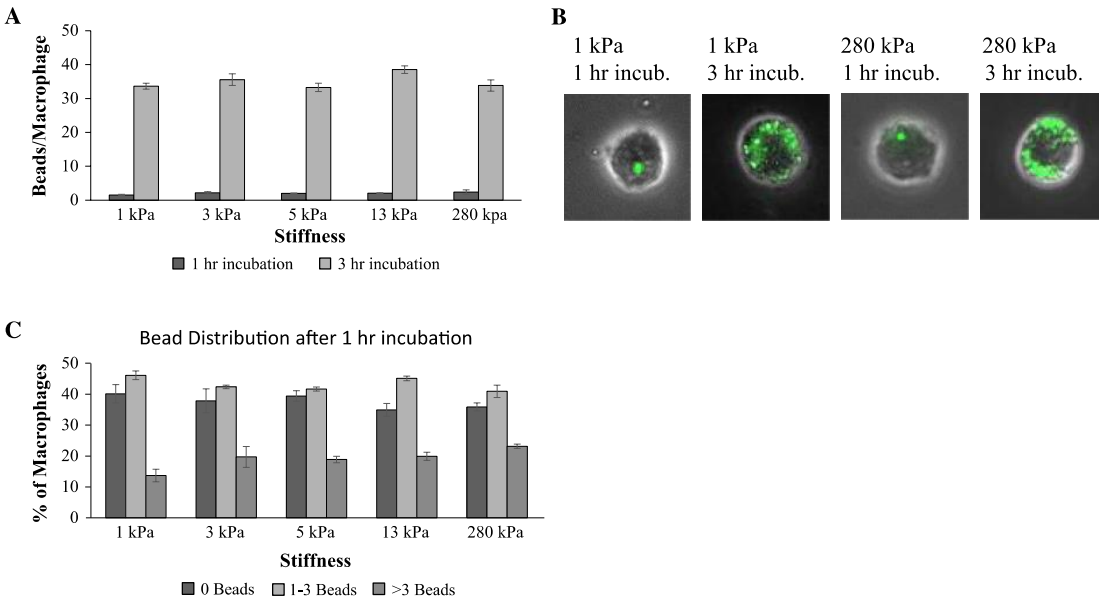

Figure 3.5 Macrophage phagocytosis of 1 µm particles does not depend on substrate stiffness. **A,B** On average, macrophages phagocytosed 2.0 ± 0.3 beads after 1 hour and 35.0 ± 1.3 beads after 3 hours. **C** Regardless of substrate stiffness, after 1 hour, on average, about 38.0 ± 2.4%, 43.0 ± 1.1%, and 19.0 ± 1.7% of macrophages had consumed no beads, 1-3 beads, and over three beads, respectively.

Together, the results emphasize that macrophage phagocytosis does not depend on substrate stiffness. Moreover, the same results were obtained using

different experimental methods (i.e., measuring fluorescence with a plate reader and taking optical images and quantifying beads/cell).

3.3.5 Doubling Time Faster on Stiff Substrates

Macrophage proliferation in fibronectin-stamped circles was observed over 72 hours and the doubling time was calculated. One hour after plating the cells there was an average of 15.0 ± 1.7 and 17.2 ± 2.4 macrophages per circle on the stiff 280 kPa and 13 kPa gels, respectively. After 70 hours, there was an average of 259.8 ± 9.9 cells per circle on the stiff substrate and 221.4 ± 18.3 cells per circle on the 13 kPa gel (Figure 3.6B). This time point was not included in the doubling time calculation, however, since limited space may have slowed cell proliferation within the circles. Forty-eight hours after plating the cells, there was an average of 121.3 ± 9.3 cells per circle on the 280 kPa gel and 85.72 ± 8.49 cells on the 13 kPa gel and images show there was room for additional cells (Figure 3.6C). Therefore, from the cell counts at 1, 24, and 48 hours it was found that, on average, cells on the 13 kPa gel doubled in 19.0 ± 0.1 h, while macrophages on the stiffest gel (280 kPa) proliferated faster with a doubling time of 14.6 ± 0.2 h (Figure 3.6A).

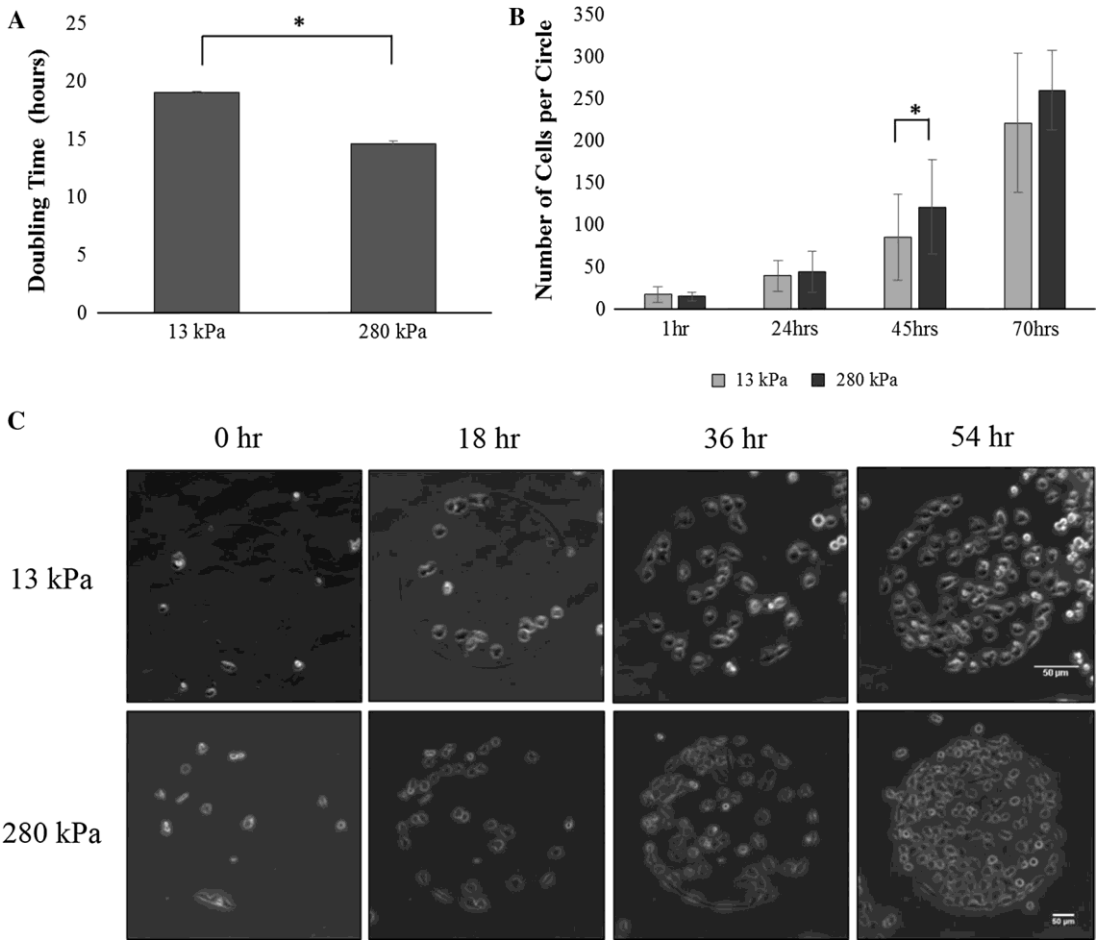

Figure 3.6 Macrophages proliferate in less time on stiffer substrates. Initially, the same number of cells were plated on gels with fibronectin-stamped circles. **A** Cells on stiff substrates (280 kPa) had a significantly smaller doubling time than cells on the substrate of intermediate stiffness (13 kPa). **B** The number of cells in each 400 µm circle was not statistically different at 1, 24, or 70 hours, but at 45 hours, the stiff substrate (280 kPa) had significantly more cells (student's t-test, $p<0.05$). **C** Images captured during timelapse microscopy show cells proliferating to fill in patterned circles at 0, 18, 36, and 54 hours. Representative of at least 20 images taken for each stiffness at each timepoint.

3.4 Discussion

Herein we report that human monocyte-derived macrophages are able to sense their mechanical environment and respond via morphological and biophysical changes. In general, on soft matrices, mechanosensitive cells take on a rounded shape with few focal adhesion complexes and no F-actin stress fibers. In contrast, on stiff

substrates, cells will flatten, form multiple strong adhesions, and form thick stress fibers.

While monocyte-derived macrophages' response to stiffness had not been studied, we can compare our results to other cell types and other macrophages. A number of cell lines have been studied like: RAW 264.7 a mouse macrophage line transformed by a leukemia virus, J774A.1 a macrophage line derived from a mouse sarcoma, and Mono Mac-6 cells originally collected from the blood of a male with acute monocytic leukemia [86]. Tissue-resident macrophages have also been used in experiments. Alveolar macrophages, for example, are collected from the lung. Our studies were conducted with primary human monocyte-derived macrophages isolated by the company Celprogen and grown on ECM-coated flasks in their medium which allows for cell passaging.

Previous studies claim stress fibers are not present in macrophages, even on stiff substrates [22], [75]. They say actin stress fibers spanning the length of a cell are seen in contractile cells with low motility (endothelial cells, fibroblasts, smooth muscle, etc.) and not macrophages. They hypothesize macrophages are not prestressed and use some other mechanism for mechanosensing the environment. However, the cytoskeletal stiffness of macrophages increases as the substrate stiffness increases [22], [74]. Moreover, Roduit et al. showed that if actin is depolymerized in macrophages, with cytochalasin, macrophage stiffness decreased from ~132 to ~28 kPa, supporting the notion that actin fibers contribute to macrophage elasticity [87]. Herein, we observed F-actin fibers are present in monocyte-derived macrophages. The F-actin fibers become more pronounced and span a greater length of the cell as

the substrate stiffness increases (Figure 3.4). These findings challenge the current paradigm and suggest a causal relationship between the formation of F-actin stress fibers (pre-stress) in macrophages and the increased stiffness in macrophages on stiffer substrates, as is seen in contractile tissue cells [88].

In addition to increased F-actin fiber formation with substrate stiffness, the morphology of the macrophages was affected by substrate stiffness. On soft substrates (1–5 kPa), the macrophages increased their area two-fold (from about 155 to 318 μm^2), whereas on stiff substrates (280 kPa and glass) the macrophages formed protrusions (e.g., lamellipodium, filopodium, etc.) resulting in an over six-fold increase in area (to 988 μm^2). Murine alveolar macrophages also spread more on stiffer substrates. However, they appear to be smaller, only spreading to about 100 μm^2 on soft and 375 μm^2 on stiff (glass) substrates [22]. There are noticeable differences in morphology and function from different lineages of macrophages. The mechanism for these differences remains to be elucidated.

Proliferation is important in lesions, in late plaques maybe even more so than monocyte recruitment [76]. It was shown that blocking macrophage proliferation with 5-FU slows progression of plaques in mice. Herein, we showed for healthy monocyte-derived macrophages the average doubling rate goes from 19.0 to 14.6 hours by increasing the substrate stiffness from 13 to 280 kPa. Understanding the cues that lead to increased proliferation could be useful as possible therapeutic targets. Interestingly, in addition to the mechanical environment, the macrophage cell line also determines the proliferation rate. The doubling time of macrophage cell lines from cancer subjects has been reported to be anywhere between 11 hours for RAW264.7 cells

[89], 27 hours [90] for J774A.1 and 50 hours [91] for Mono Mac-6 cells. Conceivably, the time required to proliferate is modulated by the mechanical environment for these macrophage cell lines as well. However, further studies are needed to confirm this.

Unlike the relatively quick proliferation rate, the track speed of monocyte-derived macrophages is relatively slow. The average migration speed for monocyte-derived macrophages was between 0.08 and 0.20 μm/min, whereas the average speed is about 0.8 μm/min for murine bone marrow-derived macrophages [83], about 4 μm/min for FNLP-stimulated murine alveolar macrophages [92], and about 12 μm/min in the tailfin of juvenile fish [93]. Van Goethem et al. found that the average velocity of human monocyte- derived macrophages was about 0.2 μm/min on soft (0.1 kPa) gels (Matrigel and gelled collagen I), and about 0.7 μm/min on soft (0.02 kPa) fibrillar collagen I substrates [94]. The investigators attributed the slow (0.2 μm/min) movement to a mesenchymal mode of migration and the 0.7 μm/min migration to an amoeboid mode where the cells stayed more round in shape.

Previously, it has been found that mouse RAW264.7 and human alveolar macrophages phagocytosed fewer 2 μm latex beads when plated on softer substrates compared to stiffer ones [74]. However, gene expression studies could not predict these results [74]. The authors also found a significant increase in phagocytosis by adding a stimulant, LPS. Conversely, we did not observe a significant increase in phagocytosis after treating the macrophages with 10 ng/ml LPS for 24 hours (data not shown). Further studies are needed to elucidate how posttranslational protein modifications in tumor and alveolar macrophages can modulate phagocytosis

sensitivity to substrate stiffness, but not in monocyte-derived macrophages. Phagocytosis can be mediated by several different receptors. For example, bacteria may display pathogen-associated molecular patterns (PAMPS) while foreign particles that circulate in the blood may be coated in opsonins. Phagocytic receptors on the macrophage recognize the different ligands on the foreign particles that lead to phagocytosis [36], [37]. Further studies might investigate whether phagocytosis of beads coated with opsonins or PAMPS is dependent on the underlying substrate stiffness macrophages are plated on. These studies could then be compared to our results with uncoated beads.

The extracellular matrix (ECM) proteins may also influence cell behavior [95], [96]. To isolate the effects of mechanical properties alone on macrophage behavior, the ECM protein remained constant in this study. Fibronectin was chosen as the extracellular matrix protein because it is a glycoprotein that connects cells with a variety of components in the ECM (e.g., collagen, fibrin, and heparin sulfate proteoglycans) and it contains an amino acid sequence [arginine-glycine-aspartic acid (RGD)] common to many ECM proteins (including elastin) [97]–[100]. The RGD sequence binds to integrins on the surface of macrophages to facilitate reorganization of the cytoskeleton and cell migration. Thus, fibronectin is an essential protein allowing macrophages to sense the environment, however, further studies are needed to elucidate if specific binding to other ECM proteins affects the behavior of macrophages.

In conclusion, in this chapter, we demonstrate that human monocyte-derived macrophages are mechanosensitive and respond to increases in substrate elasticity

with increased area, faster proliferation, the appearance of actin stress fibers, and differences in migration speed. These results add to the growing body of knowledge about the specific responses of different cell types to their mechanical environment and could have implications in understanding the progression of atherosclerosis.

Chapter 4: Centrosome Positioning During One-Dimensional Cell Migration

4.1 Introduction

Much cell migration research has focused on understanding the mechanisms involved in cells moving on a flat, two-dimensional (2D) substrate [3]. Under these conditions, cells polarize with the centrosome towards the front of the cell, send out broad, actin-based lamellipodia that attach to the substrate and propel the cell forward [3]. Cancer cells, immune cells, and stem cells moving through the body, however, encounter a variety of more confined spaces, for example between gaps in the endothelium and through extracellular matrix (ECM) [2]. Therefore, there is increasing interest in cell migration under conditions of confinement to better understand how cells migrate in the in vivo environment [4]. Under confinement, cells are unable to send out the broad lamellipodia and instead must send out smaller protrusions, polarize, and then squeeze the cytoskeleton and nucleus through small spaces [37]. To mimic the physical confinement these matrices present, cells can be seeded in three-dimensional collagen, or can be confined in microfluidic channels [44]. In vivo, cells also migrate on narrow tracks and along collagen fibers through the ECM [32]. Micropatterned lines of ECM represent a simple system that confines cells to the patterned area, recapitulating this aspect of the in vivo environment.

Additional differences between so-called one-dimensional migration on micropatterned lines, three-dimensional migration through matrices, and two-dimensional migration have been observed. For example in 1D and 3D, there is increased cell speed, decreased adhesions, and more dependence on microtubules

compared to 2D migration [33], [44]. Furthermore, a canon of cell migration in two-dimensions is the position of the centrosome in front of the nucleus in a migrating cell [3], [24]. The centrosome, which anchors microtubules, is essential in cell polarization and migration [48], [49], [101]. It has been observed, however, that in cells migrating under 1D confinement, the centrosome is not found at the front of cells, but in the back, behind the nucleus [33], [52]. The mechanism responsible for the positioning is not understood.

Microtubules, which grow from the centrosome, are one candidate for centrosome positioning. In vitro models of a microtubule aster in confined spaces showed that microtubule pushing forces against the edges of confinement could center the aster [46]. It has been seen in other cases though that the major force in centrosome positioning is not forces from the microtubules themselves, but rather from the microtubule motor dynein [26], [27], [48], [49]. This was seen in single cells spread on a 2D surface [26] and in 2D wounded monolayers of 3T3 cells where the centrosome was found to reposition towards the front of the cell except when dynein was inhibited [26], [51]. However, both confluence and shape of cells affect centrosome and nuclear positioning [102]. Therefore, it is necessary to investigate what the dominant positioning mechanism is in 1D migration.

We aimed to examine centrosome position in 1D migration of NIH-3T3 fibroblasts using 3-5 μm fibronectin lines micropatterned on a glass substrate. In this system, we found the centrosome positioned behind the nucleus in the majority of cells and that dynein-inhibition has a slight effect on cell speed and centrosome position with about 50% of the cells having the centrosome in back. Blebbistatin, a

myosin II inhibitor, caused a significant defect in the cell's ability to persist on the lines and only 35% of cells had the centrosome in the back. Treatment with a low concentration of nocodazole resulted in cells repeatedly changing directions, the centrosome not repositioning after these changes, and increased centrosome dynamics. We also found that microtubule polymerization depended on the position of the centrosome: cells with the centrosome behind the nucleus had greater EB3 intensity at the front of the cell. Together, these results suggest a model where microtubule pushing forces due to growing ends contacting the cell membrane or other organelles play a role in positioning the centrosome in fibroblasts migrating under 1D confinement.

4.2 Materials and Methods

4.2.1 3T3 Fibroblast Cell Culture

The NIH-3T3 cell line (ATCC, Manassas, VA) was cultured in DMEM supplemented with 10% fetal calf serum. The following plasmids were transfected into NIH-3T3 cells by nucleofection (Lonza): dsRed-cent2 which was a gift from Joseph Gleeson (Addgene plasmid #29523) [103], H2B-gfp, and EB3-gfp. Drug treatments were 200nM taxol, 100 nM nocodazole [104], 15 μM (-)-blebbistatin, and 50 μM Ciliobrevin D (EMD Millipore) [105].

4.2.2 Polyacrylamide Gel Preparation

Fibronectin-coated polyacrylamide gels of varying stiffness (1 kPa and 280 kPa) were made according to the following concentrations of acrylamide and bis: 1

kPa—3% acrylamide and 0.1% bis, 280 kPa 15% acryl and 1.2% bis [20]. (Additional details found in Section 3.2.1).

4.2.3 Micropatterning Lines

A silicon wafer with patterns of 3 and 5 μm lines was etched using standard photolithography techniques. The wafer was used as a mold for PDMS, mixed at a 10:1 ratio with PDMS-curing agent, poured over the wafer, put under vacuum, then baked at 80°C for two hours. The PDMS was cut into approximately 2x2 cm squares to be used as stamps [106]. The PDMS was incubated in a 0.2 mg/ml fibronectin solution for 10 minutes, rinsed, and allowed to dry. The stamp was placed into contact with either a glass coverslip or a glass-bottomed dish for 1 minute. After stamping, the glass was rinsed with PBS and left in a 1% bovine serum albumin solution to block non-specific binding for one hour. Rhodamine fibronectin was used to check the stamping.

4.2.4 Live-Cell Imaging and Analysis

3T3 fibroblasts were plated on the gels or glass substrates and allowed to adhere. Around $4x10^4$ cells were plated on each gel, to achieve single cell migration. Or 3T3 fibroblasts were plated on the stamped glass and allowed to adhere. Timelapse microscopy captured phase and fluorescent images every 5 minutes for eighteen hours. Microscopy was completed at 37°C and 5% CO_2 (Olympus IX81, Slidebook software). ImageJ was used to merge fluorescent images and individual channels were adjusted to provide a clear image. ImageJ was also used to find the cell outline, nucleus, and centrosome position. This data was imported into MATLAB and

a custom-written program analyzed the raw data (Appendices A and B). The instantaneous speed of the cell and nucleus was found using the center of the cell and nucleus respectively. The mean cell width was calculated for each cell at every timepoint then averaged over all cells.

4.2.5 2D Migration Analysis

The dot product was used to determine the position of the centrosome relative to the nucleus and the direction of migration for persistently migrating cells. The dot product was found between 1) the vector between the nucleus center and the centrosome and 2) the vector between the centers of nuclei of the first and last timepoints (MATLAB code in Appendix A). The inverse cosine of the dot product was found and this angle fell between 0 and 180°. The centrosome was classified as in front of the nucleus, if the angle was between 0 and 90°, and behind the nucleus if it was between 91 and 180° (Figure 4.1A). A second analysis narrowed the range for the front to between 0 and 60°, 121 and 180° for the back, and 61 to 120° for the side of the cell (Figure 4.1B). In this analysis, cells were imaged every 20 minutes and the analysis looked at the cell migration over at least 100 minutes.

4.2.6 1D Migration Analysis

The MATLAB function atan2 was used to find the angle between the centrosome and center of the nucleus. This function gives the angle from the positive x-axis. The angle was found for each timepoint of every cell, and the average deviation from 90 degrees of all cells is reported. The average standard deviation is

defined as the mean of each cell's standard deviation (MATLAB code in Appendix B).

For drug treatments, 3T3 fibroblasts were plated on the micropatterned glass coverslips and allowed to adhere for two hours. Excess cells were washed away with PBS and 3 ml of media with the appropriate volume of drug treatment was added to the cells before timelapse imaging began. The nucleus of blebbistatin-treated cells could not be imaged because the wavelength required to image GFP would have inactivated the blebbistatin [107].

Average EB3 intensity was calculated using ImageJ from background-subtracted images and is defined as the total intensity divided by the area of the front, that is the cell from the nucleus to the leading edge, or the area of the back, from the rear edge of the nucleus to the trailing edge of the cell. To determine the direction of cell migration, an initial image and an image taken after 30 minutes were compared.

4.2.7 Statistical Analysis

All experiments were repeated at least three times independently. Data is reported as the mean ± standard error of the mean. Statistical significance was determined using a student's t-test or a two-proportion z-test. The data met the requirements for statistical analysis including normality as tested by the chi-square goodness of fit test. These statistical tests were performed in Excel. A p-value of less than 0.05 was considered statistically significant, unless stated otherwise.

4.3 Results

4.3.1 Nucleofection Does Not Affect Cell Migration on Lines

First, to verify that nucleofection was not affecting cell behavior we compared the migration of control, untransfected 3T3 fibroblasts to 3T3 fibroblasts that had been transfected with the H2B-gfp and dsRed-cent2 plasmids. Both groups of cells migrated persistently on the lines and the average speeds of the cells, defined as the speed of the center of the cell, were statistically similar, 0.77 ± 0.08 μm/min and 0.80 ± 0.05 μm/min for untransfected and transfected cells respectively.

4.3.2 Centrosome Position on Different Stiffnesses

In addition to confinement, another important property cells encounter in vivo is the elasticity of the substrate [4]. We examined whether centrosome positioning was dependent on substrate stiffness.

3T3 fibroblast cells were imaged as they migrated on fibronectin-coated glass, a soft polyacrylamide gel (1 kPa), and a stiff polyacrylamide gel (280 kPa). The position of the centrosome relative to the nucleus was determined for persistently migrating cells on each substrate by finding the angle between the centrosome relative to the nucleus and the direction of migration (details in Appendix A). This angle falls anywhere between 0 and 180 degrees. First, we classified the centrosome as towards the front of the cell (in front of the nucleus, towards the direction of migration) if this angle was 90° or less, and towards the back if it was greater than 90° (Figure 4.1A). On glass and the stiff 280 kPa gel the centrosome was in front, towards the direction of migration for 69% and 71% of cells respectively. On the soft

substrate, however, the centrosome was in front of the nucleus in only 35% of cells (Figure 4.1A).

To better understand if the centrosome was behind, in front of, or to the side of the nucleus, especially on soft gels, the range of the angles was narrowed. In this case, for an angle between 0 and 60° the centrosome was classified as in front, from 121 to 180° it was in the back of the nucleus, and for the remainder it was on the side (Figure 4.1B). Even with this more constricting definition, on the soft gels, 23% of cells had the centrosome in front of the nucleus with 54% in back. On the stiff gels, the centrosome was found in front of the nucleus in 62% of cells and in the back in 27%. Similarly, on glass the centrosome was more often in front of the nucleus, 61%, than behind, 29%. The remainder of the time the centrosome was located towards one of the sides of the nucleus, in 23%, 12%, and 11% of the cells on 1 kPa, 280 kPa, and glass respectively (Figure 4.1B).

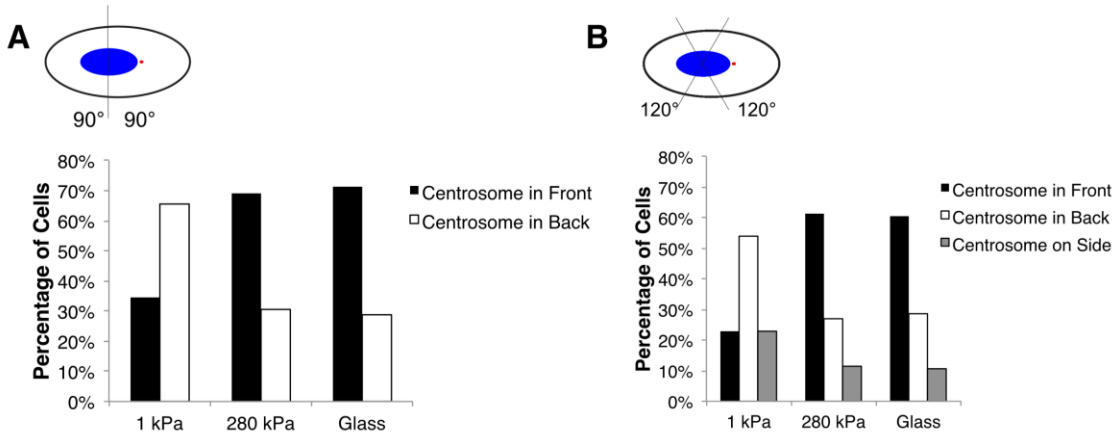

Figure 4.1 Percentage of cells migrating persistently on 1 kPa, 280 kPa, or glass substrate with the centrosome (red) in front of or behind the nucleus (blue, in the sketches above). ($n \geq 13$ cells for each condition, 3 experiments). **A** The centrosome position is defined as in front or back of the nucleus (90° angle). The majority of cells on stiff substrate and glass have the centrosome in front of the nucleus, while a majority have it in the back on the soft substrate. **B** Centrosome position is defined as in the front, back or side. The proportion of cells with the centrosome in front and back is similar to as with the previous definition.

4.3.3 Centrosome Position in 1D Migration

After discovering that the centrosome position did depend on substrate stiffness, we turned our attention to understanding if centrosome positioning for cells migrating under confinement was different from 2D migration. 3T3 fibroblast cells were imaged as they migrated on 3 or 5 μm fibronectin lines stamped on glass. 92% of the observed cells migrated persistently along the lines with only 8% changing directions. The remaining cells maintained their direction of migration and of the cells that maintained a constant centrosome position, 63% had the centrosome behind the nucleus while 37% positioned the centrosome in front of the nucleus (Figure 4.2A-B).

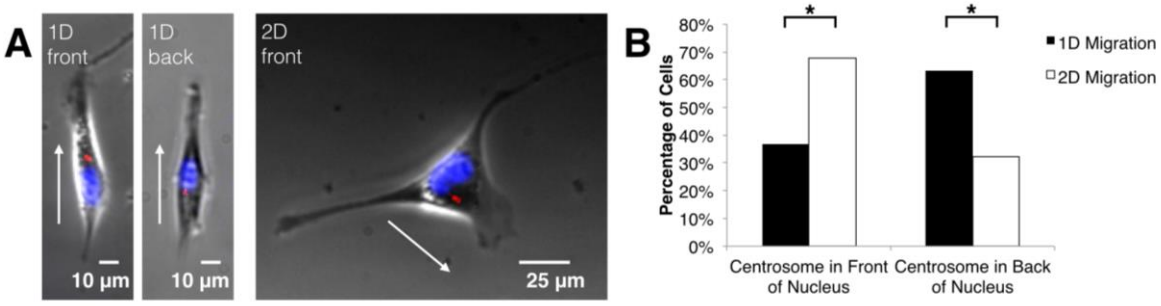

Figure 4.2 Centrosome position depends on geometrical constraints. **A** Phase images merged with fluorescent images of centrosome (red) and nucleus (blue) of 3T3 fibroblasts migrating on 1D micropatterned lines show a cell migrating with the centrosome in front of the nucleus (left), behind the nucleus (middle), and a cell migrating with the centrosome in front during 2D migration on glass (right). **B** Comparison of centrosome position in front of or behind the nucleus for 3T3 fibroblasts during 1D and 2D migration. (1D migration n=19 cells, 7 experiments. 2D migration n=14 cells, 4 experiments. Two proportion z-test, *p=0.016).

Instead of the centrosome always being at the center of the cell, we observed that the position of the centrosome behind or in front of the nucleus resulted in the centrosome being closer to the back or front of the cell (Figure 4.3A). When the centrosome was in the back of the nucleus it was closer to the back of the cell. If the

centrosome was in front of the nucleus, the centrosome was located closer to the center of the cell (Figure 4.3B).

4.3.4 Centrosome Position Does Not Affect Cell Migration

The next questions were whether the position of the centrosome depended on cell phenotype or affected cell migration. First, we looked at whether the cell width differed with centrosome position, which might indicate the cells were being confined to different degrees. The mean width of the cell when the centrosome was in back of the nucleus was 5.99 ± 1.32 μm, similar to the mean width when the centrosome was in front, 5.00 ± 0.78 μm (Figure 4.3C).

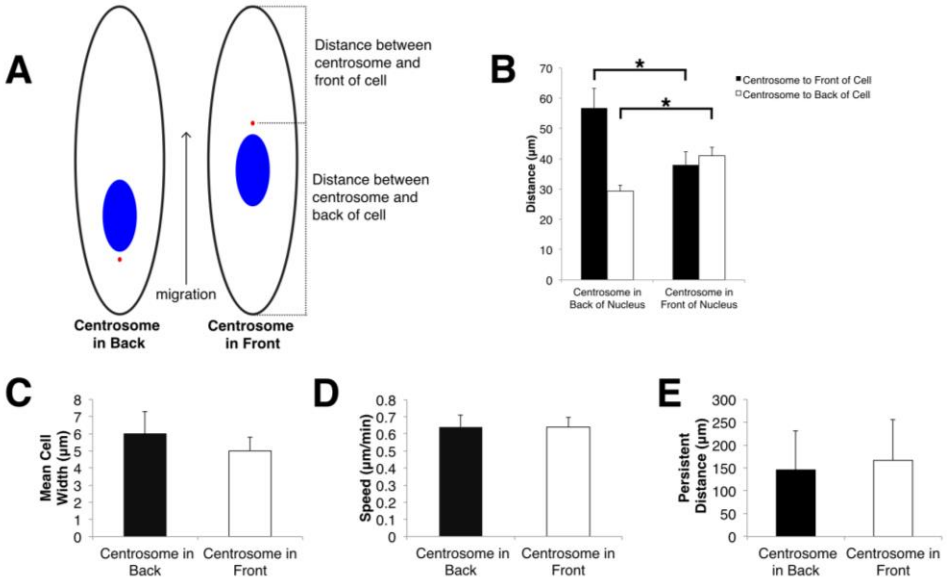

Figure 4.3 Biophysical parameters of migration do not depend on centrosome position. **A** Depiction of cells moving on 1D micropatterned lines and the definitions of the distance between centrosome (red) and back and front of a cell (nucleus in blue). **B** The distance between the centrosome and the back of the cell is shorter when the centrosome is behind the nucleus compared to when it is in front. **C-E** The mean cell width, speed as measured by tracking the centrosome, and distance travelled persistently of 3T3 fibroblasts migrating on 1D micropatterned lines do not depend on the position of the centrosome in front of or behind the nucleus. Mean + s.e.m. is shown, centrosome in back n=12, centrosome in front n=7, 7 experiments, all non-significant student's t-test.

Next, we explored if the position of the centrosome was affecting cell migration. The mean speed was measured by tracking the centrosome as the 3T3 cells migrated on the micropatterned lines. When the centrosome was in back of the nucleus the mean speed was 0.64 μm/min compared to 0.65μm/min when the centrosome was in front of the nucleus (Figure 4.3D).

The persistence of the 3T3 cells migrating on the micropatterned lines is greatly increased compared to 2D migration. It was observed that only 8% of cells changed direction while migrating on the 1D lines. The average distance travelled persistently, that is until the cell switched directions, stopped, divided, or went off screen, was similar whether the centrosome was behind or in front of the nucleus, 145.7 ± 84.9 μm and 166.8 ± 89.9 μm respectively (Figure 4.3E). That these biophysical parameters did not change with centrosome position led us to question whether centrosome position is maintained or is random.

4.3.5 Centrosome Position is Maintained During Change of Directions

When a cell did change directions during migration, the centrosome maintained its position in front of or behind the nucleus, suggesting that centrosome positioning is actively maintained in fibroblasts. Figure 4.4A shows images of the nucleus and centrosome captured during a timelapse. The cell is moving down on a micropatterned line with the centrosome behind the nucleus, the cell then switches to move up on the micropatterned line and the centrosome moves across the nucleus to resume its position behind the nucleus (Figures 4.4A-B). The instantaneous speed of the center of the nucleus and centrosome is plotted versus time in Figure 4.4C, and peaks are seen in the centrosome speed. The cell depicted in this figure is

representative of the behavior observed for all cells that changed directions on the lines. We observed 3 cells migrating with the centrosome behind the nucleus and 1 cell with the centrosome in front of the nucleus which all repositioned the centrosome to the new back or front, respectively.

A micropipette was used to try to induce changes of direction for cells migrating on lines. The cells were imaged to determine which direction they were migrating then a micromanipulator was used to nudge the leading edge protrusion. Only 2 out of the 32 cells tested changed directions of migration. The remaining cells reattached and continued to migrate in the same direction. In the cells that did change directions, the centrosome was observed to maintain its position relative to the nucleus like in the spontaneous changes of direction. In both of these cases the centrosome was in back of the nucleus.

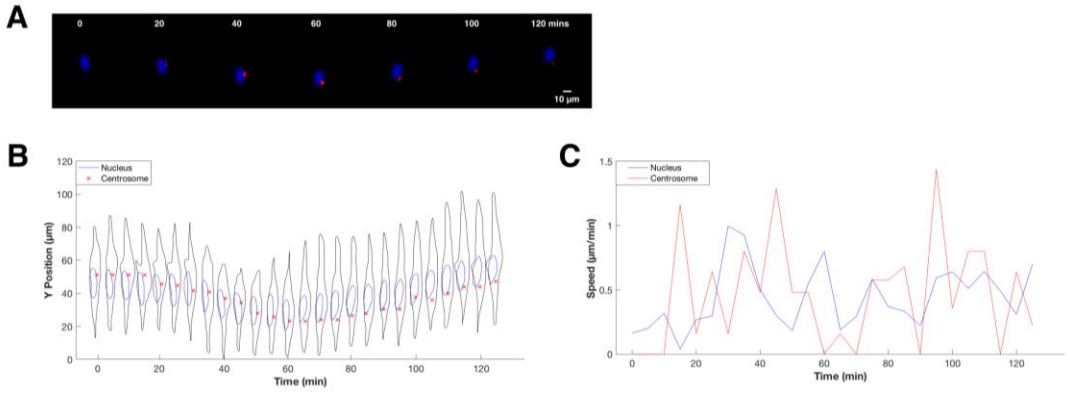

Figure 4.4 Centrosome position is maintained as evidenced when cells change directions on lines. **A** Fluorescent images from timelapse of nucleus (blue) and centrosome (red) during a change of directions on lines. **B** Outline of the cell changing direction. The centrosome (red x) changes positions to remain behind the nucleus (blue outline) as the cell switches from migrating down to migrating up. **C** The speeds of the centrosome and nucleus during the change of directions suggests the centrosome has a faster speed than the nucleus.

4.3.6 Centrosome after Cell Division

6 cells were observed to divide and then reattach and continue migration on the micropatterned lines. In these cases, the two daughter cells positioned their centrosomes in the same orientation, relative to the nucleus, as the dividing cell once they resumed migration after division. That is, if a cell was migrating with the centrosome in back of the nucleus, after division the two daughter cells also had the centrosome in back of the nucleus during migration on the line.

4.3.7 Microtubules Exhibit Polarity

To investigate microtubule dynamics in migrating cells, microtubule ends were visualized as cells migrated on lines by transfecting the cells with an EB3-gfp plasmid (Figure 4.5A). 73% of cells with the centrosome in back of the nucleus had a greater EB3 intensity at the front of the cell (Figure 4.5B). On average, cells with the centrosome in back of the nucleus had 18.7 ± 0.06% more EB3 in the front than the back of the cell. Cells with the centrosome in front of the nucleus had a 0.7 ± 0.05% difference (Figure 4.5C). This polarization led us to hypothesize that growing microtubules played a role in centrosome positioning.

To further test this hypothesis we used cytoskeletal inhibitors to observe both cell migration and centrosome positioning on lines.

4.3.8 Microtubules Needed for Migration and Persistence

Treatment of 3T3 cells migrating on micropatterned lines with 200 nM taxol resulted in halted migration (cell trajectories plotted in Figure 4.6C). Cells did not

move along the line, although they did have dynamic protrusions with both extension and contraction. These dynamics were not correlated to centrosome dynamics.

A low dose of nocodazole (100 nM) was used to inhibit microtubule dynamics without causing complete depolymerization seen at higher concentrations [104]. 3T3 cells treated with 100 nM nocodazole changed direction more often than untreated cells. 57% of cells changed direction at least once over the 18 hour timelapses after being treated with nocodazole compared to only 8% of untreated cells.

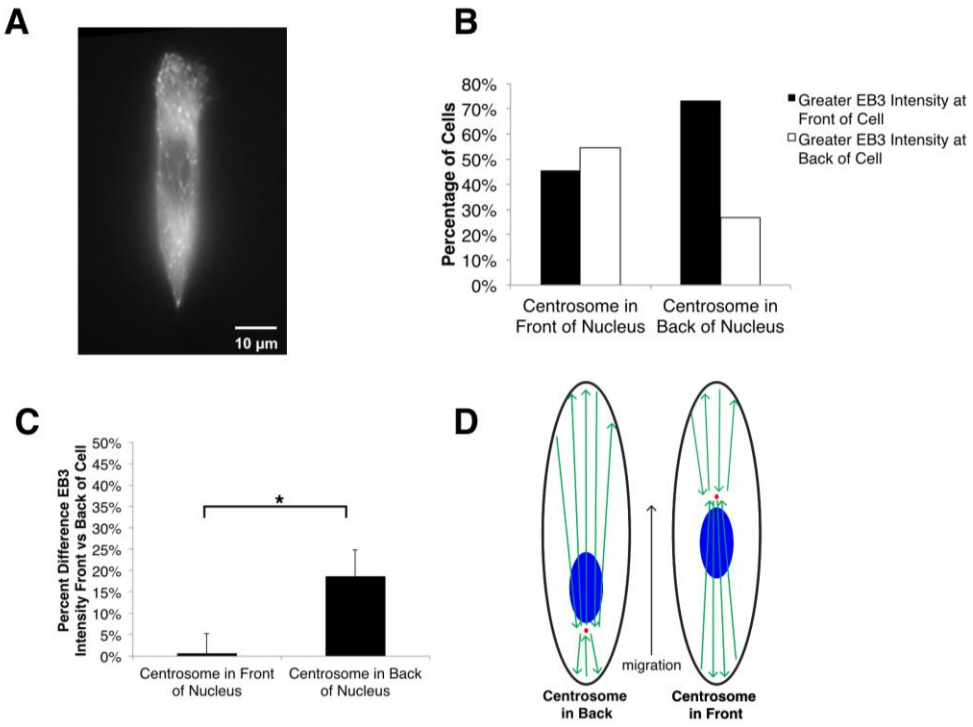

Figure 4.5 Microtubule polymerization depends on centrosome position. **A** Fibroblast transfected with EB3-gfp migrating on a 1D line. **B** When the centrosome is in back, a higher percentage of cells have greater EB3 intensity at the front of the cell. (Back: n=8 cells, Front: n=6 cells, 3 experiments, two proportion z-test, p=0.059). **C** The percent difference in fluorescent intensity of EB3 between the front and back of the cell is higher for cells with the centrosome in back, meaning that they have more EB3 towards the front. (Student's t-test p=0.029). **D** Schematic of microtubule polarization with microtubules in green, nucleus in blue, and centrosome in red. When the centrosome is in back of the nucleus more microtubules push against the front of the cell (left).

4.3.9 Blebbistatin-Treated Cells Do Not Migrate Persistently on Lines

Cells were allowed to adhere to the micropatterned lines, then treated with blebbistatin, a myosin II inhibitor. Examining the trajectories of the cells shows they were not as confined to the lines and migration in 1D (Figure 4.6C). Instead, the blebbistatin-treated cells were wider than control cells and at times, cells would move in the x-direction, perpendicular to the fibronectin lines, until they came across another line when many would resume migrating primarily in the y-direction (Representative images shown in Figure 4.6D).

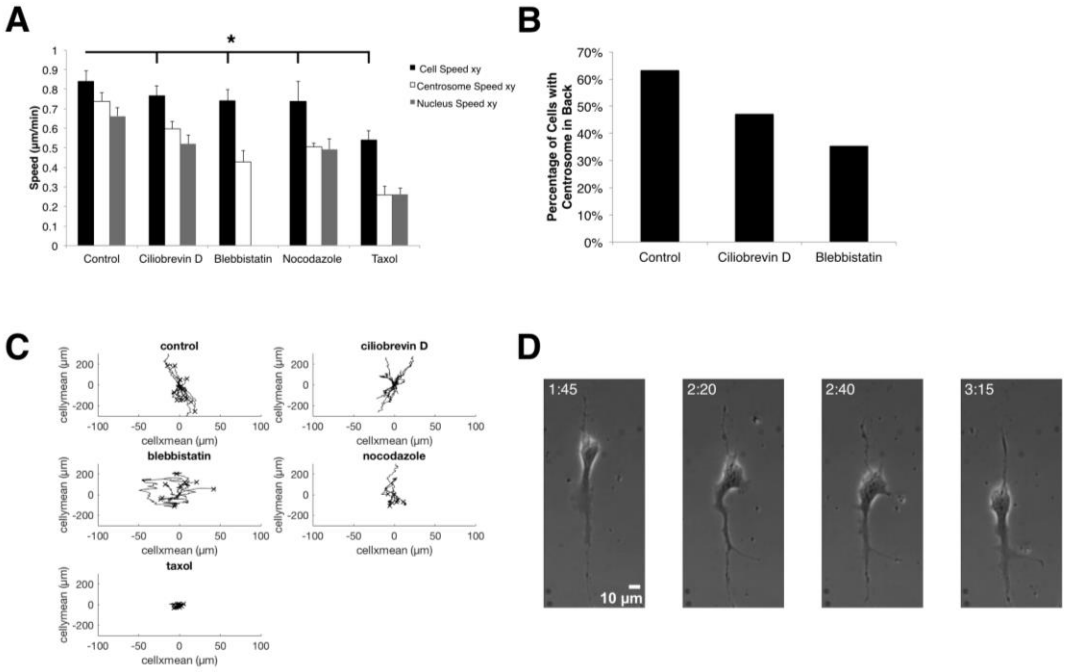

Figure 4.6 Disruption of actin and microtubule polymerization affects fibroblast migration on lines. **A** Cell speed as measured by tracking the cell center, centrosome, and nucleus is affected by drugs to dynein, myosin II, microtubule polymerization, and microtubule dynamics. Mean + s.e.m. is shown, control n=19 cells, 7 experiments, cytoplasmic dynein inhibitor n=24, 6 experiments, blebbistatin n=9, 2 experiments, nocodazole n=7, 3 experiments, taxol n=10, 3 experiments. Student's t-test for mean cell speed for each drug treatment compared to control * $p<0.05$. **B** Percentage of 3T3 cells migrating on 1D lines with the centrosome in back comparing control cells and cells treated with blebbistatin or cytoplasmic dynein inhibitor. (Two-proportion z-test p=0.153, 0.116). **C** Trajectory plots of cell centroids for cells observed migrating on 1D lines show the cytoskeleton's role in cell migration. **D** Representative phase images of a blebbistatin-treated cell moving along the micropatterned line. Time stamp (h:min).

During migration, significant membrane trails were left behind. Furthermore, the centrosome position when the cells were migrating on the lines was altered. In blebbistatin-treated cells, 35% of cells positioned their centrosome towards the back of the cell during migration on lines and the cell speed was 0.74 μm/min compared to 0.84 μm/min for untreated cells (Figure 4.6A-B).

4.3.10 Dynein Inhibition has Small Impact on Centrosome Position

Ciliobrevin D-treated cells moved at a similar speed on lines compared to untreated cells (0.76 μm/min compared to 0.84 μm/min). There was also a slight, not statistically significant difference in centrosome position, 47% of cells had the centrosome in back compared to 63% in untreated cells (Figure 4.6).

4.3.11 Microtubules and Centrosome Dynamics

The angle between the center of the nucleus and the centrosome, defined in Figure 4.7A, was used to measure the centrosome's position relative to the nucleus. For a cell migrating up, an angle of -90° means the centrosome is directly behind the center of the nucleus. An angle of 90° means that the centrosome is in front of the nucleus, and 0 or 180° means that the centrosome is located to the side of the nucleus. The deviation from 90° was calculated for each cell, and the average of the absolute values for control cells was 19.9 ± 3.81°. This means that, on average, the centrosome did not deviate from directly in front of or behind the nucleus by more than 20°. This was very similar to ciliobrevin D treated cells, 21.4 ± 4.51°. When the microtubules were perturbed with either taxol or nocodazole, however, the cells had a significantly greater deviation from 90 degrees: 46.4 ± 8.18° and 44.3 ± 8.24° (Figure 4.7B)

suggesting the centrosome was displaced from directly behind or in front of the nucleus after treatment with these drugs.

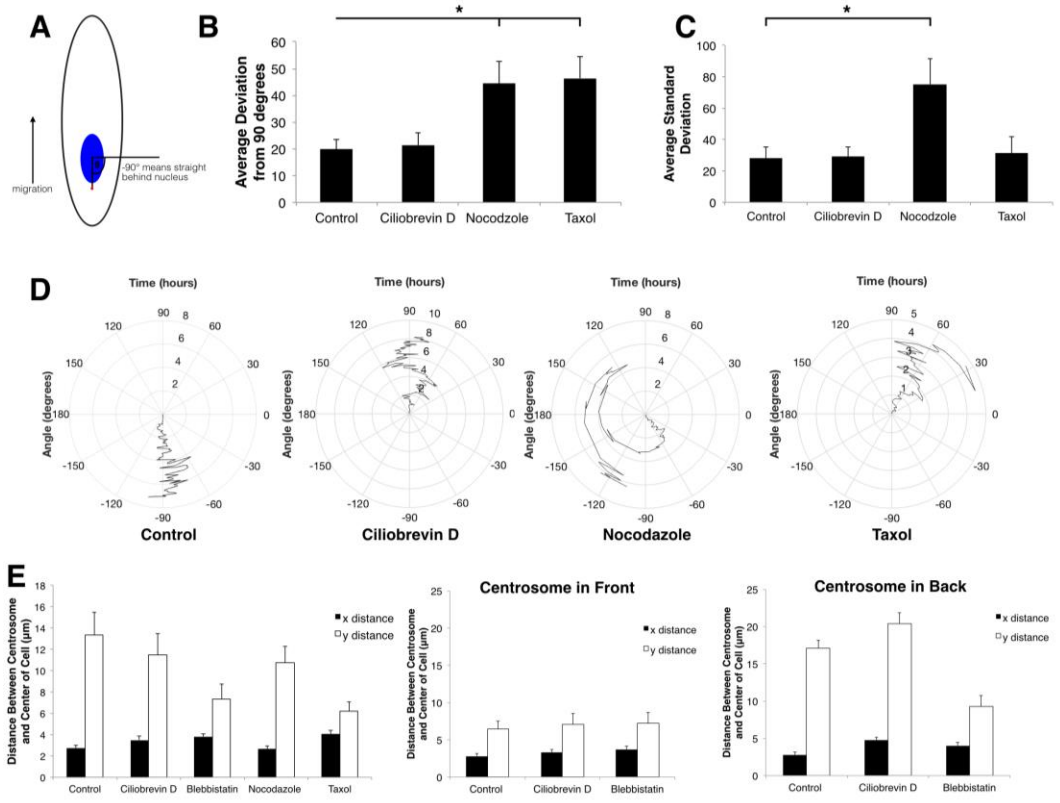

Figure 4.7 Actin and microtubule polymerization disruption affects centrosome dynamics. **A** Definition of the angle between the centrosome and center of the nucleus. **B** Average deviation from 90 degrees of the angle between the centrosome and nucleus shows the centrosome is displaced from directly in front of or behind the nucleus in nocodazole and taxol treated cells. Mean + s.e.m. is shown, control n=19 cells, 7 experiments, cytoplasmic dynein inhibitor n=24, 6 experiments, nocodazole n=7, 3 experiments, taxol n=10, 3 experiments. Student's t-test nocodazole compared to control p=0.005, taxol compared to control p=0.002. **C** Average standard deviation of the angle between the centrosome and nucleus shows increased dynamics of the centrosome for nocdazole-treated cells. Student's t-test nocodazole compared to control p=0.005. **D** Representative plots of the angle between the centrosome and nucleus over the time course of an experiment, with time=0 starting at the origin for control and drug-treated cells. **E** The distance between the center of the cell and the centrosome for all cells (left). The distance depends on the position of the centrosome in front of the nucleus (middle) or in back of the nucleus (right).

As a measure of centrosome dynamics, the standard deviations of the angle over all time points of a single cell were averaged across all cells. The average

standard deviation of control cells was 28.1° similar to taxol and ciliobrevin D-treated cells (29.1° and 31.4°). Nocodazole-treated cells had a significantly larger mean standard deviation, 75.1°, shown in Figure 4.7C.

Figure 4.7D shows representative polar plots of the angle between the centrosome and nucleus as a function of time. The control cell and ciliobrevin D-treated cell maintain an angle of around -90 or 90° over time. The taxol-treated cell is slightly less than 90° while the nocodazole-treated cell varies widely between 120 and -60° affirming that microtubule polymerization is involved in regulating centrosome position.

The distance between the centrosome and the center of the cell has been used as a measure of centrosome positioning. Similar to the distance between the centrosome and the edge of the cell shown in Figure 4.3B, we observed that the distance between the center of the cell and centrosome depended on whether the centrosome was found in front or behind the nucleus (Figure 4.7E). Another measure of centrosome position is the average distance between the centrosome and the closest edge of the nucleus. The average distance was 1.96 ± 0.14 μm and was not statistically different between treatment groups.

4.4 Discussion

It is now clear that the centrosome plays an important role in cell polarization. In fact, the centrosome position in relation to the nucleus and the leading edge indicates how the cell is polarized [3]. Our results indicate that the centrosome position towards the front of the cell is influenced by both substrate stiffness and confinement. Very recently, a paper was published by Discher and colleagues

investigating centrosome position in mesenchymal stem cells (MSCs) on substrates of different stiffness [108]. Similar to our results, they reported that the centrosome position was found in front of the nucleus for cells on stiff substrates, and was not polarized for cells on soft substrates [108]. Microtubules in the MSCs were polarized towards the front on stiff gels but unpolarized on soft gels. They also found that myosin IIb was unpolarized on soft gels and towards the rear of the cell on stiff substrates [108], [109]. These results further support that centrosome positioning and polarization of the cell is affected by substrate stiffness in not just fibroblasts, but MSCs as well.

Centrosome positioning can be controlled by pulling forces due to dynein motors interacting with microtubules and by pushing forces due to microtubule polymerization. In vitro experiments have shown that both dynein motors [48], [49] and microtubule pushing forces [46] are able to center the centrosome in microfabricated chambers that mimic the confining environment of a cell. For fibroblasts migrating at the leading edge of wounded monolayers, dynein is necessary for centrosome positioning towards the front of the cell [26], [51]. Dynein, microtubule pushing forces, and retrograde actin flow all contributed in various degrees to centrosome positioning in single cells plated on a two-dimensional glass surface [26], [27].

Migration in complex 3D environments is quite different from 2D migration though. Research from Yamada's group has shown that the cell phenotype in 3D environments is more similar to cells migrating in 1D than 2D [33]. Centrosome positioning is also different between 2D and 1D migration. In 1D migration, the

centrosome was often seen behind the nucleus. We found that the centrosome is behind the nucleus in 63% of cells during 1D migration. For the centrosome to be positioned behind the nucleus, dynein pulling forces that originate from interactions with microtubules directed towards the back of the cell would be dominating. Alternatively, pushing forces due to microtubules growing towards the front of the cell could position the centrosome towards the back. We found that microtubules polymerize more towards the front of the cell when the centrosome is behind the nucleus, and are similar when the centrosome is in front of the nucleus (Figure 4.5). This polarization suggests that microtubule pushing forces are important.

A simplified force balance on the centrosome, considering only pushing forces due to growing microtubules, suggests that these forces could be enough to influence the centrosome's position towards the back of the cell. We assume that the total force (F_{tot}) acting on the centrosome is the sum of pushing forces from microtubules growing towards the front of the cell (F^{+}_{f}) and towards the back of the cell (F^{+}_{b}), $F_{tot} = F^{+}_{b} + F^{+}_{f}$. The pushing force of one microtubule (f^{+}) is $f^{+} = \frac{p^2 k}{L^2}$ where κ denotes the microtubule bending rigidity [25]. The pushing force F^{+} is simply the pushing force of one microtubule multiplied by the number of microtubules, then $F_{tot} = N_b \frac{p^2 k}{L_b^2} - N_f \frac{p^2 k}{L_f^2}$. Where, N_b is the number of microtubules towards the back of the cell and N_f is the number towards the front of the cell. L_b is the length from the centrosome to the back of the cell, L_f is the length from the front of the cell to the centrosome, and L is the total length of the cell. We plotted this function in MATLAB and looked for the value of L_b where F_{tot} was equal to zero, which means that the

forces acting on the centrosome from microtubules directed towards the front and back of the cell are balanced, to see where the centrosome would be positioned in this case.

Based on our results, when the centrosome is in the back, 20% more microtubules are towards the front (Figure 4.5). Using this value and a cell length of 83 μm, we find that L_b is 39.6 μm, meaning that the centrosome would be positioned more towards the back of the cell. This agrees with our data. We found that when the centrosome is behind the nucleus, it is pushed towards the back of the cell with an average distance of 28 μm between the centrosome and back of the cell (Figure 4.3B). When the centrosome is in front of the nucleus, there is no difference in microtubules towards the front or back, therefore the centrosome should be towards the center, which is our result (Figure 4.3B).

Obviously, this force balance is an over-simplification of the actual conditions inside the cell: we have only considered pushing microtubules; we assumed that all microtubules reached the cell membrane; and we do not take into account microtubules pushing on other organelles in the cell. A better model would need to be developed to incorporate all of these factors and predict centrosome position with more certainty. Even so, this simple force balance shows that pushing forces could in fact bias the centrosome towards the back of the cell.

During observation of cells migrating on lines we were able to follow the position of the centrosome. Of particular interest was when the cells changed directions. We observed, similar to what has been seen in epithelial cells [52], that when a cell changes direction the centrosome switches to retain its position relative to

the nucleus (Figure 4.3). These results suggest that the centrosome position is indeed maintained by the cell and not random. This repositioning of the centrosome requires that the microtubules also redistribute and begin growing asymmetrically towards the new front or back of the cell depending on centrosome position.

To further dissect the forces acting on centrosome positioning we used cytoskeletal inhibitors to depolymerize microtubules (100 nM Nocodazole), inhibit dynein (50 µM Ciliobrevin D), and inhibit myosin II (15 µM Blebbistatin). Our results indicate that the most important effects are seen after depolymerizing microtubules. When cells were incubated with nocodazole they changed directions much more frequently. Microtubule polymerization was also essential for centrosome positioning. As discussed in the results and Figure 4.7, disruption of microtubule polymerization resulted in increased centrosome dynamics and with the centrosome no longer found directly in front of or behind the nucleus as a cell migrated. During changes of direction the centrosome was not repositioned as it was in control cells.

It is important to note that there are interactions between actin and microtubules and perhaps between microtubule polymerization and dynein accumulation [110]. For example, our results show that the majority of blebbistatin-treated cells have the centrosome towards the front of the cell. This could be due to reduced actin membrane contractility and the interaction of microtubule ends with the membrane. Another possibility is that actin and the centrosome may interact, recent experiments have shown that the centrosome is able to promote actin filament assembly and organization [111].

While our results focus on centrosome positioning, nuclear positioning is also important during migration. It is now well-established that the nucleus is the limiting factor during migration [35], [65]. The mechanisms of nuclear positioning have not been examined in 1D migration, although actin has been shown to play a role in cells at the leading edge of wounded monolayers [50]. Furthermore, the nucleus is connected to the cytoskeleton network through LINC complexes [112]–[114]. Because of these connections and the close proximity of the centrosome and the nucleus, it has been speculated that there may be a link between the nucleus and centrosome, although the nature of the link and its properties are unknown [115]. It was previously shown though that dynein and microtubules control nuclear rotation in a cell [110], [116]. In these experiments, the centrosome did not rotate with the nucleus. Similarly, in our results, the nucleus does not appear to rotate as the centrosome is repositioned during changes of direction (Figure 4.4). This adds evidence that if the nucleus and centrosome are linked, it is not a rigid tether.

Our results also have implications in cell division. During cell division the two centrosomes are positioned on opposite sides, and after division the daughter cells move away from each other with the centrosome in between the nucleus and the leading edge. This would indicate that eventually all cells should have the centrosome in the front, contrary to our observations. Our results indicate that the daughter cells instead move the centrosome to the position it was in before division. It has been seen that cell geometry prior to division can influence the division axis orientation [60] which may help explain our findings.

An understanding of fibroblast cells moving under 1D confinement offers a reference point to understand how immune cells and cancer cells move in the body. For example, in T cells the centrosome orientation seems to be important for polarized secretion at the immunological synapse [117]. And cancer cells often have centrosome amplification [118] and mutations in nesprins that could affect LINC complexes [7] among other genetic abnormalities. A more thorough understanding of cell polarization and migration under confinement would offer additional insights into these cells' in vivo behaviors. Finally, it is of note that while migration in 1D and 3D environments are similar, centrosome positioning has not been well studied in the context of 3D migration. These studies could be important since extreme confinement may prevent the centrosome from repositioning. It would be interesting to see if this prevents a cell from changing directions since centrosome repositioning was observed in cells that changed directions in 1D migration (Figure 4.4).

In conclusion, the centrosome has traditionally been described as a key indicator of cell polarization, found towards the leading edge of the cell. The results described in this chapter show that the position of the centrosome is not as definitive as this. Instead, the centrosome position actually depends on the stiffness of the substrate the cells are migrating on as well as the degree of confinement. Our results show that cells migrating on soft gels do not display polarization of the centrosome towards the leading edge. Additionally, for cells migrating on 1D lines, the centrosome is actually primarily found behind the nucleus and this position is maintained even when cells change directions. Finally, we show that the centrosome position for cells migrating on 1D lines depends on microtubule polymerization.

These results have implications in understanding cell polarization for cells migrating under confinement.

Chapter 5: Centrosome and Nucleus Positioning During Migration Under Three-Dimensional Confinement‡

5.1 Introduction

Cell migration is a central process in the development and maintenance of the body. It also plays a key role in pathological process such as cancer development. In both normal and pathological processes, cells must move through a variety of microenvironments that physically confine the cell [8], [119]. Much of the understanding of cell movement comes from studies done on 2D surfaces. There has been increased interest in studying cells as they migrate in complex environments.

Since it is difficult to image single cells migrating in the body, microfluidic devices are a popular tool to study cells migrating under confinement. These more closely mimic the environments cells encounter in vivo than 2D substrates. Konstantopoulos and colleagues developed a microfluidic device that incorporates a chemoattractant gradient to induce cells to move from a cell seeding region into and through narrow channels [120]. These narrow channels resemble microtracks found in extracellular matrix that allow for persistent, directed cell migration. This type of chemotactic migration is seen in cancer cells migrating away from a primary tumor [121]–[123]. This microfluidic device also includes entrances into the channels, where cells move from an unconfined environment into 3D confinement. This transition requires significant cellular deformation, similar to the way cells must

‡ This work was done in collaboration with Marina Shumakovich and Dr. Kimberly Stroka's laboratory.

deform their cytoskeleton and nucleus to enter small pores in the ECM or move through endothelial cell junctions during metastases formation [119], [121].

A number of studies have investigated cell migration in channels and found that cancer cells are able to enter and migrate through channels more quickly than healthy cells [120], [124]–[126]. It has also been shown that cells are extremely persistent once inside channels [124], [125]. One possibility is that the cancer cell's softer nucleus offers less of an obstacle than in healthy cells [35], [38]. In fact, it is thought that the nucleus, as the stiffest organelle in the cell, may be the limiting factor in migration through three-dimensional matrices [35], [37], [65]. The nucleus is not migrating independently though; it is directly connected to the cytoskeleton through LINC complexes [41]. The cytoskeleton is involved in moving the cell and nucleus forward [50], [127]. The cytoskeleton also polarizes the cell which is necessary for directed migration [3], [101].

In 1D confinement, where the cell is confined by its adhesive area, cells also travel more persistently than in 2D, as described in Chapter 4. Importantly, the position of the microtubule-organizing center was found to be different in 1D confinement than for cells migrating on 2D surfaces. The centrosome is positioned behind the nucleus in 1D whereas in 2D migration it is towards the front of the cell. While the majority of cells migrated persistently in 1D, a small number of cells changed directions. In this case the position of the centrosome was maintained (Chapter 4). That is, the centrosome switched to the new back of the cell as the cell changed directions. This implies that the polarity of the cell is important and maintained even under 1D confinement.

It is not known how the microtubule-organizing center is positioned for cells moving through microfluidic channels. Based on cell migration in 1D, we hypothesized that the centrosome and the nucleus would have a preferred orientation, with the centrosome towards the back of the cell during migration in 3D environments. We were also interested in studying if cells would be able to change directions and change polarity in a more confining environment. We used a chemotactic microfluidic device with small channels and found that under confinement the position of the centrosome was in fact behind the nucleus in nearly all cells during migration in the smallest channels, although not in wider channels. Interestingly, cells did not have a clear preference for centrosome position entering the channel, and entry time into the channels was not dependent on centrosome position. We also found that even when the cell is under three-dimensional confinement, the centrosome will maintain its position behind the nucleus when a cell changes directions.

5.2 Methods

5.2.1 Cell Culture and Reagents

The NIH-3T3 cell line (ATCC, Manassas, VA) was cultured in DMEM (Life Technologies, Grand Island, NY) supplemented with 10% fetal calf serum (Colorado Serum, Denver, CO). To visualize the nucleus and centrosome, cells were transfected using nucleofection (Lonza) with an H2b-gfp plasmid and dsRed-cent2 plasmid which was a gift from Joseph Gleeson (Addgene plasmid #29523) [103].

5.2.2 Microfluidic Device

A silicon wafer with channels was etched using standard photolithography techniques. More details on the device can be found in reference [120]. The wafer was used as a mold for polydimethylsiloxane (PDMS), mixed at a 10:1 ratio with PDMS-curing agent, poured over the wafer, put under vacuum, then baked at 85°C for two hours. The PDMS was cut out into individual devices and a hole punch was used to create inlets and outlets to the channels that also serve as media reservoirs. The PDMS and a clean glass slide were treated with oxygen plasma (Harrick Plasma) for 2.5 minutes then pressed together for 3 minutes to ensure good bonding. A 0.2 mg/ml fibronectin solution (Sigma) was added to all inlets and outlets to coat the channels, the devices were left to incubate for 1 hour, then rinsed with PBS.

5.2.3 Cell Seeding into Device and Imaging

3T3 fibroblasts were seeded into the channel by adding about 1x 10^5 cells suspended in 25 µl media to the cell inlet of the microfluidic device. Cells were allowed to flow through and populate the cell seeding channel for 5 minutes before the cell suspension was removed and DMEM and DMEM supplemented with calf serum were added to the medium and chemokine channels respectively. More details on the stability of the chemoattractant gradient can be found in reference [120].

Timelapse microscopy captured phase and fluorescent images every 10 minutes for eighteen hours. Microscopy was completed at 37°C and 5% CO_2 (Olympus IX81 and Olympus IX83).

5.2.4 Switching the Chemoattractant

To induce cells to switch directions, the chemoattractant gradient was switched. The device was first set up as described above and cells were allowed to enter and migrate into channels overnight. Then, all the media was removed from the device and media supplemented with serum was added to what was the cell inlet channel. The other channels were filled with unsupplemented media. The cells were then imaged (Figure 5.4A).

5.2.5 Migration and Position Analysis

ImageJ was used to find the nucleus outline and centrosome position. This data was imported into MATLAB (MathWorks) and a custom-written program analyzed the raw data (Appendix B). The instantaneous speed of the nucleus was found using the center of the nucleus.

5.2.6 Statistical Analysis

Data is reported as the mean ± standard error of the mean. Statistical significance was determined using analysis of variance between groups (ANOVA), followed by a multicomparison t-test or a two-proportion z-test. These statistical tests were performed in MATLAB. A p-value of less than 0.05 was considered statistically significant, unless stated otherwise.

5.3 Results

5.3.1 Microfluidic Device for 3D Confinement

3T3 fibroblasts were imaged as cells migrated into and through the narrow channels of the microfluidic device shown in Figure 5.1A. The cells were suspended in media and migrated towards a gradient of media supplemented with serum, more details about the device can be found in reference [120]. Two different channel widths were investigated: a 6 μm wide channel that was 10 μm high (referred to as the 6 μm channel), and a more confining 3 μm wide, 6 μm high channel (referred to as the 3 μm channel). Figure 5.1B shows cells in the seeding region and cells moving through the channels towards the chemoattractant. The migration of cells in channels is compared to cell migration on 1D micropatterned fibronectin lines (Figure 5.1C) and cells on a fibronectin-coated 2D glass substrate (Figure 5.1C). Additional details on these experiments can be found in Chapter 4.

5.3.2 Migration Speed Depends on Degree of Confinement

The first observation was that, as expected, the nucleus had a narrower width in channels and on 1D lines compared to 2D migration (Figure 5.2A). The average nuclear width was 2.58 μm for cells in 3 μm channels, 2.59 μm for cells in 6 μm channels, 4.08 μm in 1D migration, and 11.4 μm in 2D migration. The area of the nucleus in the 3 μm channels, 108.5 ± 5.0 μm^2, was greater than the area in 6 μm channels, 92.7 ± 3.9 μm^2, suggesting that the nucleus had to elongate in the 3 μm channels which are 4 μm shallower than the 6 μm channels to accommodate its

volume. Figure 5.1.C shows that cells in the 3 μm channels appeared more deformed than cells in the 6 μm channels.

To investigate the effects of the various confining microenvironments on cell migration, the speed of the nucleus was examined. The center of the nucleus for cells migrating inside the channels was tracked over the course of the timelapse. The speed of the nucleus for cells in the narrow 3 μm channels was 0.24 ± 0.02 μm/min which was slower than cells in the 6 μm channels that migrated at 0.35 ± 0.04 μm/min (Figure 5.2B). Cells moving in the 6 μm channels actually had a more similar speed to cells on 2D surfaces, 0.34±0.05 μm/min. Cells migrating on 1D lines were significantly faster than any other condition, with a speed of 0.63 ± 0.05μm/min.

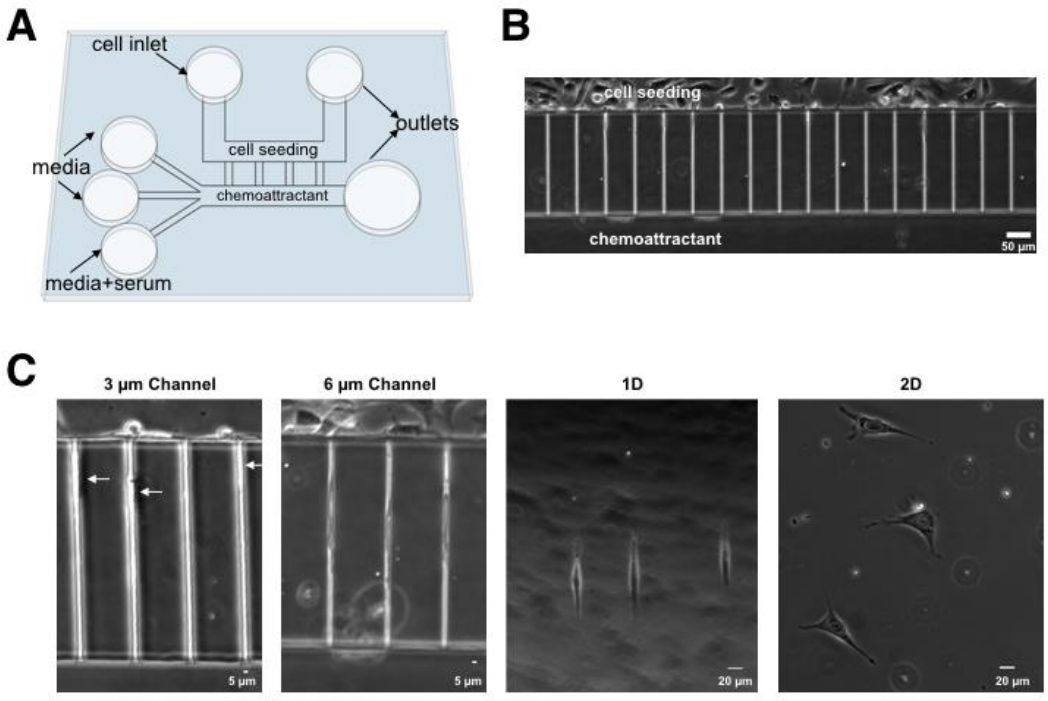

Figure 5.1 Microfluidic device to study 3D migration. **A** Schematic of the microfluidic device, image based on one from **[120]**. **B** Phase image of the channels portion of the microfluidic device with cells moving from the cell seeding channel towards the chemoattractant. **C** 3T3 fibroblasts migrating in 3 μm channels (cells are significantly deformed and hard to see in a single frame from the timelapse, they are indicated by arrows), 6 μm channels, on micropatterned 1D fibronectin lines, and on a fibronectin-coated 2D glass substrate. Scale bars as indicated.

5.3.3 3D Confinement Affects Centrosome and Nucleus Position

In 2D migration, the centrosome is in front of the nucleus, towards the leading edge, in 71% of persistently migrating cells. In the majority of cells migrating on 1D surfaces, however, the centrosome is behind the nucleus. To determine the positioning of the centrosome for cells in channels, we classified the centrosome position relative to the nucleus and the direction of migration for cells migrating in the channel. In 6 μm channels, 20% of cells changed the centrosome position during migration. In the remaining 80% of cells, the centrosome was found almost equally in front of the nucleus as behind. In the more confining 3 μm channel, for migrating cells, the centrosome was behind the nucleus, towards the back of the cell, in nearly all cells (Figure 5.2E).

It was observed for some cells migrating in the 3 μm channels that the centrosome appeared to be far from the edge of the nucleus (Figure 5.2D). Indeed, after quantifying the distance between the centrosome and the closest edge of the nucleus, some cells had an increased distance between the centrosome and the nucleus, with the average distance of one cell reaching 10.9 μm (Figure 5.2C). These cells contributed to an overall average distance of 4.9 ± 0.6 μm. The average nuclear length or area of these cells was not different from cells with a shorter distance. This was not seen for cells in the wider 6 μm channels or in 1D or 2D migration where the average distances between the centrosome and nucleus were 2.6 ± 0.2, 2.2 ± 0.3, and 3.14 ± 0.3 μm respectively.

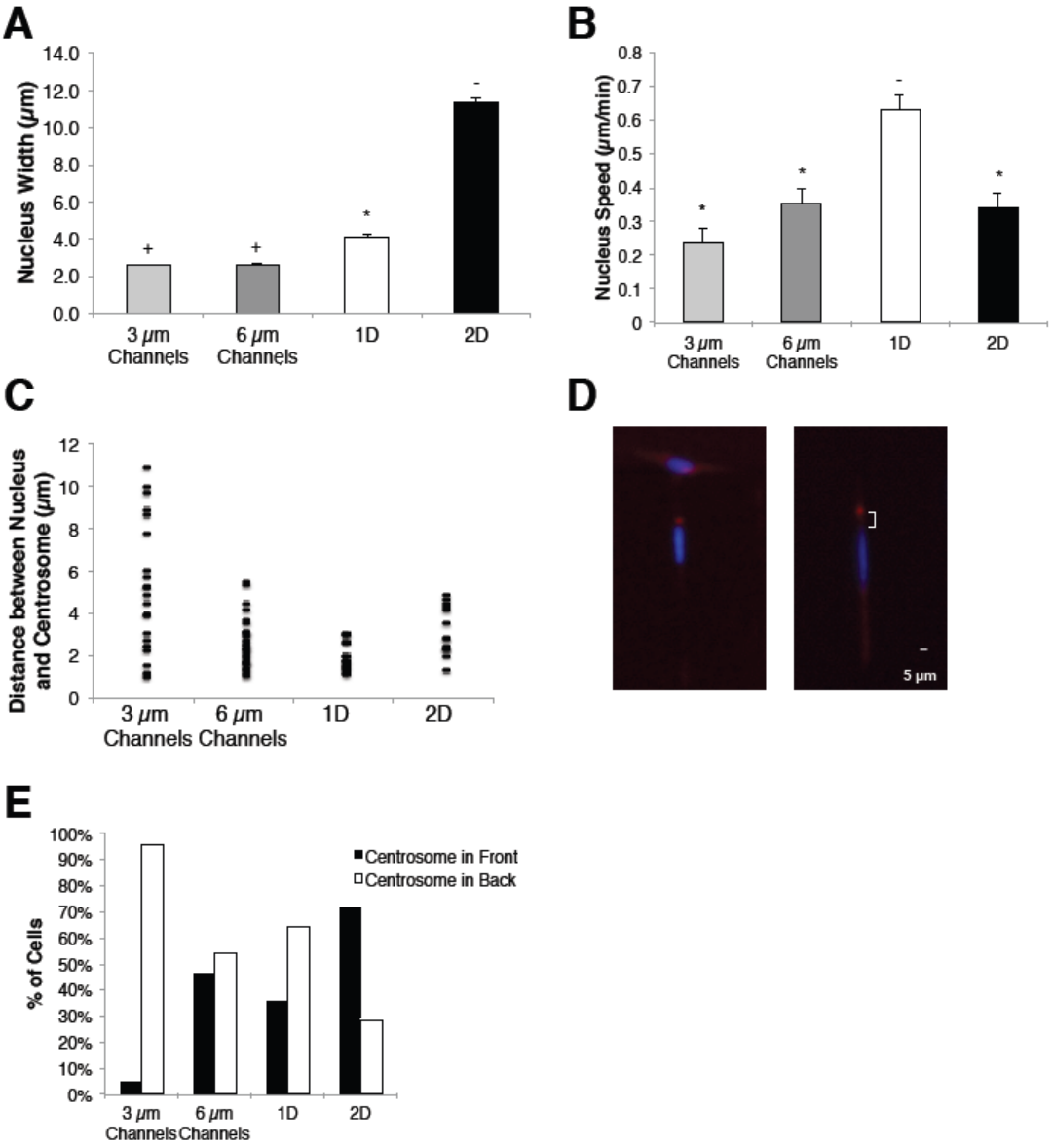

Figure 5.2 Centrosome position depends on confinement. **A** Average nucleus width for cells migrating in the 3 μm channels (n=25 cells, 4 independent experiments), 6 μm channels (n=34 cells, 7 experiments), on 1D lines (n=19 cells, 7 experiments), or on a 2D glass substrate (n=14 cells, 4 experiments). Mean + s.e.m. is shown, ANOVA p=9.7e-19 followed by multicomparison tests p < 1e-8 between groups with different symbols. The same symbol indicates the groups are not statistically different. **B** Cell speed as measured by tracking the nucleus center. The symbols represent statistical significance. Mean + s.e.m. is shown, ANOVA p=1.7e-9 followed by multicomparison tests p < 1e-4. **C** Scatter plot of the distances between the centrosome and closest edge of the nucleus. **D** Two cells in 3 μm channels. Cell on left has small distance between the nucleus (blue) and centrosome (red), cell on right has increased distance, scale bar 5 μm. **E** Percentage of cells with the centrosome positioned in front of the nucleus (black) or in back (white).

5.3.4 Centrosome Position Entering Channel

We examined cells as they moved from the cell seeding channel, which is similar to 2D migration, into the channels. 55% of cells entered the 3μm channel with the centrosome behind the nucleus. Figure 5.3A shows a cell approaching and entering a channel with the centrosome behind the nucleus. 45% of cells entered the 3 μm channels with the centrosome in front but then quickly switched the centrosome to the back of the nucleus once in the channel (Figure 5.3B). About 50% of cells entered the 6 μm channel with the centrosome in the front (Figure 5.3B).

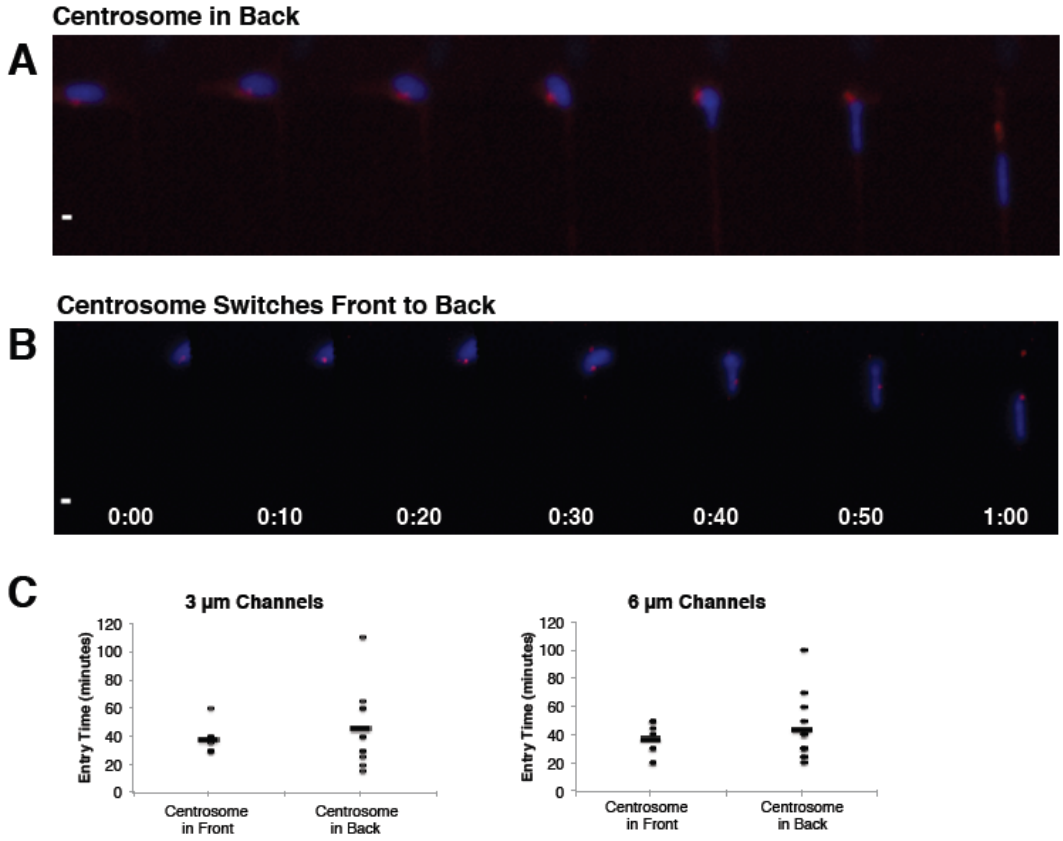

Figure 5.3 Centrosome and nucleus entering the channels. **A** Cell entering the 3 μm channel with centrosome (red) behind the nucleus (blue), scale bar 5 μm, time stamp (hrs:mins). **B** Cell entering the 3 μm channel with centrosome initially leading the nucleus then switching to the back, scale bar 5μm, time stamp (hrs:mins). **C** Plots of the time it takes for the nucleus to enter the channel when the centrosome is in front or behind the nucleus, each tick represents one cell, mean entry time depicted as bold tick. Entry time for 3 μm channels is on the left (n=20, 4 experiments), 6 μm channels is on the right (n=21 cells, 7 experiments), difference between means is non-significant by student's t-test.

Interestingly, the amount of time it took the nucleus to enter the channel was not significantly different depending on the centrosome position or on the width of the channel. It took an average of 41.5 ± 4.9 minutes for the nucleus to enter the 3 μm channel and 40.7 ± 4.3 minutes to enter the 6 μm channel (Figure 5.3C). The centrosome position was also not correlated with the nuclear area. Similarly, the nucleus speed once inside the 6 μm channels did not depend on centrosome position.

5.3.5 Centrosome Position During Changes of Direction

To investigate whether confinement would affect the ability of cells to change direction, the cells were allowed to migrate into the channel. The chemoattractant gradient was then switched (as explained in Figure 5.4A). Cells were able to change directions in both the 6 μm channels and the smaller 3 μm channels. Interestingly, the centrosome also changed positions to maintain its position relative to the nucleus. Figure 5.4B shows the nucleus of a cell that was migrating down in the channel with the centrosome in the back. The chemoattractant gradient was switched and imaging was started. Figure 5.4B shows the nucleus moving up towards the new direction of the chemoattractant and the centrosome moving to behind the nucleus, towards the new back of the cell. It took an average of 88.6 ± 18.6 minutes for the centrosome position to change in the 3 μm channels.

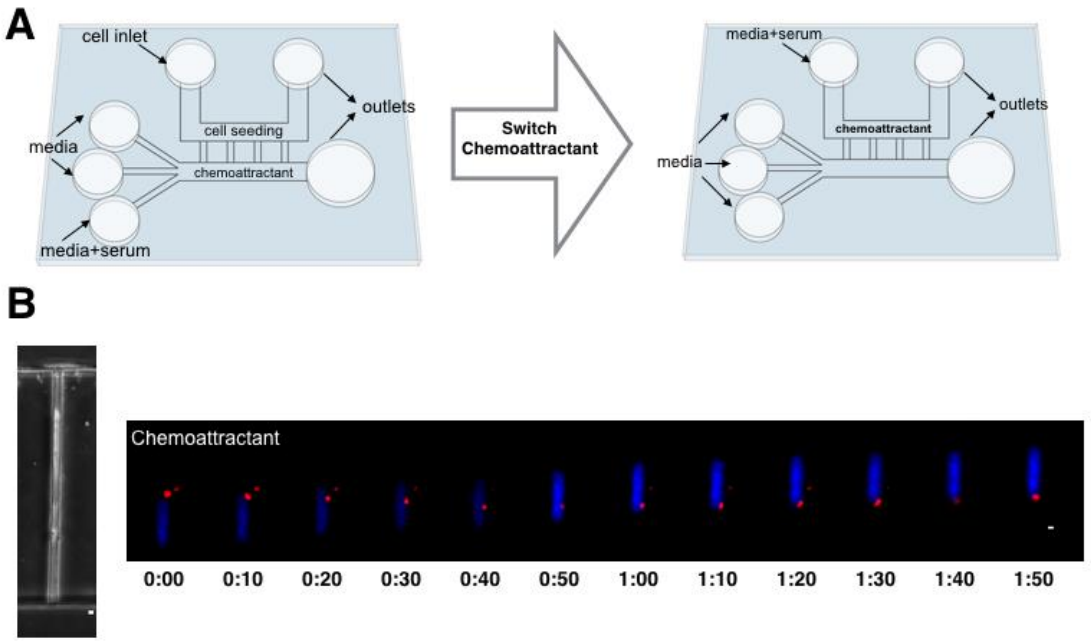

Figure 5.4 Cells repolarize during change of directions in the microchannels. **A** Schematic of how cells were induced to reverse directions by changing which channel contains the media+serum that acts as a chemoattractant. **B** Representative cell after the chemoattractant was switched in a 3μm channel. The centrosome (red) is repositioned towards the new back of the cell, behind the nucleus (blue), scale bar 5 μm, time stamp is the time after the switch (hrs:mins). The channel is shown in brightfield to the left. The image is representative of 7 cells in 3 experiments in the 3μm channel.

Discussion

Chemotaxis is a key step during cancer progression and metastasis. Endothelial cells lining the bloodstream secrete chemoattractant signals that cancer cells sense, prompting their migration away from a primary tumor towards the bloodstream where they travel to distant sites in the body, extravasate, and form secondary tumors [123]. Chemotaxis requires that cells sense a chemoattractant, establish polarity, and then persistently migrate towards the chemoattractant [3], [123]. As described in Chapter 4, for a persistently migrating cell in 2D, the centrosome, a marker of polarity, is found anterior to the nucleus; for a cell migrating in 1D, it is found toward the rear of the cell. Moreover, the centrosome position is

maintained when a cell changes directions on lines. The centrosome position in the confining environment of a microchannel and the ability of cells to repolarize the centrosome in more confined spaces in response to a chemoattractant gradient had not previously been studied.

We found that the position of the centrosome depended on the size of the channel. In channels 3 μm wide x 6 μm high nearly all the cells positioned the centrosome behind the nucleus. In a slightly wider and taller channel, 6 μm wide x 10 μm high, the centrosome was found almost equally in front of as behind the nucleus. It could be that the degree of confinement in the 6 μm channel was not extreme enough to influence the migration of all cells. Other studies with similarly sized channels have seen that cells in these partially confining 6 μm channels sometimes migrate down one side of the channel and have similar migration modes to cells in wider, less constricting channels [44], [120]. In the 3 μm channels, however, the cytoplasm is clearly deformed in the channel (Figure 5.1C) and the speed is slower than in the 6 μm channels and on the 2D glass surface, suggesting that the confinement of the cell is influencing centrosome position. Others have also seen that cells move slower in more confining channels, except for cancer cells which actually migrate with increased speed in smaller channels [124]–[126].

In 2D migration, the centrosome is found less than 4 μm from the edge of the nucleus (Figure 5.2C) and close to the center of the cell [101]. This close proximity between the nucleus and centrosome led to the hypothesis that there might be some linkage between the two [115]. Indeed, the centrosome and the nucleus are connected through the LINC complex [41]. It has been discovered, however, that this tether

must not be rigid, since nuclear rotation in a fibroblast was observed without a similar rotation of the centrosome [110], [116]. Our result that the distance between the centrosome and the nucleus depends on confinement, provides further proof that it must be a flexible link. In the 3 μm channels the average distance between the centrosome and nucleus in a cell was as large as 10.9 μm. Only cells in the 3 μm channels were observed to have this increased distance between the centrosome and nucleus though. This suggests that the increase in distance is the result of confinement, and not simply due to migration in channels, although the exact mechanism and implications on cell and nuclear migration require more study.

Cells entering the microfluidic channels from the seeding channel is a model for how cells enter small spaces, for example, cells moving through pores in the extracellular matrix [4]. We observed significant differences in migration speed and centrosome positioning once cells were inside the channels (Figure 5.2). Surprisingly though, we did not observe significant differences in the time it took for the nucleus to enter the 3 μm channels compared to the 6 μm channels (Figure 5.3C). For cells entering the 3 μm channel, the nucleus does appear to deform (Figure 5.3A-B), even so, the channel may not be small enough to pose a significant restricting obstacle that would slow down nuclear entry. Others have seen similar results, Davidson et al. performed experiments with fibroblasts looking at the transit time of a nucleus through a series of constrictions measuring 2, 3, or 5 μm wide x 5 μm high and saw that the nucleus took significantly longer to move through the 2 x 5μm constrictions but migration through the 3 and 5 μm wide constrictions were similar [35]. Another study looked at a variety of cell types and found that almost all cells were able to

transmigrate through a polycarbonate membrane with a pore diameter of 3 μm but transmigration was nearly arrested at a diameter of 1 μm [37]. These confirm that, like we observed, 3 μm wide spaces require deformation of the nucleus, but do not present a limiting obstacle.

While we observed that cells migrated with the centrosome behind the nucleus in 3 μm channels, the cells did not all enter the channel that way. 45% of cells entered the 3 μm channel with the centrosome in front of the nucleus then switched it to the back (Figure 5.3B). This ratio is similar to cells entering the 6 μm channel where 50% of cells entered with the centrosome in front. However, the cells in the 6 μm channel did not change the centrosome position once inside the channels. We also observed that there is no difference in entry time between cells with the centrosome positioned in front or in back of the nucleus (Figure 5.3C). During nuclear entry, part of the cytoplasm of the cell is still in the unconfined channel and it may be that the cell is still sensing an unconfined environment. Indeed, fibroblasts cells migrating on micropatterns alternating between 1D and 2D migration showed a clear preference for remaining on the larger patterns where they could migrate unconfined [33], [128]. This was also seen for endothelial cells migrating between two different widths of channels, the majority of cells did not move from the 15 μm wide channel to the 4 μm channel [124]. In our case, though, we have a chemoattractant gradient stimulating cells to move into and through the channels. For cells entering the channel with the centrosome in front, it is after the initial transition from 2D to 3D migration that the centrosome is positioned behind the nucleus.

Next, we investigated the ability of cells to change directions under confinement. During chemotaxis in 2D, cells sense a chemoattractant, form a new front by actin polymerization, the cell then repolarizes, and finally, the rear of the cell retracts, leading to cell movement [3], [123]. We were interested in whether cells could repolarize in response to a chemotactic switch when confined in the microchannels. We found that cells were able to reposition the centrosome and switch directions when confined in the 3 μm channels. The centrosome seems to move across the nucleus to the new rear of the cell in these cases (Figure 5.4B). Confocal imaging suggests that the nucleus does not fill the entire height of the channel. Therefore, we expect that the centrosome is moving over the nucleus during repositioning. It would be interesting to investigate more extreme confinement where the nucleus filled the channel to determine the effects on cell migration and whether the cell's potential inability to repolarize could play a limiting role in migration through narrow spaces. With more confining channels, we could also investigate nuclear entry into smaller channels that would require greater nuclear deformation to determine if the centrosome is positioned primarily in the back before entry in this case, or if it takes longer or hinders the cell's ability to enter when the centrosome is positioned in the front.

In conclusion, cells migrating on 2D substrates typically position the centrosome in front of the nucleus. We showed in Chapter 4 that the centrosome position actually depends on the substrate stiffness and confinement and is found towards the back of the cell in the majority of cells migrating under 1D confinement. In this chapter, our results suggest that in the most confining channels of a

microfluidic device the centrosome is also positioned towards the rear of the cell and that this positioning takes place after the cell has entered the channel. Furthermore, the centrosome position is maintained in cells when they switch directions even in the confining channels. Previously, cell polarization and the centrosome position for cells migrating in microfluidic channels had not been investigated. Therefore, these results contribute towards a better understanding of the mechanisms that cells use to move in confined environments.

Chapter 6: Conclusions and Future Work

Cell migration is well understood for cells moving on two-dimensional surfaces like glass or tissue culture plastic dishes. In the body, however, cells encounter a wide variety of microenvironments and their response to these is less understood. Two parameters cells encounter during migration in both healthy processes and in disease are varying stiffnesses of the environment, and geometric confinement. It has been shown that many cell types are mechanosensitive and can adapt their area, cytoskeleton, and speed depending on the substrate stiffness [4], [129]. Similarly, cells respond to the various geometric confinements they encounter in vivo by changing cell shape and using different migration processes [4], [8]. However, the effect of substrate stiffness on macrophages had not been studied nor had the effects of substrate stiffness and confinement on cell polarization, the first step in cell migration. Therefore, the overall objective of this work was to investigate the effects of substrate elasticity and confinement on cell polarization and migration. Below follows a summary of the results presented in this dissertation as well as an exploration of possible future work motivated out of our results.

6.1 Monocotye-derived Macrophages are Mechanosensitive

We first investigated whether monocyte-derived macrophages, a key player in the progression of atherosclerosis [12], are sensitive to the elasticity of their environment. An atherosclerotic plaque progresses through different stages of stiffening and has regions of soft and stiff variability [15]. The response of monocyte-derived macrophages to different stiffness had not been investigated. We let

macrophages adhere and migrate on polyacrylamide gels of varying stiffness and found that macrophages are indeed sensitive to the elasticity of their environment. On soft substrates, macrophages remained rounded while on stiffer substrates macrophages had a larger area and more prominent F-actin stress fibers. Macrophage doubling time was also dependent on substrate stiffness. Macrophages proliferated more quickly on stiffer gels than on soft. Macrophage migration into plaques and their inability to migrate out is a factor in atherosclerosis. Therefore, the migration of macrophages was of specific interest. Macrophage speed was also found to respond to stiffness, with cells moving fastest on stiff 280 kPa gels and slowest on 3 kPa gels.

Future studies could investigate the polarization of macrophages in response to substrate stiffness. Macrophages can polarize into two subsets, classical (M1) and alternative (M2), based on different signaling pathways [130]. Both M2 and M1 macrophages can be found in an atherosclerotic plaque. M2 macrophages, however, are associated with inflammation resolution that is largely absent in atherosclerosis [131]. Moreover, stable plaques are associated with a higher number of M2 macrophages [131]. It has been shown that in addition to signaling molecules, the shape of a cell can also influence macrophage polarization. Macrophages micropatterned into a more elongated shape were polarized towards the M2 phenotype as measured by cytokine production [132]. Based on our results that cells elongate more on stiff substrates, we hypothesize that stiff substrates may also skew macrophage polarization towards the M2 subset. Future experiments could investigate whether soft and stiff substrates influence macrophage polarization.

6.2 Cell Polarization is Affected by Substrate Elasticity

Our results with macrophage migration prompted us to further investigate migration on substrates of different stiffness. We looked specifically at cell polarization, which is the first step of migration and a necessary step for directed migration [3]. The centrosome was used as an indicator for cell polarization, and also because of its role in the cell as the microtubule-organizing center. Here, we found that the centrosome position was only in front of the nucleus, towards the leading edge for cells on stiff substrates: glass and the 280 kPa gel. On a softer gel, it was more often towards the back of the cell indicating that stiffness affects centrosome positioning.

6.3 Future Work with Substrate Stiffness Gradients

It has been shown that fibroblasts are sensitive to gradients of stiffness and will migrate persistently towards stiffer substrates, a process called durotaxis [18], [109]. To further examine centrosome positioning in response to changes in substrate elasticity, future experiments could investigate the centrosome position in cells as they migrate from soft to stiff substrates. We have been able to create polyacrylamide gels that vary from soft to stiff (1 kPa to 280 kPa) (Figure 6.1) and we observed persistent fibroblast migration from the soft towards the stiff substrate.

This system could be used to further investigate the mechanisms of cell polarization. We hypothesize that the centrosome would switch positions as cells moved from soft to stiff. With this gradient gel, that hypothesis could be investigated and different cytoskeletal elements could be perturbed to see their effect on

persistence and centrosome positioning as well. These gradient gels could also be used to investigate macrophage durotaxis since a single plaque has variations in stiffness.

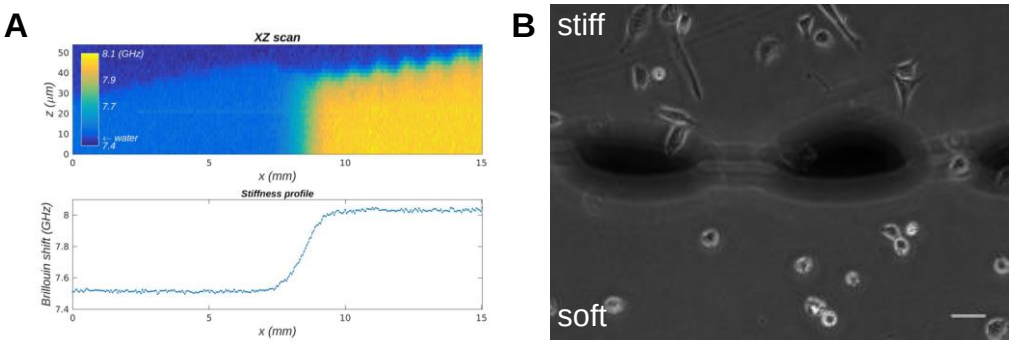

Figure 6.1 A Characterization of gels with a stiffness gradient shows that over a length of 1.5 mm there is a gradual increase in stiffness. Characterization done with Brillouin microscopy by Milos Nikolic in Dr. Giuliano Scarcelli's lab. **B** Fibroblast cells plated on a gel with a stiffness gradient. The dark line indicates where the transition from soft to stiff takes place as indicated by fluorescent micobeads mixed into the stiff gel. Cells are more rounded at first on the soft gel and more elongated on the stiff side of the gel. Scale bar 50 μm.

6.4 Centrosome Position is Maintained by Microtubule Pushing Forces in 1D Migration

After finding that the polarization of the cell is affected by substrate stiffness, we investigated whether confinement, another important microenvironment parameter for cells in the body, could affect centrosome position. We found that the centrosome position was more often behind the nucleus, towards the rear of the cell, as fibroblasts migrated persistently on micropatterned 1D lines. We compared the speed, persistence, and width of cells with their centrosome in front of or behind the nucleus and found that these biophysical parameters were not changed by the position of the centrosome. Furthermore, we found that when microtubule polymerization was perturbed, the centrosome position was not maintained in front of or behind the

nucleus, and was more dynamic. This indicates that microtubule pushing forces are important for centrosome positioning in 1D migration.

6.5 Centrosome is Polarized in Microchannels

We also observed that the centrosome position was maintained when cells changed directions on lines. This result led us to our next study to investigate what happens when the cell is under more extreme confinement where there is less room for the centrosome to be displaced across the nucleus. We used a microfluidic device with channels to investigate whether the centrosome would have a preferred orientation in more extreme 3D confinement. Indeed, centrosome position followed 1D migration and was found towards the back of the cell during migration in the narrowest channels but did not have a preferred orientation during entry into the channels.

6.6 Changing Directions in Confinement

We observed that the centrosome was reoriented to the new back of the cell when cells changed directions in small channels in response to a chemoattractant gradient switch. We believe, from confocal microscopy, that in these 3 μm wide x 6 μm high channels, the nucleus is not filling the entire volume of the channel. If the nucleus were to cover the entire channel, we expect that the cells will not change directions as easily because the centrosome will not be able to reposition without deforming the nucleus in some manner. Future experiments could investigate cells changing directions under more extreme confinement to determine if confinement poses an obstacle to repolarization.

Furthermore, since we found that microtubules are important in centrosome positioning in 1D migration, cytoskeletal drug inhibitors could be used to determine whether microtubule polymerization forces are necessary for centrosome positioning in 3D confinement. Additionally, other in vitro models of confinement could be explored. For example, instead of microfluidic devices, collagen gels could be used as a model of the extracellular matrix that captures the porosity and stiffness of the in vivo environment [28].

6.7 Future Work Investigating Cancer Cells

We chose to use monocyte-derived macrophages in the first aim of the work since we were specifically interested in this cell type's unique response to substrate stiffness in the context of atherosclerosis. In the next aims where we investigated polarity and migration under confinement, we chose to use 3T3 fibroblasts. Fibroblasts have physiological relevance since they must move through tissue to reach wound sites. Another benefit to fibroblasts is that they have been well studied in two-dimensional migration and their migration follows the canonical migration cycle [3].

Future work could investigate centrosome positioning in cancerous cells during confined migration. It has been documented that cancer cells move faster than epithelial cells in small channels [125], [133]. One possible reason is that cancer nuclei are more deformable [130], [131]. But it is also possible that some of the other abnormalities in cancer cells could play a role as well. For instance a few potentially relevant differences in cancer cells are that the LINC complex is disrupted [136] and cancer cells often have centrosome amplification [137], [138]. Future experiments

could investigate how the nucleus and centrosome migrate differently in confinement compared to epithelial cells.

6.8 Conclusions

This dissertation investigated two important parameters that cells confront as they migrate in the body. The first, substrate stiffness is important in both the progression of cancer and atherosclerosis as both of these diseases include a component of changing elasticity. Our finding that monocyte-derived macrophages are mechanosensitive adds to existing knowledge about their behavior in the progression of cardiovascular disease. We also presented our results investigating cell polarization, the first step of directed migration, in response to stiffness and confinement. We found that polarization is sensitive to both of these parameters. This offers further evidence that cells migrating in different geometric environments utilize different mechanisms and suggests that migration under confinement requires more study. These results further the understanding of cell migration in the body by investigating in isolation the specific parameters of stiffness and confinement that cells encounter and understanding their effects on migration and polarization.

Appendices

Appendix A: MATLAB Program for Analyzing Migration and Centrosome Position on Gels and Glass

Program to analyze a cell randomly migrating on a glass or gel substrate to find the position of the centrosome relative to the nucleus and the direction of migration.

How to use:

1. Find nucleus outlines using ImageJ macro (below) for each frame of the timelapse. Save these in a folder.
2. In the same folder save a spreadsheet entitled “cent” with the x and y position of the centrosome (tracked with ImageJ manual tracking plugin) in the D and E columns respectively.
3. Save this program in that folder as well and then run.

```
close all;
clc; clear;


%Import nucleus positions from spline fit
for k=1:1:53
    filename=[num2str(k)];
    data{k}=importdata([filename '.txt']);
end
data=data(1:53);
data=data(1:10);

%Import centrosome positions
centx=xlsread('cent.xlsx',1,'D:D');
centy=xlsread('cent.xlsx',1,'E:E');
centx=centx.*0.6445; %Hsieh microscope, 10x conversion
centy=centy.*0.6445;
centx=centx(1:10);
centy=centy(1:10);

%Flip coordinates from imagej coordinate system
for i=1:length(data)
data{i}(:,2)=660.48-data{i}(:,2);
centy(i)=660.48-centy(i);
end
```

```
c=[centx centy];

%Use center of nucleus not edge for speed, y direction only
 for i=1:length(centx)
       nucymean(i)=mean(data{i}(:,2));
       nucxmean(i)=mean(data{i}(:,1));
 end

%Find minimum distance between nucleus and centrosome
for i=1:100
      for j=1:length(centx)

           dist(i,j)=sqrt([c(j,1)-data{j}(i,1)]^2+[c(j,2)-
      data{j}(i,2)]^2);
    end
end

[r,I]=min(dist);

%Find point on nucleus closest to centrosome
for i=1:length(centx)
    nucx(i)=data{i}(I(i),1);
    nucy(i)=data{i}(I(i),2);
end

%Find speed of centrosome based on x and y movement
for n = 1:(length(centx)-1)
     msdcentxy(n) = (centx(n+1)-centx(n))^2+(centy(n+1)-centy(n))^2;
end

sqrt_msd_centxy=msdcentxy.^(1/2);
vcentxy = sqrt_msd_centxy./20; %20 is interval between    frames
speedcent=mean(vcentxy); %um/min

%Find speed of nucleus based on mean nucleus position
for n = 1:(length(nucx)-1)
      msdnuc(n) = (nucymean(n+1)-nucymean(n))^2 + (nucxmean(n+1) -
      nucxmean(n))^2;
end

sqrt_msdnuc = msdnuc.^(1/2);
vnuc=sqrt_msdnuc./20;
speednuc=mean(vnuc);

figure;
hold on;
for i=1:1:length(data)
     plot(data{i}(:,1),data{i}(:,2),'b')
     plot(c(i,1),c(i,2),'xr')
end
   legend('Nucleus','Centrosome');
  % xlabel('x position (um)')
   ylabel('y position (\mum)')
   xlabel('Time (min)')
      set(gca,'FontSize',14);
```

```
%Find total distance travelled (contour length)
L_cent=sum(sqrt_msd_centxy)
L_nuc=sum(sqrt_msdnuc)

%Find angle between migration vector and centrosome vector
for i=1:length(centx)
    veccent(i,1)=(centx(i)-nucxmean(i));
    veccent(i,2)=(centy(i)-nucymean(i));
end


%Find angle between timepoints (direction of movement)
 for i=1:length(centx)-1
     vecnuc(i,1)=(nucxmean(end)-nucxmean(1));
     vecnuc(i,2)=(nucymean(end)-nucymean(1));
 end

 for i=1:length(centx)-1
      magvecnuc(i)=sqrt(vecnuc(i,1)^2+vecnuc(i,2)^2);
      magveccent(i)=sqrt(veccent(i,1)^2+veccent(i,2)^2);
 end


%Dotproduct of veccent and vecnuc
 for i=1:length(centx)-1
     dotc(i)=dot(veccent(i,:),vecnuc(i,:));
 end

  for i=1:length(centx)-1
       anglec(i)=acosd(dotc(i)/(magvecnuc(i) *  magveccent(i)));
 end

for i=1:length(anglec)
    if anglec(i)<45 %If the direction angle and centrosome position
angle are close, it is towards the front
        centposd(i)=({'F'});
    elseif anglec(i)<180 && anglec(i)>135 %if they are opposite it
is towards the back
        centposd(i)=({'B'});
    else centposd(i)=({'S'}); %otherwise the centrosome is on the
side
    end
end

a=unique(centposd,'stable')
b=cellfun(@(x)sum(ismember(centposd,x)),a,'un',0)

%Find end to end length
E_cent=sqrt((centx(end)-centx(1))^2+(centy(end)-centy(1))^2);
E_nuc=sqrt((nucxmean(end)-nucxmean(1))^2+(nucymean(end)-
nucymean(1))^2);
R_cent=E_cent/L_cent
R_nuc=E_nuc/L_nuc

%Find a "chemotactic index" parameter over time
%Find vector for every other displacement, compare that to
```

```
displacement before
for i=1:length(centx)-2
    vecnucskip(i,1)=nucxmean(i+2)-nucxmean(i);
    vecnucskip(i,2)=nucymean(i+2)-nucymean(i);
end

for i=1:length(vecnucskip)
    magnucskip(i)=sqrt(vecnucskip(i,1)^2+vecnucskip(i,2)^2);
end

for i=1:length(centx)-2
    dotcskip(i)=dot(vecnucskip(i,:),vecnuc(i,:));
end
%Angle close to 0 degrees means vectors pointing in same direction/
persistent
%Angle close to 180 degrees means vectors pointing in opposite
direction
for i=1:length(centx)-2
      angleskip(i)=acosd(dotcskip(i)/(magnucskip(i)*magvecnuc(i)));
end

%Nucleus circularity, C=4*pi*Area/perimeter^2
%Find point on nucleus farthest from center (long axis)
for i=1:100
for j=1:length(nucxmean)
     nuclength(i,j)=sqrt([nucxmean(j)-data{j}(i,1)]^2+[nucymean(j)-
data{j}(i,2)]^2);
    end
end

[nucminor,I]=min(nuclength);
[nucmajor,I]=max(nuclength);

area=pi*nucminor.*nucmajor;
perimeter=2*pi*sqrt((nucminor.^2+nucmajor.^2)/2);
circform=4*pi*area./perimeter.^2;
```

ImageJ Macro to Find the Outline of the Nucleus

```
dir="/Users/Katrina/Desktop/2-14-17 lines/position 3/nucleus
position/cell 1/"
name=getSliceNumber( );
txtPath=dir+name+".txt";
run("Fit Spline");
saveAs("xy Coordinates",dir+name);
run("Next Slice [>]");
```

Appendix B: MATLAB Program to Analyze Cell Migration and Centrosome Position on 1D Lines or in Channels

Program to analyze a cell migrating on a micropatterned 1D line or in a channel. Cell migration direction should be in the y direction.

How to use:

1. Find nucleus outlines using ImageJ macro (in Appendix A) for each frame of the timelapse. Save these in a folder.
2. In the same folder save a spreadsheet entitled “cent” with the x and y position of the centrosome (tracked with ImageJ manual tracking plugin) in the D and E columns respectively.
3. Save this program in that folder as well and then run.

```
close all;
clc; clear;


%Import nucleus outlines from ImageJ spline fit
for k=1:1:29
    filename=[num2str(k)];
    data{k}=importdata([filename '.txt']);
end


%Import cell positions from spline fit in imagej
for k=1:1:29
   filename=sprintf('cell%d.txt',k);
   celldata{k}=importdata([filename]);
end


%Import centrosome positions from Excel spreadsheet with ImageJ
tracking results and convert from pixels to microns
centx=xlsread('cent.xlsx',1,'D:D');
centy=xlsread('cent.xlsx',1,'E:E');
centx=centx.*0.8; %Convert from pixels to µm
centy=centy.*0.8;

c=[centx centy];


%Find center of cell
```

```
 for i=1:length(data)
      cellymean(i)=mean(celldata{i}(:,2));
      cellxmean(i)=mean(celldata{i}(:,1));
 end


%Find center of nucleus
 for i=1:length(data)
      nucymean(i)=mean(data{i}(:,2));
      nucxmean(i)=mean(data{i}(:,1));
 end


%Find minimum distance between nucleus and centrosome
for i=1:100
    for j=1:length(data)
      dist(i,j)=sqrt([c(j,1)-data{j}(i,1)]^2+[c(j,2)-
      data{j}(i,2)]^2);
    end
end

[r,I]=min(dist);


%Find point on nucleus closest to centrosome
for i=1:length(data)
    nucx(i)=data{i}(I(i),1);
    nucy(i)=data{i}(I(i),2);
end


%Find width of the nucleus at each timepoint
 Method: Find similar y points, then subtract x points at
 same y position, Find max difference and call that the
 width at that y position
for k=1:length(data)
 for i=1:100
      pn{i,k}=find(abs(data{k}(:,2)-data{k}(i,2))<1);
   for j=1:length(pn{i,k})
      dist2n{i,k}=abs(data{k}(i,1)-data{k}(pn{i,k}(j),1));
    end
 end
end

dist3n=cell2mat(dist2n);

%Find the widest point of the nucleus at each timepoint
maxdistn=max(dist3n);



%Find the average maximum width for the cell over all timepoints
meanmaxwidthnuc=mean(maxdistn); medianmaxwitdthnuc=median(maxdistn);
stdmaxwidthnuc=std(maxdistn);


%Find the mean width of the nucleus over all timepoints
```

```
meandistnuc=mean(dist3n);
meanwidthnuc=mean(meandistnuc) %mean cell width over all frames
stdevwidthnuc=std(meandistnuc)


%Find the width of the cell at each timepoint
for k=1:length(data)
 for i=1:100
      pncell{i,k}=find(abs(celldata{k}(:,2)-
       celldata{k}(i,2))<1);
   for j=1:length(pncell{i,k})
      dist2cell{i,k}=abs(celldata{k}(i,1)-
       celldata{k}(pncell{i,k}(j),1));
    end
 end
end

dist3cell=cell2mat(dist2cell);

%Find the widest point of the cell at each timepoint
maxdistcell=max(dist3cell);


%Find the mean width of the nucleus over all timepoints
meanmaxwidthcell=mean(maxdistcell);
medianmaxwitdthcell=median(maxdistcell);
stdmaxwidthcell=std(maxdistcell);


%Mean width cell
meandistcell=mean(dist3cell);
meanwidthcell=mean(meandistcell); %mean cell width over all frames
stdevwidthcell=std(meandistcell);


%Find whether the centrosome is on long side or short side of cell
%First, find maximum y position and minimum y position of cell
(furthest points) at each timepoint
for i=1:length(celldata)
      maxcelly(i)=max(celldata{i}(:,2));
      mincelly(i)=min(celldata{i}(:,2));
end


%Then find the distance between each of these and the centrosome
A=abs(centy-mincelly'); %from centrosome to cell edge at top of
image (b/c imagej starts 0 at the top)
B=abs(centy-maxcelly'); %from cent to cell edge near bottom of image

%Find which is larger A or B at each time point and record
for i=1:length(celldata)
    if A(i)>B(i) record(i)=1;
    elseif A(i)<B(i)  record(i)=2;
    end
end
```

```
%How many timepoints have A longer, how many have B longer
counts=hist(record,2)


%Find the difference between top and bottom protrusions to see if
there is a correlation between this and the centrosome position
for i=1:length(celldata)-1
      diffmax(i)=maxcelly(i+1)-maxcelly(i);
      diffmin(i)=mincelly(i+1)-mincelly(i);
      diffcent(i)=centy(i+1)-centy(i);
end


%Find the distance between the center of the cell and centrosome
for i=1:length(celldata)
      distcellcentx(i)=abs(cellxmean(i)-centx(i));
      distcellcenty(i)=abs(cellymean(i)-centy(i));
end


%Find speed of centrosome based on x and y movement
for n = 1:(length(centx)-1)
     msdcentxy(n) = (centx(n+1)-centx(n))^2+(centy(n+1)-centy(n))^2;
end

sqrt_msd_centxy=msdcentxy.^(1/2);
vcentxy = sqrt_msd_centxy./5; %5 min is interval between frames
speedcentxy=mean(vcentxy); %µm/min


%Find speed of centrosome for y direction only
for n = 1:(length(centx)-1)
    msdcent(n) = (centy(n+1)-centy(n))^2;
end
sqrt_msd_cent=msdcent.^(1/2);
vcent = sqrt_msd_cent./5;
speedcent=mean(vcent);


%Find speed of nucleus based on mean nucleus position for y
direction only
for n = 1:(length(nucx)-1)
  msdnucy(n) = (nucymean(n+1)-nucymean(n))^2;
end
sqrt_msdnucy = msdnucy.^(1/2);
vnucy=sqrt_msdnucy./5;
speednucy=mean(vnucy);


%Find speed of nucleus based on mean nucleus position
for n = 1:(length(nucx)-1)
  msdnuc(n) = (nucymean(n+1)-nucymean(n))^2+(nucxmean(n+1)-
  nucxmean(n))^2;
end
sqrt_msdnuc = msdnuc.^(1/2);
vnuc=sqrt_msdnuc./5;
speednuc=mean(vnuc);
```

```
%Find speed of cell xy based on mean cell position
for n = 1:(length(nucx)-1)
  msdcell(n) = (cellymean(n+1)-cellymean(n))^2+(cellxmean(n+1)-
  cellxmean(n))^2;
end
sqrt_msdcell = msdcell.^(1/2);
vcell=sqrt_msdcell./5;
speedcell=mean(vcell);


%Find angle between center of nucleus and centrosome
for i=1:length(centx)
     ang(i)=atan2(nucymean(i)-centy(i),nucxmean(i)-
     centx(i));
 end
  ang=ang*(180/pi);
  meanang=mean(ang)
  stdang=std(ang)


%%Draw gif of nuclear outline and centrosome position
figure;
h=animatedline('Color','k');
r=animatedline('Color','r');
axis([100,200,150,250])
legend('Centrosome','Nucleus')
for k=71:91
addpoints(h,data{k}(:,1),data{k}(:,2))
addpoints(r,c(k,1),c(k,2))
drawnow;
      frame = getframe(1);
      im = frame2im(frame);
       [A,map] = rgb2ind(im,256);
   if k == 1;
      imwrite(A,map,'Plotzoom.gif','gif','Loopcount',inf);
      else
      imwrite(A,map,'Plotzoom.gif','gif','WriteMode','append');
      end
  end
```

Appendix C: Analysis of Salmonella Motility

I used the data analysis procedures I established to analyze bacteria motility in a collaboration project with Dr. Biswas group. Included in this appendix is the published paper I am a co-author on and the MATLAB code I used to analyze the bacteria motility.

Bioactive Extracts from Berry Byproducts on the Pathogenicity of *Salmonella* Typhimurium[§]

C.1 Introduction

Salmonella, a major foodborne enteric pathogen, is among the leading causative agents of acute gastroenteritis in the world. According to the Centers for Disease Control and Prevention (CDC), Salmonella causes one million illnesses, 19,000 hospitalizations and 380 deaths per annum in the US [139]. Raw and undercooked poultry and poultry products are considered one of the major sources of salmonellosis [140]. A number of Salmonella serovars colonize in the poultry gut as normal flora. The ability of Salmonella to adhere to host intestinal epithelial cells plays a primary role in the enteropathogenesis, multiplication and colonization. Therefore, the adherence phase can be considered as a critical control point in early intervention strategies to prevent the colonization of Salmonella in host gut. Important physicochemical and mechanical properties, i.e., auto-aggregation, hydrophobicity, cellular motility are associated with the adhesion ability of bacterial pathogens to the host epithelial cells [141], [142], and these properties eventually lead

[§] Reprinted from *International Journal of Food Microbiology*, vol. 237, S. Salaheen *et al.*, Bioactive extracts from berry byproducts on the pathogenicity of Salmonella Typhimurium, pp. 128–135, Copyright (2016) with permission from Elsevier.

to bacterial colonization followed by invasion. Furthermore, at the initiation of invasion, the pathogenicity island 1 in Salmonella is involved in the process of colonization and invasion through the type III secretion system [143], [144]. The expression of the genes, those regulate the type III secretion system, are involved in completion of invasion, intracellular survival and multiplication, is induced by the transcriptional regulator proteins such as HilA, HilC, HilD, InvA, InvC, InvF, SirA, and SirB [145], [146]. These phases of activities should be considered in the quest of intervention strategies to reduce the colonization of Salmonella in poultry gut with the ultimate goal to prevent Salmonella cross-contamination in poultry products and reduce the Salmonella associated foodborne infections in humans.

Commonly used control measures against the colonization of Salmonella in poultry gut include the use of antibiotics, synbiotics, and bacteriophages in feed and water. However, development of antibiotic resistance, low efficacy of synbiotics, and high strain specificity of bacteriophages render these control measures tricky. In response to increased public health concern on antibiotic resistance, the U.S. Food and Drug Administration has announced to gradually withdraw non-therapeutic use of antibiotics from farm animal production [147]. Consequently, the search for alternative natural and green antimicrobials is now more essential than ever. Bioactive phenolics from berries, especially blackberry (*Rubus fruticosus*) and blueberry (*Vaccinium corymbosum*) pomace as feed or water supplements to reduce pre-harvest levels of Salmonella contamination in farm animals, specifically poultry, might be a feasible alternative. Antimicrobial effects of phenolics present in berry fruits and their pomaces against enteric bacterial pathogens have been extensively

studied [148]–[151]. In our previous studies, we showed the bactericidal effect of phenolic extracts from berry fruits on Campylobacter jejuni, Salmonella Gallinarum, Salmonella Pullorum, and Pasteurella multocida [150], [152], [153]. Proposed mechanisms of pathogen inhibition of these phenolics include damage of bacterial cell membrane [154], inhibition of extracellular microbial enzymes [155], distortion of microbial metabolism, and deprivation of substrates mandatory for microbial cell proliferation and pathogenicity [149]. Importantly, synergisms among various phenolic derivatives act indiscriminately against benign and pathogenic bacteria.

Therefore, in this study we aimed to evaluate the phenotypic and genotypic changes of Salmonella exposed to lethal and sub-lethal concentrations (SLC_{2LOG}) of blackberry and blueberry pomace extracts in vitro. We also investigated the effect of these extracts on the natural colonization of Salmonella in chick cecum. Findings from this study will provide significant insight into the alternative preventive and therapeutic antimicrobial regime to reduce Salmonella infection by developing a new, effective, and green antimicrobial against bacterial infections.

C.2 Materials and Methods

C.2.1. Preparation of Pomace Extracts and HPLC-Tandem Mass Spectrometry (LC-MS/MS) Analysis

Extracts were prepared according to the protocol previously described [150]. Total phenolic content in each extract was determined using spectrophotometric method [156]. Total phenolic content was expressed as Gallic Acid Equivalent (GAE). The pH values of the crude extracts were 4.5–5 and pH varied depending on the treatment concentration. A phenolic screen was accomplished using HPLC-MS [157]. Sample injections were 5 μL and separations were performed on an Agilent

1100 system, coupled to an Agilent MSD-TOF (time-of-flight) mass spectrometer. Reversed phase liquid chromatography was used to separate the samples. A Waters Atlantis T3 column (3 μm, 150 x 2.1 mm i.d.) was used. A binary mobile phase consisting of solvent systems A and B was used in gradient elution where A was 0.1% formic acid (v/v) in ddH2O and B was 0.1% formic acid (v/v) in acetonitrile. Mobile phase flow rate was 0.3 mL/ min. The linear gradient was as follows: time 0–1 min, 0% B; time 40 min, 90% B; time 41 min, 90% B; time 42 min, 0% B; time 52 min, 0% B. Following the separation, the column effluent was introduced by electrospray ionization (ESI) into the MSD-TOF. Samples were assayed, using positive mode ESI. Source parameters were: gas temperature 350 °C, gas flow 9 L/min, nebulizer 35 psi, fragmentor 125 V, capillary voltage 3500 V. Data was acquired with a mass range of 75–1000 m/ z. Accurate mass accuracy was guaranteed by the continuous infusion of Agilent Reference Mass Solution (G1969-85001). Individual chromatographic peaks were identified using Agilent's Mass Hunter Qualitative Analysis software (v. B.06). Compounds were identified using Agilent's Mass Profiler Professional software (v. 13.1). Peaks in duplicate injections were aligned to account for instrumental drifts in retention time and mass. Compounds were retained only if they appeared in both duplicate samples. Compounds were annotated by querying Agilent's METLIN human metabolite database, with a mass error criteria of 5< ppm.

C.2.2. Bacterial Strain and Antimicrobial Susceptibility Assay

Salmonella enterica serovar Typhimurium (ST, ATCC 14028) was used in the current study for in vitro assays. Minimum Inhibitory Concentration (MIC) was

determined using broth micro-dilution method described previously [150]. The lowest concentration that caused a significant reduction compared to the control (>3-logs, 99.9%) was considered as Minimum Bactericidal Concentration (MBC). MBC:MIC ratio was also determined which illustrates a relationship between in vitro MBC and MIC of any drug against specific pathogen. If the value is <2, the drug is considered to be bactericidal against that pathogen; if this ratio exceeds 16 the drug is considered bacteriostatic and the ratio is >32, the pathogen is regarded as tolerant to that drug [158], [159].

The antimicrobial activity patterns were determined by a concentration- kill curve of ST (5x 10^5 CFU/mL each) cultured in Luria Bertani (LB, Himedia, India) broth containing different concentrations (0 to 2.0 mg GAE/mL) of blackberry (Blk) and blueberry (Blb) pomace extracts and their 1:1 combination (BPE) at 37 °C for 18 h. The broth containing 0 mg GAE/mL extract was considered as a control. Growth inhibition assay was carried out in triplicate. The dose-response curves were analyzed using the Nonlinear Curve Fitting Function of Microcal Origin 7.5 (Microcal Software Inc., Northampton, MA) and we determined that the sublethal concentration (SLC_{2LOG}) at which microbial numbers were lesser by a factor of ~2 logs compared with the control [160]. The SLC_{2LOG} values were 1.35 mg GAE/mL for all of the extracts (Blk, Blb, and BPE) against ST, and this concentration was used to induce sublethal stress condition in the future assays.

C.2.3. Physicochemical Properties of ST Treated with Berry Pomace Extracts

Physicochemical properties, e.g., cell surface hydrophobicity, autoaggregation, injured cell rate, and swimming and swarming motility, were

evaluated following the methodologies previously described [160]–[162]. All the tests were carried out with 3 technical and 3 biological replicates. The bacterial cells were grown in LB broth in absence (no treatment) and predetermined SLC_{2LOG} of Blk, Blb, and BPE at 37°C for 18 h. The ST cells were harvested by centrifuging at 3000xg for 20 min followed by hydrophobicity, auto-aggregation, and injured cell rate assays. For motility assay, OD600 of ST suspension was adjusted to 0.10. Two microliters of the bacterial suspension was stabbed onto 0.45% (swarming motility) or 0.25% (swimming motility) Muller Hinton (MH, Himedia, India) agar containing SLC_{2LOG} of Blk, Blb, and BPE. The plates were incubated at 37°C for 24–48 h. For microscopic analysis of ST motility, OD600 of ST suspension was adjusted to 0.1 in PBS followed by inclusion of SLC_{2LOG} of BPE into the bacterial suspension and incubation at 37°C for 5 min and 60 min. Cells were imaged with pictures taken every 0.25 s over 2 min with time-lapse microscopy at 37°C with an Olympus IX71 microscope. The resulting movies were analyzed using the TrackMate plugin for Fiji software (http://fiji.sc/TrackMate). A custom MATLAB code (MathWorks, MA) was used to calculate the velocities of the cells based on the mean-squared displacement and to plot the resulting histograms.

C.2.4. Adhesion and Invasion Assay

Adhesion and invasion assays were performed after pre-treatment and post-treatment of ST with Blk, Blb, and BPE, according to the method described previously [150]. For pre-treatment, the bacterial cells were grown in LB broth in absence (no treatment) and SLC_{2LOG} of Blk, Blb, and BPE at 37 °C for 18 h. 100 μL of these bacterial suspensions, containing CFU approximately 100 times higher than

host (INT407, HD11, and DF1) cell number, was inoculated into triplicate wells (technical replicates) of a 24-well tissue culture plate (Greiner Bio-One CellStar, NC). For post-treatment, 100 μL of bacterial suspensions was inoculated into triplicate wells of a 24-well tissue culture plate containing semi-confluent monolayers of host cells covered with DMEM with 10% Fetal Bovine Serum (FBS) and SLC_{2LOG} of Blk, Blb, and BPE, respectively, to a final volume of 1mL. Adhesion and invasion assay was carried out with 3 biological replicates.

C.2.5. Quantitative RT-PCR Assay

The cells were grown in LB broth in the absence (control) or presence (test) of SLC_{2LOG} of Blk, Blb, and BPE at 37°C for 18 h. Then the bacterial cells were harvested and RNA extraction was carried out, followed by cDNA synthesis and qRT-PCR was performed in Eco™ (Illumina, CA) according to the protocol previously described [150]. PCR cycle was: 95°C for 30 s, followed by 40 cycles of 95°C for 5 s, 55°C for 15 s, and 72°C for 10 s. The custom-synthesized oligonucleotides (Erofins MWG Operon; Huntsville, AL) were used as primers to target conserved regions of ST (Table C.1). The relative expression levels of genes were calculated by the comparative method [163]. The housekeeping gene, 50S rRNA, was used as the reference gene for normalization of target gene expression. Quantitative RT-PCR assay was carried out in triplicate.

Table C.1 Molecular functions and primer sequences of target genes used in qRT-PCR analysis for S. Tymphimurium.

Function/protein	Gene	Primer sequences (5′-3′)	Accession no.
50S ribosomal protein L5	50S rRNA	F: GTAGTACGATGGCGAAACTGC R: CTTCTCGACCCGAGGGACTT	M36266
Invasion protein regulator	*hilA*	F: AATGGTCACAGGCTGAGGTG R: ACATCGTCGCGACTTGTGAA	U25352
Invasion regulatory protein	*hilC*	F: TATGGTGTAGAAAAAAGTCGCATCA R: ATCCGCTCTACCTTCTTTAGTGTCA	AF134856
Invasion protein	*invA*	F: CGCGCTTGATGAGCTTTACC R: CTCGTAATTCGCCGCCATTG	U43237
Type III secretion system ATPase	*invC*	F: GCTGACGCTTATCGCAACTG R: GGCGGTGCGACATCAATAAC	U08279
Invasion regulatory protein	*invF*	F: TCGCCAAACGTCACGTAGAA R: CATCCCGTGTATAACCCCCG	U08280
Transcriptional regulator	*sirA*	F: TCCAGCTACTTTCGCAGCAA R: AACACGTTGTAACGCGGTTG	U88651
Transcription factor	*sirB*	F: AGGCGCGTTTTATCGCTTTC R: CCAGACTGACCAGACGTTCC	AF134855

C.2.6. Biofilm Formation Assay

The ability of ST to form biofilms on glass surfaces in the absence and presence of SLC_{2LOG} of BPE was determined. ST was inoculated at approximately $5x10^5$ CFU/mL in triplicate wells of 6-well plates (Corning, NY) containing 22 x 22 mm^2 glass slides and LB broth (control) or LB broth with SLC_{2LOG} of BPE and incubated for 24, 48, and 72 h without shaking at 37°C. After each time point, the glass slides were rinsed with PBS five times and ST cells were recovered using sterile cell scraper (VWR, PA) from the glass surface. Planktonic cells (culture from overlaying broth) and bio-filmed cells (scraped from glass slides) were serially diluted and plated on LB agar for enumeration.

C.2.7. Natural Colonization of Chicks with Salmonella

Natural colonization of Salmonella in chick model provided with various concentrations of BPE was determined. One hundred 1-day-old Cobb-500 broiler chicks were obtained from Longenecker's Hatchery Inc., PA. They were assigned into four groups of 25 chicks each in floor pans, using a Completely Randomized Design. Chicks were provided with commercially available crumbles (Purina Animal

Nutrition, MO) with no antibiotic supplementation and this way the chicks were raised for seven weeks. After three weeks, five chicks from each group were euthanized to check the natural colonization level of Salmonella in chick cecum. After 3 weeks, BPE supplementation in water was started; group A was provided with only tap water, whereas group B, group C, and group D were provided with tap water with 0.1, 0.5, and 1.0 g GAE/L of BPE, respectively. After seven weeks, all the birds were euthanized and ceca were separated. To check the Salmonella colonization, approximately 200 g of cecum content was homogenized in 1 mL PBS, serially diluted and plated on Xylose Lysine Deoxycholate (XLD) agar for enumeration. Three representative presumptive isolates from each group were tested with Salmonella specific PCR according to the protocol described by Peng et al. [157]. Cecum from each bird was considered an experimental unit for statistical analysis. The number of birds colonized by Salmonella was compared using Fisher's exact test. Differences in the level of colonization (CFUs/g cecum content) were compared by first ranking the data and performing one-way analysis of variance (ANOVA) on the ranked data. Comparison of mean ranks was performed using Tukey's test.

C.2.8. Statistical Analysis

All data were analyzed using the Statistical Analysis System software (SAS, Institute Inc., Cary, NC, USA). One-way analysis of variance (ANOVA) was used, followed by Tukey's test to determine significant differences among treatments at $p<0.05$.

C.3 Results

C.3.1. Total Phenolic Contents and Component Analysis of Berry Pomace Extracts

We re-suspended the dried phenolic powder in 10% v/v ethanol and measured the total phenolic content for Blk, and Blb. The concentrations of the stock solutions were adjusted to 6–8 mg GAE/mL in both Blk and Blb. HPLC-MS analysis of these crude extracts showed the presence of a wide variety of components. In the positive ionization mode, 1638 and 1103 compounds were detected in Blk and Blb, respectively. Among these compounds, we found 985 and 605 unique compounds in Blk and Blb, respectively. Major compounds in Blk and Blb included, but not limited to, flavan, flavanone, flavones, glucuronides, glucosides, quinolones, catechol, coumarin, phenols, luteolines, tannins, quercetin, chlorogenic acid, ellagic acid, gallic acid, and xanthoxic acid. Wide structural variability in the phenolic derivatives was observed depending of their presence in Blk or Blb.

C.3.2. Inhibition of ST Growth with Pomace Extracts

The effects of Blk, Blb, and BPE on ST growth are shown in Table C.2. We found that the MIC of both Blk and Blb was 1.5 mg GAE/mL on ST, whereas MIC of BPE was 1.4 mg GAE/mL. However, the MBC was 1.7 mg GAE/mL for all Blk, Blb, and BPE. MBC:MIC ratio values were <2 for all the extracts indicating their bactericidal nature. The antimicrobial activity patterns with a concentration-kill curve of ST showed that the growth of ST was reduced by less than two logs in the presence of 1.35mg GAE/mL of Blk, Blb, and BPE, compared to the control. So, we used 1.35 mg GAE/mL of Blk, Blb, and BPE to induce sub-lethal stress condition to ST for further assays.

Table C.2 Antibacterial effect of blackberry and blueberry pomace extracts on S. Tymphimurium.

Treatment	MIC (mg/mL GAE)	MBC (mg/mL GAE)	MBC/MIC	Bactericidal/bacteriostatic
Blk	1.5	1.7	1.13	Bactericidal
Blb	1.5	1.7	1.13	Bactericidal
1:1 Blk Blb	1.4	1.7	1.21	Bactericidal

Abbreviations: MIC, Minimum Inhibitory Concentration; MBC, Minimum Bactericidal Concentration; GAE, Gallic Acid Equivalent; Blk, blackberry pomace extract; Blb, blueberry pomace extract.

C.3.3. Alteration of Physicochemical Properties of ST in the Presence of Berry Pomace Extracts

The effects of the SLC_{2LOG} of Blk, Blb, and BPE on the physicochemical properties, e.g., hydrophobicity, auto-aggregation, injured cell rate, swimming motility, and swarming motility have been presented in Table C.3. In the presence of SLC_{2LOG} of Blk, Blb, and BPE, auto-aggregation capability of ST decreased significantly. Untreated bacterial cells showed higher auto-aggregation, approximately 12% whereas in presence of Blk, Blb, and BPE the values were reduced to 5, 3, and 6% ($p<0.05$), respectively.

Table C.3 Physiochemical properties and mechanical behaviors of S. Tymphimurium treated with blackberry (Blk), blueberry (Blb) pomace extracts and 1:1 combination (BPE).

Treatments	Auto-aggregation (%)	Hydrophobicity (%)	Swimming motility (%)	Swarming motility (%)	Injured cell (%)
Control	$12 \pm 4^{\ddagger, a}$	18 ± 4^{a}	$100^{A, a}$	$100^{A, a}$	26 ± 4^{a}
Blk	5 ± 1^{b}	8 ± 5^{b}	41 ± 4^{b}	47 ± 7^{b}	54 ± 3^{b}
Blb	3 ± 4^{b}	1 ± 1^{c}	41 ± 3^{b}	43 ± 3^{b}	49 ± 9^{b}
BPE	7 ± 2^{b}	4 ± 2^{b}	40 ± 2^{b}	26 ± 2^{c}	49 ± 9^{b}

‡ Means with different letters within an individual column (a–c) are significantly different at $p < 0.05$.
A Motility values are normalized to untreated control (100%).

Alteration in auto-aggregation capacity of ST did not show significant dependence on any specific extract. (See Table C.3).

Cell surface hydrophobicity of ST was also decreased due to treatment with all the extracts. Hydrophobicity of ST was found to be in the untreated control which significantly reduced to 8, 1, and 4% after treatments with SLC_{2LOG} of Blk, Blb, and BPE, respectively. Unlike auto-aggregation, cell surface hydrophobicity of ST showed significant dependence ($p<0.05$) on the type of extract, i.e., Blb treatment

resulted in significantly lower hydrophobicity in ST compared to Blk or BPE. The Blk, Blb, and BPE-induced cell injury has been presented in Table C.3. The rates of injured ST cells were significantly increased, ranging from 49 to 54% by the treatment with SLC_{2LOG} of Blk, Blb, and BPE. However, alteration in injured cell rate was not significantly dependent on whether Blk, Blb, or BPE was used as treatment.

C.3.4. Soft-agar and Microscopic Analysis of the Motility of ST in the Presence of Berry Pomace Extracts

The motility phenotypes of ST treated with berry pomace extracts were examined through solid-based movement (swarming motility) and liquid-based movement (swimming motility) on semi-solid agar plates containing SLC_{2LOG} of Blk, Blb, and BPE (Table C.3). The motility of the control (no treatment) was considered 100%. All the extracts, Blk, Blb, and BPE reduced bacterial migration to a range of 25–47%. We found that BPE reduced the swimming motility of ST more effectively (75% reduction) than Blk and Blb, which resulted in 53% and 58% reductions, respectively. For swarming motility, all three treatments reduced the motility of ST by 58 to 60% with no significant variation among treatments.

Microscopic analysis of ST motility indicated that the mean velocities of ST at 0, 5, and 60 min of treatment with SLC_{2LOG} of BPE were 88, 44, and 20 μm/min, respectively (Table C.4). Large populations of ST with 5 and 60 min of BPE treatment (64 and 71% detected cells, respectively) showed lower velocity (0–20 μm/min) whereas a large number of cells (64% of detected cells) without treatment had high velocity between 80 and 140 μm/min. We also determined the contour path length, i.e., the total distance the cell travels. ST in the absence of BPE had an average longer contour path than ST treated with BPE for 5 and 60 min. On an

average 57, 23, and 19% of tracked ST cells travelled >50 μm in the presence of BPE after 0, 5, and 60 min, respectively.

Table C.4 Analysis of motility pattern in ST treated with SLC_{2LOG} of BPE.

Motility parameters	BPE 0 min	BPE 5 min	BPE 60 min	*p*-Value
Contour path length (μm)	99 ± 5[1,a]	38 ± 3[b]	27 ± 2[c]	<0.001
% detected cells: contour path > 50 μm	57[2]	23	19	
% detected cells: velocity 0–20 μm/min	22	64	71	
% detected cells: velocity 80–160 μm/min	64	25	10	
Overall velocity (μm/min)	88 ± 4[a]	44 ± 4[b]	20 ± 2[c]	
Velocity (μm/min): contour path > 50 μm	118 ± 5[a]	118 ± 5[a]	66 ± 6[b]	

[1] Values indicate Mean ± Standard Error; means with different letters within an individual row (a–c) are significantly different at $p < 0.001$.
[2] Statistical analysis: % detected cells were analyzed with Chi-square test; path length and velocity were analyzed with one way ANOVA.

C.3.5. Role of Berry Pomace Extracts on Host Cell-ST Interactions

Association and invasiveness of ST to intestinal epithelial cell (INT407), chicken macrophage cell (HD11) and chicken fibroblast cell (DF1) have been presented in Fig. C.1.

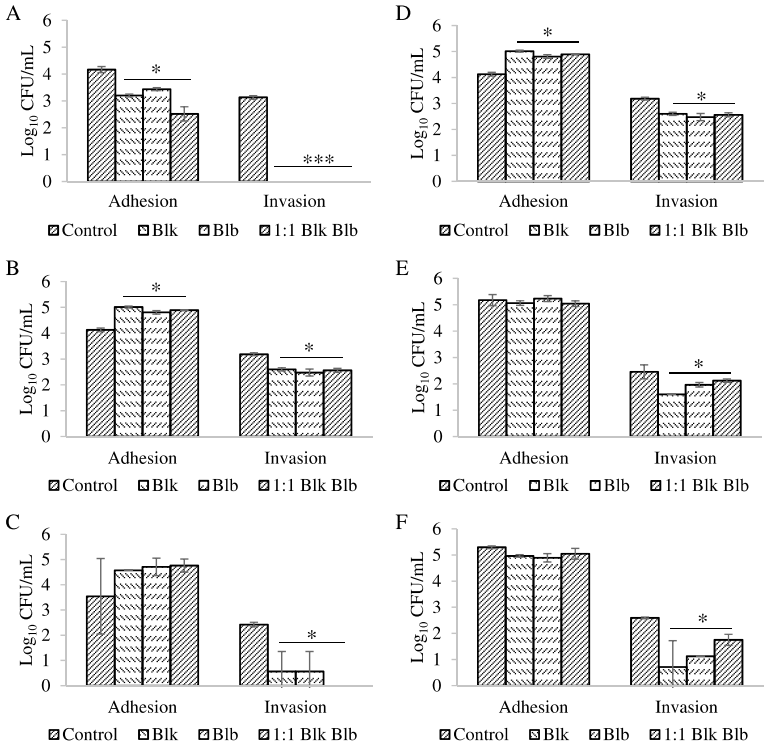

Figure C.1 Adhesion and invasiveness of ST to INT407 (Pre-treatment: A & Post-treatment: B), HD11 (Pre-treatment: C & Post-treatment: D) and DF1 (Pre-treatment: E & Post-treatment: F) respectively in the presence of blackberry (blk), blueberry (Blb) pomace extracts and their 1:1 combination.

After pre-treatment of ST with SLC_{2LOG} of Blk, Blb, and BPE, association to INT407 was reduced by 1– 1.5 logs, association to HD11was increased by 0.5–1.0 log, and no statistical difference was observed in DF1 cells. Only treatment specific difference in association was observed in INT407 cells, where BPE caused significant reduction in the association of ST compared to Blk or Blb. Invasion of ST was reduced significantly regardless of host-cell type due to pre-treatment with SLC_{2LOG} of Blk, Blb, and BPE. All the three treatments inhibited the invasion of ST into INT407 cells completely and reduced the invasion into HD11 and DF1 cells by 0–1.5 logs and 0.5–1.0 log, respectively.

After post-treatment, where the SLC_{2LOG} of Blk, Blb, and BPE were present during the infection period of 1 h, association to INT407 and HD11 cells was increased by 0.5–1.0 logs, and no statistical difference was observed in DF1 cells. Invasion of ST was reduced significantly regardless of host-cell type due to post-treatment with SLC2LOG of Blk, Blb, and BPE. All the three treatments reduced the invasion of ST into INT407, HD11, and DF1 cells by 0.25–0.5, 0.25–0.5, and 0.5–2.0 logs, respectively.

C.3.6. Differential Gene Expression of ST Grown in Presence of Berry Pomace Extracts

The relative expression patterns of Salmonella Type III secretion system associated genes responsible for bacterial invasion were examined in ST treated with SLC_{2LOG} of Blk, Blb, and BPE (Fig. C.2). The transcript levels of all the genes tested, i.e., *hilA, hilC, invA, invF, sirA,* and *sirB,* were declined except one (*invC*) in ST with Blk, Blb, and BPE treatments. The relative expression level of *invC* gene was

increased by more than two-fold in ST with SLC_{2LOG} of Blk treatment only, but no change due to treatment with Blb or BPE. All the other genes, *hilA*, *hilC*, *invA*, *invF*, *sirA*, and *sirB* were down-regulated by ~7, 5, 8, 9, and 6 fold, respectively. No significant treatment-specific differences in expression level of these genes were observed in this study.

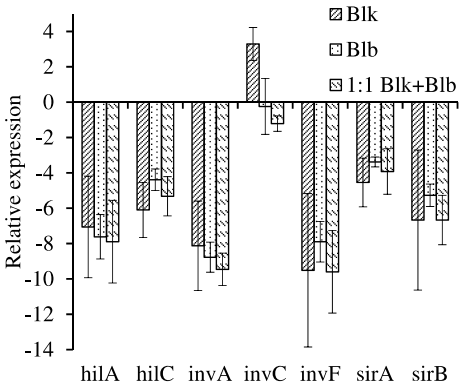

Figure C.2 Relative expression of virulence genes of ST treated with SLC_{2LOG} of blackberry (Blk), blueberry (Blb) pomace extracts and their 1:1 combination.

C.3.7. Growth of Planktonic Cells and Biofilm Formation by ST in Presence of Berry Pomace Extracts

The growth of ST in planktonic state and formation of biofilm in presence of SLC_{2LOG} of BPE have been presented in Fig. C.3. In the presence of BPE, biofilm formation by ST was significantly lower compared to the control (without BPE) after 24 h. However, after 48 h, biofilm formation in presence or absence of BPE became similar and after 72 h, biofilm formation by ST was significantly higher ($p < 0.05$) in the presence of BPE compared to the control. The growth of ST under planktonic state was also altered in presence of SLC_{2LOG} of BPE after 24 h, which showed ~2.0 log reduced growth in presence of BPE compared to the control. However, the CFU of ST in presence or absence of BPE was equilibrated after 48 and 72 h.

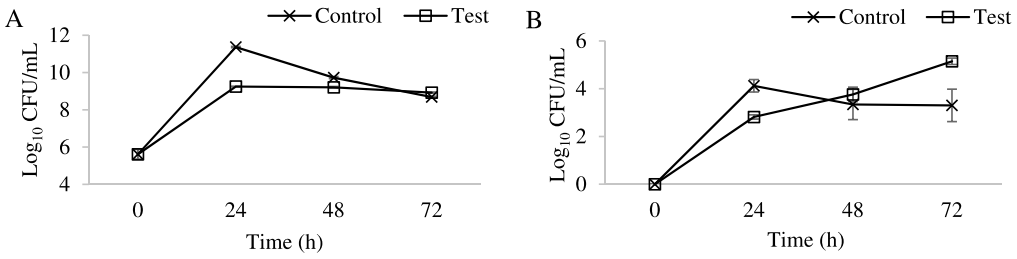

Figure C.3 ST planktonic cell growth (A) and biofilm formation (B) on glass slides in the presence of SLC_{2LOG} of BPE.

C.3.8. Colonization of Chicks with Salmonella

We tested the natural colonization of chicks with Salmonella when provided with 0–1.0 g GAE/L of BPE as water supplement. We checked the natural colonization level by euthanizing five chicks from each of the four groups after three weeks. 100% of the euthanized chicks were naturally colonized with Salmonella after three weeks in groups A, B, and C but 20% chicks in group D, given 0–1.0 g GAE/L of BPE as water supplement (Fig. C.4A). After seven weeks, all the chicks were euthanized. Salmonella was present in 55, 57.89, 50, and 25% chicks from group A, B, C, and D, respectively. The observed median level of colonization of the cecum contents by Salmonella was three logs lower ($p<0.001$) in groups C and D (provided with 0.5 and 1.0 g GAE/L of BPE, respectively) than group A (0 g GAE/L BPE). These two concentrations, 0.5 and 1.0 g GAE/L, of BPE did not show any significant effect on the growth performance and behavior of the chicks.

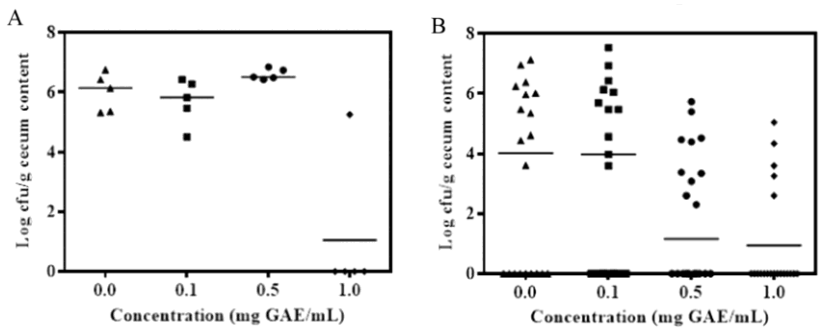

Figure C.4 Natural colonization of Salmonella in chick cecum after three weeks (A) and seven weeks (B). Each dot indicates Salmonella CFU per g of cecum content from one chick and the horizontal bars indicate median value in each group.

C.4 Discussion

Since berries, specifically blackberry and blueberry as well as their pomaces, are rich sources of phenolic compounds [149], [164], and berry pomaces are abundant from the fruit juice industry in the US, berry pomaces are a plausible and economic raw material for extraction of phenolic extracts and can be used in the biomedical sector as well as farm animal production. HPLC/ high mass accuracy TOF mass spectrometry analysis indicated that major phenolic compounds in both Blk and Blb pomaces included, flavan, flavanone, flavones, glucuronides, glucosides, quinolones, catechol, coumarin, phenols, luteolines, tannins, quercetin, chlorogenic acid, ellagic acid, gallic acid, and xanthoxic acid. This finding remains consistent with previous literature which also reported the presence of these compounds in berries [149], [164], [165] though structural and categorical diversity can be noticed among the phenolic compounds. Factors influencing this diversity include, but are not limited to, species and genetic makeup of berries, agricultural practices, season of harvest, irrigation, soil constituent, types of fertilizers used, processing during juice extraction, and storage of the pomaces. A literature survey demonstrates that crude extracts show better antimicrobial efficacy compared to individual compounds [166] and we also

found that combined mixture of commercially available quercetin, gallic acid, teichoic acid, catechol, and coumaric acid had lower MIC value on Salmonella and Campylobacter compared to each of the individual compounds (data not shown). Due to the reported synergism among various types of phenolic compounds, the use of crude extract instead of purified compounds is justifiable.

After a series of studies on the effect of phenolic extracts from berry pomaces on pathogenic bacteria and probiotics [150]–[153], in this study, we present the bactericidal effect of these extracts against pathogenesis and colonization of Salmonella in chicken gut. However, this does not deny the bacteriostatic nature that was noticed from the use of sublethal concentrations of these phenolic extracts that showed growth inhibition after 24 h but revealed reduced or no effect after longer period of exposure. This finding agrees with Puupponen-Pimiä et al. who also reported that raspberry and cloudberry phenolic extracts inhibited growth of Salmonella at the beginning of the incubation but regrowth occurred after prolonged incubation [149]. The mechanism behind the inhibition of Salmonella did not solely depend on pH. Depending on the concentration of berry pomace extracts, pH of the solution ranged from 4.5 to 6.5; whereas Salmonella can withstand over a range of pH values from 3.8 to 9.5 [167]. The number of injured (but still viable) Salmonella cells doubled after treatment with sublethal concentration of berry pomace extracts in a batch culture, hence the exhaustion of phenolic compounds from the system or stress response in Salmonella or both contributed in the lower efficacy of berry pomace extracts after prolonged period of time.

Auto-aggregation and cell surface hydrophobicity are two major physicochemical surface properties of pathogenic bacteria. In several Gram-negative bacteria, auto-aggregation capacity serves as virulence marker [168], [169]. Hydrophobicity is another important cell surface physicochemical property. Cell surface hydrophobicity and auto-aggregation were reported to be positively correlated to bacterial association to the host cells [142]. We found that due to treatment with sublethal concentration of berry pomace extracts, auto-aggregation and cell surface hydrophobicity in Salmonella decreased significantly, while in a similar study on *Campylobacter jejuni*, we found decreased auto-aggregation and increased hydrophobicity [150]. This might be the result of specific alterations of the distribution and proportions of cell surface-associated proteins and polysaccharides that act as the mediators in the aggregation process Schachtsiek et al. and Wang et al. reported that the presence of protein could result in higher hydrophobicity, whereas a more hydrophilic surface is associated with the presence of polysaccharides [170], [171]. Previously Nohynek et al. showed that phenolic extracts disintegrated and altered the permeability of the outer membrane (OM) of Salmonella while addition of $MgCl_2$ abolished the majority of the OM-disintegrating activity of phenolic extracts which suggests chelation of divalent cations from the OM may be another mechanism of OM disintegration [164].

Sublethal concentrations of berry pomace extracts also reduced the liquid-based movement (swimming motility) and solid-based movement (swarming motility) of Salmonella on semi-solid agar plate. Partial immobilization in Salmonella was also reported after treatment with cloudberry, strawberry, and bilberry extracts

[164]. Swimming motility mediated by flagella is mainly involved in bacterial translocation to evade the host immune system [172] whereas the surface-associated swarming motility is important in bacterial colonization [173]. Reduced motility was also observed in Campylobacter when treated with berry pomace extracts [150]. The decrease in swimming and swarming motility bears evidence for the potential role of berry pomace extracts to alter bacterial attachment and invasiveness into host cells.

Attachment is the prerequisite for Salmonella colonization on intestinal epithelial cells followed by invasiveness, which are considered to be important virulence properties. Association of Salmonella to cultured host cells, e.g., intestinal epithelial INT407, chick macrophage HD11, and chick fibroblast DF1 was altered; decreased association to INT407, increased association to HD11, and association remained unchanged in DF1 cells, after treatment with sublethal concentration of berry pomace extracts. Altered OM protein profile in Salmonella can be a probable cause of increased associated bacterial number to HD11 cells. Hydrophobicity and surface charge of bacterial cells play an important role in the adhesion process as demonstrated previously [174]. In the present case, the extent of adhesion seems to be directly related with cell surface hydrophobicity of Salmonella. Unlike association, treatment with sublethal concentration of berry pomace extract significantly reduced Salmonella invasion into all the host cell types. Alteration of mechanical and physicochemical properties (decreased auto-aggregation and motility) may have an impact on the reduction of invasiveness in Salmonella which is supported by previous studies who showed a positive correlation between bacterial motility and invasiveness into host cells [150], [175]. Reduction in Salmonella invasiveness can be further

explained by expression levels of Type III secretion system related genes that are responsible for invasion and intracellular survival. Our results suggest that berry pomace extracts can negatively affect transcriptional regulatory proteins that are involved in bacterial invasion. Salmonella pathogenicity island (SPI) 1 encoded transcriptional regulators are essential for bacterial uptake into intestinal epithelial cells followed by inflammation [160]. Differential expression of *hilA*, that encodes the transcriptional activator of the SPI1 structural genes, is influenced by three AraC-like regulators (HilD, HilC, and RtsA) and each of them can activate the *hilD*, *hilC*, *rtsA*, and *hilA* genes that form a complex feed-forward regulatory loop [176], [177]. Conversely, HilC and HilD act as transcription activators to induce the expression of *hilA* by binding to the upstream repression sites [178], [179]. Decreased motility, hence decreased invasiveness in Salmonella treated with sublethal concentration of berry pomace extracts can also be attributed to the down-regulation of HilC that controls flagellum synthesis (FliZ) [180]. A two component regulatory system (BarA/SirA) that includes SirA plays role in Salmonella virulence and motility [181]. SirA,when activated, positively regulates the transcription of *hilA* and *hilC*, that serves as an initial effector of bacterial invasion pathway [145], [181]; therefore the induction of *sirA* in Salmonella leads to bacterial association and biofilm formation [182].

Findings from this study suggested that sublethal concentrations of berry pomace extracts deferred the Salmonella biofilm formation initially but prolonged exposure resulted in higher level of biofilm formation. A positive correlation between Salmonella auto-aggregation, cell surface hydrophobicity, and motility to biofilm

formation has been reported [171] while another study proposed that instead of motility, flagellar filaments are conducive to biofilm formation [183]. Disrupted lipopolysaccharide of Salmonella cell membrane was also shown to help the rapid formation of biofilm on glass slide [183]. Our finding is consistent with previous reports that sublethal concentrations of phenolics are capable of inducing biofilm formation by Salmonella [184], [185]. In this study we found that 0.5–1.0 g GAE/L, which is far below the MIC value, of berry pomace extract significantly reduced the natural colonization of Salmonella in chick cecum. This phenomenon can be explained by previous report from Clifford, who documented that dietary phenolics are poorly absorbed in the small intestine and 90–95% accumulated in colon resulting high abundance of bioactive phenolic compounds to be interacted with resident bacteria [186]. To conclude, our findings suggest that phenolic extracts of blackberry and blueberry pomaces have high potential for application in the reduction of pre-harvest colonization level of Salmonella in poultry gut and in controlling the growth of this enteric pathogen in meat and meat products by acting as a natural and green preservative. Novel prophylactic substitutes can be developed targeting the altered pathogenicity of Salmonella due to treatment with berry pomace extracts. The berry pomace extracts will not only replace the synthetic antimicrobial use in food production, but they will also have a positive impact on consumer confidence on the safety of the products and on the general public health climate. In addition, waste management problem in the berry juice industry can be addressed by proper application of these cheap and vastly abundant byproducts while increasing profit.

C.5 Matlab Program That Analyzes Trackmate Raw Data to Find the Speed of Bacteria.

```
data=ans;
cellsz = cellfun(@size,data,'uni',false);
tracks=size(data);
time_step=2; %seconds (2secs for Campylobacter A)

for i=1:tracks(1)
      data{i}=data{i}.*0.3171; %pixels to um 20x
end

for i=1:tracks(1) %go through # of tracks
    for j=1:cellsz{i}(1)-1 %go through all timepoints of 1 track
     msdv{i}(j,:) = (data{i}(j+1,2)-data{i}(j,2))^2+(data{i}(j+1,3)-
    data{i}(j,3))^2;
   end
end

for i=1:tracks(1)
    sqrt_msd{i} = msdv{i}.^(1/2);
    v{i} = sqrt_msd{i}./time_step;
    speed{i} = mean(v{i})*60; %convert to um/min
end

    speed=cell2mat(speed)';
    meanspeed=mean(speed)
    medianspeed=median(speed)
    stdevspeed=std(speed)
```

C.6 MATLAB Program That Collects All Trackmate Raw Data and Compiles into a Histogram.

```
t3=xlsread('/Users/Katrina/Desktop/bacteria motility/Salmonella A
10fps/trackmate3/Speed_trackmate3.xlsx');
t4=xlsread('/Users/Katrina/Desktop/bacteria motility/Salmonella A
10fps/trackmate4/Speed_trackmate4.xlsx');
t5=xlsread('/Users/Katrina/Desktop/bacteria motility/Salmonella A
10fps/trackmate5/Speed_trackmate5.xlsx');
t6=xlsread('/Users/Katrina/Desktop/bacteria motility/Salmonella A
10fps/trackmate6/Speed_trackmate6.xlsx');
t7=xlsread('/Users/Katrina/Desktop/bacteria motility/Salmonella A
10fps/trackmate7/Speed_trackmate7.xlsx');
t8=xlsread('/Users/Katrina/Desktop/bacteria motility/Salmonella A
10fps/trackmate8/Speed_trackmate8.xlsx');

tracklength=[t3(:,1); t4(:,1); t5(:,1); t6(:,1); t7(:,1) ;t8(:,1)];
speed=[t3(:,2); t4(:,2); t5(:,2); t6(:,2) ;t7(:,2); t8(:,2)];

meanspeed=mean(speed)
medianspeed=median(speed)
stdevspeed=std(speed)

meantrack=mean(tracklength)
mediantrack=median(tracklength)
stdevtrack=std(tracklength)


figure;

histogram(speed,100); set(gca,'FontSize',14);xlabel('speed
(um/min)','FontSize',14); title('Histogram Salmonella A');
```

Bibliography

[1] V. te Boekhorst, L. Preziosi, and P. Friedl, “Plasticity of Cell Migration In Vivo and In Silico,” 06-Oct-2016. .

[2] P. Friedl and K. Wolf, “Plasticity of cell migration: a multiscale tuning model,” *J. Cell Biol.*, vol. 188, no. 1, pp. 11–19, Jan. 2010.

[3] A. J. Ridley *et al.*, “Cell migration: integrating signals from front to back,” *Science*, vol. 302, no. 5651, pp. 1704–1709, Dec. 2003.

[4] G. Charras and E. Sahai, “Physical influences of the extracellular environment on cell migration,” *Nat. Rev. Mol. Cell Biol.*, vol. 15, no. 12, pp. 813–824, Dec. 2014.

[5] W. J. Polacheck, I. K. Zervantonakis, and R. D. Kamm, “Tumor cell migration in complex microenvironments,” *Cell. Mol. Life Sci.*, vol. 70, no. 8, pp. 1335–1356, 2013.

[6] A. F. Chambers, A. C. Groom, and I. C. MacDonald, “Dissemination and growth of cancer cells in metastatic sites,” *Nat. Rev. Cancer*, vol. 2, pp. 563–572, 2002.

[7] D. Wirtz, K. Konstantopoulos, and P. C. Searson, “The physics of cancer: the role of physical interactions and mechanical forces in metastasis,” *Nat. Rev. Cancer*, vol. 11, no. 7, pp. 512–522, Jul. 2011.

[8] K. M. Stroka, Z. Gu, S. X. Sun, and K. Konstantopoulos, “Bioengineering Paradigms for Cell Migration in Confined Microenvironments,” *Curr. Opin. Cell Biol.*, vol. 30, pp. 41–50, Oct. 2014.

[9] S. Suresh, “Biomechanics and biophysics of cancer cells,” *Acta Biomater.*, vol. 3, no. 4, pp. 413–438, Jul. 2007.

[10] M. J. Paszek *et al.*, “Tensional homeostasis and the malignant phenotype,” *Cancer Cell*, vol. 8, no. 3, pp. 241–254, Sep. 2005.

[11] W. A. Muller, “Mechanisms of Leukocyte Transendothelial Migration,” *Annu. Rev. Pathol.*, vol. 6, pp. 323–344, 2011.

[12] G. K. Hansson and A. Hermansson, “The immune system in atherosclerosis,” *Nat. Immunol.*, vol. 12, no. 3, pp. 204–212, Mar. 2011.

[13] K. J. Moore, F. J. Sheedy, and E. A. Fisher, “Macrophages in atherosclerosis: a dynamic balance,” *Nat. Rev. Immunol.*, vol. 13, no. 10, pp. 709–721, Oct. 2013.

[14] G. J. Randolph, “Emigration of monocyte-derived cells to lymph nodes during resolution of inflammation and its failure in atherosclerosis,” *Curr. Opin. Lipidol.*, vol. 19, no. 5, pp. 462–468, Oct. 2008.

[15] C. Weber and H. Noels, “Atherosclerosis: current pathogenesis and therapeutic options,” *Nat. Med.*, vol. 17, no. 11, pp. 1410–1422, Nov. 2011.

[16] D. T. Butcher, T. Alliston, and V. M. Weaver, “A tense situation: forcing tumour progression,” *Nat. Rev. Cancer*, vol. 9, no. 2, pp. 108–122, Feb. 2009.

[17] D. E. Discher, P. Janmey, and Y. Wang, “Tissue cells feel and respond to the stiffness of their substrate,” *Science*, vol. 310, no. 5751, pp. 1139–1143, 2005.

[18] C.-M. Lo, H.-B. Wang, M. Dembo, and Y. Wang, “Cell Movement Is Guided by the Rigidity of the Substrate,” *Biophys. J.*, vol. 79, no. 1, pp. 144–152, Jul. 2000.

[19] A. J. Engler, S. Sen, H. L. Sweeney, and D. E. Discher, “Matrix elasticity directs stem cell lineage specification,” *Cell*, vol. 126, no. 4, pp. 677–689, 2006.

[20] K. M. Stroka and H. Aranda-Espinoza, “Neutrophils display biphasic relationship between migration and substrate stiffness,” *Cell Motil. Cytoskeleton*, vol. 66, no. 6, pp. 328–341, Jun. 2009.

[21] K. M. Stroka and H. Aranda-Espinoza, “Endothelial cell substrate stiffness influences neutrophil transmigration via myosin light chain kinase-dependent cell contraction,” *Blood*, vol. 118, no. 6, pp. 1632–1640, Aug. 2011.

[22] S. Féréol *et al.*, “Sensitivity of alveolar macrophages to substrate mechanical and adhesive properties,” *Cell Motil. Cytoskeleton*, vol. 63, no. 6, pp. 321–340, 2006.

[23] B. Alberts, A. Johnson, J. Lewis, M. Raff, K. Roberts, and P. Walter, *Molecular Biology of the Cell, 5th Edition*, 5th edition. New York: Garland Science, 2007.

[24] G. G. Luxton and G. G. Gundersen, “Orientation and function of the nuclear–centrosomal axis during cell migration,” *Curr. Opin. Cell Biol.*, vol. 23, no. 5, pp. 579–588, Oct. 2011.

[25] N. Pavin, L. Laan, R. Ma, M. Dogterom, and F. Jülicher, “Positioning of microtubule organizing centers by cortical pushing and pulling forces,” *New J. Phys.*, vol. 14, no. 10, p. 105025, 2012.

[26] A. Burakov, E. Nadezhdina, B. Slepchenko, and V. Rodionov, “Centrosome positioning in interphase cells,” *J. Cell Biol.*, vol. 162, no. 6, pp. 963–969, Sep. 2003.

[27] J. Zhu, A. Burakov, V. Rodionov, and A. Mogilner, “Finding the cell center by a balance of dynein and myosin pulling and microtubule pushing: a computational study,” *Mol. Biol. Cell*, vol. 21, no. 24, pp. 4418–4427, Dec. 2010.

[28] K. Wolf *et al.*, “Collagen-based cell migration models in vitro and in vivo,” *Semin. Cell Dev. Biol.*, vol. 20, no. 8, pp. 931–941, Oct. 2009.

[29] M. Sidani, J. Wyckoff, C. Xue, J. E. Segall, and J. Condeelis, “Probing the microenvironment of mammary tumors using multiphoton microscopy,” *J. Mammary Gland Biol. Neoplasia*, vol. 11, no. 2, pp. 151–163, Apr. 2006.

[30] S. Gabriele, A.-M. Benoliel, P. Bongrand, and O. Théodoly, “Microfluidic investigation reveals distinct roles for actin cytoskeleton and myosin II activity in capillary leukocyte trafficking,” *Biophys. J.*, vol. 96, no. 10, pp. 4308–4318, May 2009.

[31] S. K. Shaw, P. S. Bamba, B. N. Perkins, and F. W. Luscinskas, “Real-Time Imaging of Vascular Endothelial-Cadherin During Leukocyte Transmigration Across Endothelium,” *J. Immunol.*, vol. 167, no. 4, pp. 2323–2330, Aug. 2001.

[32] B. Weigelin, G.-J. Bakker, and P. Friedl, “Intravital third harmonic generation microscopy of collective melanoma cell invasion,” *IntraVital*, vol. 1, no. 1, pp. 32–43, Jul. 2012.

[33] A. D. Doyle, F. W. Wang, K. Matsumoto, and K. M. Yamada, "One-dimensional topography underlies three-dimensional fibrillar cell migration," *J. Cell Biol.*, vol. 184, no. 4, pp. 481–490, Feb. 2009.

[34] K. N. Dahl, A. J. Ribeiro, and J. Lammerding, "Nuclear shape, mechanics, and mechanotransduction," *Circ. Res.*, vol. 102, no. 11, pp. 1307–1318, 2008.

[35] P. M. Davidson, C. Denais, M. C. Bakshi, and J. Lammerding, "Nuclear deformability constitutes a rate-limiting step during cell migration in 3-D environments," *Cell. Mol. Bioeng.*, vol. 7, no. 3, pp. 293–306, Sep. 2014.

[36] N. Caille, O. Thoumine, Y. Tardy, and J.-J. Meister, "Contribution of the nucleus to the mechanical properties of endothelial cells," *J. Biomech.*, vol. 35, no. 2, pp. 177–187, Feb. 2002.

[37] K. Wolf *et al.*, "Physical limits of cell migration: Control by ECM space and nuclear deformation and tuning by proteolysis and traction force," *J. Cell Biol.*, vol. 201, no. 7, pp. 1069–1084, Jun. 2013.

[38] Y. Fu, L. K. Chin, T. Bourouina, A. Q. Liu, and A. M. J. VanDongen, "Nuclear deformation during breast cancer cell transmigration," *Lab. Chip*, vol. 12, no. 19, pp. 3774–3778, Oct. 2012.

[39] J. Swift *et al.*, "Nuclear lamin-A scales with tissue stiffness and enhances matrix-directed differentiation," *Science*, vol. 341, no. 6149, p. 1240104, Aug. 2013.

[40] T. Harada *et al.*, "Nuclear lamin stiffness is a barrier to 3D migration, but softness can limit survival," *J. Cell Biol.*, vol. 204, no. 5, pp. 669–682, Mar. 2014.

[41] D. Razafsky, S. Zang, and D. Hodzic, “UnLINCing the nuclear envelope: towards an understanding of the physiological significance of nuclear positioning,” *Biochem. Soc. Trans.*, vol. 39, no. 6, pp. 1790–1794, Dec. 2011.

[42] D. Razafsky, D. Wirtz, and D. Hodzic, “Nuclear envelope in nuclear positioning and cell migration,” *Adv. Exp. Med. Biol.*, vol. 773, pp. 471–490, 2014.

[43] S. Huda, D. Pilans, M. Makurath, T. M. Hermans, K. Kandere-Grzybowska, and B. A. Grzybowski, “Microfabricated Systems and Assays for Studying the Cytoskeletal Organization, Micromechanics, and Motility Patterns of Cancerous Cells,” *Adv. Mater. Interfaces*, vol. 1, no. 7, p. n/a–n/a, 2014.

[44] E. M. Balzer *et al.*, “Physical confinement alters tumor cell adhesion and migration phenotypes,” *FASEB J.*, vol. 26, no. 10, pp. 4045–4056, Oct. 2012.

[45] K. M. Stroka *et al.*, “Water permeation drives tumor cell migration in confined microenvironments,” *Cell*, vol. 157, no. 3, pp. 611–623, Apr. 2014.

[46] T. E. Holy, M. Dogterom, B. Yurke, and S. Leibler, “Assembly and positioning of microtubule asters in microfabricated chambers,” *Proc. Natl. Acad. Sci. U. S. A.*, vol. 94, no. 12, pp. 6228–6231, 1997.

[47] M. Dogterom, J. W. Kerssemakers, G. Romet-Lemonne, and M. E. Janson, “Force generation by dynamic microtubules,” *Curr. Opin. Cell Biol.*, vol. 17, no. 1, pp. 67–74, 2005.

[48] L. Laan *et al.*, “Cortical dynein controls microtubule dynamics to generate pulling forces that position microtubule asters,” *Cell*, vol. 148, no. 3, pp. 502–514, Feb. 2012.

[49] J. Wu, G. Misra, R. J. Russell, A. J. C. Ladd, T. P. Lele, and R. B. Dickinson, "Effects of dynein on microtubule mechanics and centrosome positioning," *Mol. Biol. Cell*, vol. 22, no. 24, pp. 4834–4841, Dec. 2011.

[50] E. R. Gomes, S. Jani, and G. G. Gundersen, "Nuclear movement regulated by cdc42, MRCK, myosin, and actin flow establishes MTOC polarization in migrating cells," *Cell*, vol. 121, no. 3, pp. 451–463, May 2005.

[51] A. F. Palazzo *et al.*, "Cdc42, dynein, and dynactin regulate MTOC reorientation independent of Rho-regulated microtubule stabilization," *Curr. Biol.*, vol. 11, no. 19, pp. 1536–1541, Oct. 2001.

[52] F. Pouthas *et al.*, "In migrating cells, the Golgi complex and the position of the centrosome depend on geometrical constraints of the substratum," *J. Cell Sci.*, vol. 121, no. 14, pp. 2406–2414, Jul. 2008.

[53] B. C. Isenberg, P. A. DiMilla, M. Walker, S. Kim, and J. Y. Wong, "Vascular Smooth Muscle Cell Durotaxis Depends on Substrate Stiffness Gradient Strength," *Biophys. J.*, vol. 97, no. 5, pp. 1313–1322, Sep. 2009.

[54] R. J. Pelham and Y. Wang, "Cell locomotion and focal adhesions are regulated by substrate flexibility," *Proc. Natl. Acad. Sci.*, vol. 94, no. 25, pp. 13661–13665, Dec. 1997.

[55] T. Yeung *et al.*, "Effects of substrate stiffness on cell morphology, cytoskeletal structure, and adhesion," *Cell Motil. Cytoskeleton*, vol. 60, no. 1, pp. 24–34, Jan. 2005.

[56] H. N. Hayenga and H. Aranda-Espinoza, “Stiffness Increases Mononuclear Cell Transendothelial Migration,” *Cell. Mol. Bioeng.*, vol. 6, no. 3, pp. 253–265, Sep. 2013.

[57] S. M. Hamilla, K. M. Stroka, and H. Aranda-Espinoza, “VE-Cadherin-Independent Cancer Cell Incorporation into the Vascular Endothelium Precedes Transmigration,” *PLOS ONE*, vol. 9, no. 10, p. e109748, Oct. 2014.

[58] M. Théry, “Micropatterning as a tool to decipher cell morphogenesis and functions,” *J Cell Sci*, vol. 123, no. 24, pp. 4201–4213, Dec. 2010.

[59] S. A. Ruiz and C. S. Chen, “Microcontact printing: a tool to pattern,” *Soft Matter*, vol. 3, no. 2, pp. 168–177, 2007.

[60] M. Théry *et al.*, “The extracellular matrix guides the orientation of the cell division axis,” *Nat. Cell Biol.*, vol. 7, no. 10, pp. 947–953, Oct. 2005.

[61] X. Jiang, D. A. Bruzewicz, A. P. Wong, M. Piel, and G. M. Whitesides, “Directing cell migration with asymmetric micropatterns,” *Proc. Natl. Acad. Sci. U. S. A.*, vol. 102, no. 4, pp. 975–978, Jan. 2005.

[62] W. J. Polacheck, R. Li, S. G. M. Uzel, and R. D. Kamm, “Microfluidic platforms for mechanobiology,” *Lab. Chip*, vol. 13, no. 12, pp. 2252–2267, Jun. 2013.

[63] M. Mak, C. A. Reinhart-King, and D. Erickson, “Elucidating mechanical transition effects of invading cancer cells with a subnucleus-scaled microfluidic serial dimensional modulation device,” *Lab. Chip*, vol. 13, no. 3, pp. 340–348, Feb. 2013.

[64] H. V. Prentice-Mott, C.-H. Chang, L. Mahadevan, T. J. Mitchison, D. Irimia, and J. V. Shah, “Biased migration of confined neutrophil-like cells in asymmetric hydraulic environments,” *Proc. Natl. Acad. Sci.*, vol. 110, no. 52, pp. 21006–21011, Dec. 2013.

[65] P. Friedl, K. Wolf, and J. Lammerding, “Nuclear mechanics during cell migration,” *Curr. Opin. Cell Biol.*, vol. 23, no. 1, pp. 55–64, Feb. 2011.

[66] J. D. Humphrey, “Mechanisms of Arterial Remodeling in Hypertension,” *Hypertension*, vol. 52, no. 2, pp. 195–200, Aug. 2008.

[67] S. H. Rambhia *et al.*, “Microcalcifications Increase Coronary Vulnerable Plaque Rupture Potential: A Patient-Based Micro-CT Fluid–Structure Interaction Study,” *Ann. Biomed. Eng.*, vol. 40, no. 7, pp. 1443–1454, Jul. 2012.

[68] Y. Vengrenyuk *et al.*, “A hypothesis for vulnerable plaque rupture due to stress-induced debonding around cellular microcalcifications in thin fibrous caps,” *Proc. Natl. Acad. Sci. U. S. A.*, vol. 103, no. 40, pp. 14678–14683, Oct. 2006.

[69] Y.-T. Yeh *et al.*, “Matrix stiffness regulates endothelial cell proliferation through septin 9,” *PloS One*, vol. 7, no. 10, p. e46889, 2012.

[70] J. Huynh *et al.*, “Age-Related Intimal Stiffening Enhances Endothelial Permeability and Leukocyte Transmigration,” *Sci. Transl. Med.*, vol. 3, no. 112, pp. 112ra122–112ra122, Dec. 2011.

[71] J. Peloquin, J. Huynh, R. M. Williams, and C. A. Reinhart-King, “Indentation measurements of the subendothelial matrix in bovine carotid arteries,” *J. Biomech.*, vol. 44, no. 5, pp. 815–821, Mar. 2011.

[72] J. P. Califano and C. A. Reinhart-King, “Exogenous and endogenous force regulation of endothelial cell behavior,” *J. Biomech.*, vol. 43, no. 1, pp. 79–86, Jan. 2010.

[73] J. Lee, M. Leonard, T. Oliver, A. Ishihara, and K. Jacobson, “Traction forces generated by locomoting keratocytes.,” *J. Cell Biol.*, vol. 127, no. 6, pp. 1957–1964, Dec. 1994.

[74] N. R. Patel *et al.*, “Cell Elasticity Determines Macrophage Function,” *PLOS ONE*, vol. 7, no. 9, p. e41024, Sep. 2012.

[75] A. K. Blakney, M. D. Swartzlander, and S. J. Bryant, “The effects of substrate stiffness on the in vitro activation of macrophages and in vivo host response to poly(ethylene glycol)-based hydrogels,” *J. Biomed. Mater. Res. A*, vol. 100, no. 6, pp. 1375–1386, Jun. 2012.

[76] C. S. Robbins *et al.*, “Local proliferation dominates lesional macrophage accumulation in atherosclerosis,” *Nat. Med.*, vol. 19, no. 9, pp. 1166–1172, Sep. 2013.

[77] D. Gordon, M. A. Reidy, E. P. Benditt, and S. M. Schwartz, “Cell proliferation in human coronary arteries,” *Proc. Natl. Acad. Sci. U. S. A.*, vol. 87, no. 12, pp. 4600–4604, Jun. 1990.

[78] S. Katsuda, M. D. Coltrera, R. Ross, and A. M. Gown, “Human atherosclerosis. IV. Immunocytochemical analysis of cell activation and proliferation in lesions of young adults,” *Am. J. Pathol.*, vol. 142, no. 6, pp. 1787–1793, Jun. 1993.

[79] E. Lutgens *et al.*, “Atherosclerosis in APOE*3-Leiden transgenic mice: from proliferative to atheromatous stage,” *Circulation*, vol. 99, no. 2, pp. 276–283, Jan. 1999.

[80] M. D. Rekhter and D. Gordon, “Active proliferation of different cell types, including lymphocytes, in human atherosclerotic plaques,” *Am. J. Pathol.*, vol. 147, no. 3, pp. 668–677, Sep. 1995.

[81] M. Aikawa *et al.*, “An HMG-CoA reductase inhibitor, cerivastatin, suppresses growth of macrophages expressing matrix metalloproteinases and tissue factor in vivo and in vitro,” *Circulation*, vol. 103, no. 2, pp. 276–283, Jan. 2001.

[82] L. L. Norman and H. Aranda-Espinoza, “Cortical Neuron Outgrowth is Insensitive to Substrate Stiffness,” *Cell. Mol. Bioeng.*, vol. 3, no. 4, pp. 398–414, Jul. 2010.

[83] M. Y. Murray *et al.*, “Macrophage migration and invasion is regulated by MMP10 expression,” *PloS One*, vol. 8, no. 5, p. e63555, 2013.

[84] M. Théry and M. Piel, “Adhesive micropatterns for cells: A microcontact printing protocol,” *Cold Spring Harb. Protoc.*, vol. 2009, no. 7, p. pdb.prot5255, Jul. 2009.

[85] L. A. Flanagan, Y.-E. Ju, B. Marg, M. Osterfield, and P. A. Janmey, “Neurite branching on deformable substrates,” *Neuroreport*, vol. 13, no. 18, pp. 2411–2415, Dec. 2002.

[86] “ATCC Cell Lines.” [Online]. Available: https://www.atcc.org/en/Products/Cells_and_Microorganisms/Cell_Lines.aspx.

[87] C. Roduit *et al.*, “Stiffness tomography exploration of living and fixed macrophages,” *J. Mol. Recognit. JMR*, vol. 25, no. 5, pp. 241–246, May 2012.

[88] N. Wang *et al.*, “Cell prestress. I. Stiffness and prestress are closely associated in adherent contractile cells,” *Am. J. Physiol. Cell Physiol.*, vol. 282, no. 3, pp. C606–616, Mar. 2002.

[89] H. Sakagami *et al.*, “Cell death induced by nutritional starvation in mouse macrophage-like RAW264.7 cells,” *Anticancer Res.*, vol. 29, no. 1, pp. 343–347, Jan. 2009.

[90] R. van Furth, I. Elzenga-Claasen, M. van Schadewijk-Nieuwstad, M. M. Diesselhoff-den Dulk, H. Toivonen, and T. Rytömaa, “Cell kinetic analysis of a murine macrophage cell line,” *Eur. J. Cell Biol.*, vol. 44, no. 1, pp. 93–96, Aug. 1987.

[91] H. W. Ziegler-Heitbrock, E. Thiel, A. Fütterer, V. Herzog, A. Wirtz, and G. Riethmüller, “Establishment of a human cell line (Mono Mac 6) with characteristics of mature monocytes,” *Int. J. Cancer*, vol. 41, no. 3, pp. 456–461, Mar. 1988.

[92] J. E. Glasgow, B. E. Farrell, E. S. Fisher, D. A. Lauffenburger, and R. P. Daniele, “The motile response of alveolar macrophages. An experimental study using single-cell and cell population approaches,” *Am. Rev. Respir. Dis.*, vol. 139, no. 2, pp. 320–329, Feb. 1989.

[93] C. Grabher *et al.*, “Birth and life of tissue macrophages and their migration in embryogenesis and inflammation in medaka,” *J. Leukoc. Biol.*, vol. 81, no. 1, pp. 263–271, Jan. 2007.

[94] E. Van Goethem, R. Poincloux, F. Gauffre, I. Maridonneau-Parini, and V. Le Cabec, “Matrix architecture dictates three-dimensional migration modes of human macrophages: differential involvement of proteases and podosome-like structures,” *J. Immunol. Baltim. Md 1950*, vol. 184, no. 2, pp. 1049–1061, Jan. 2010.

[95] V. J. Uitto and H. Larjava, “Extracellular matrix molecules and their receptors: an overview with special emphasis on periodontal tissues,” *Crit. Rev. Oral Biol. Med. Off. Publ. Am. Assoc. Oral Biol.*, vol. 2, no. 3, pp. 323–354, 1991.

[96] A. Teti, “Regulation of cellular functions by extracellular matrix,” *J. Am. Soc. Nephrol. JASN*, vol. 2, no. 10 Suppl, pp. S83–87, Apr. 1992.

[97] J. S. Jeon, I. K. Zervantonakis, S. Chung, R. D. Kamm, and J. L. Charest, “In vitro model of tumor cell extravasation,” *PloS One*, vol. 8, no. 2, p. e56910, 2013.

[98] J. Halper and M. Kjaer, “Basic components of connective tissues and extracellular matrix: elastin, fibrillin, fibulins, fibrinogen, fibronectin, laminin, tenascins and thrombospondins,” *Adv. Exp. Med. Biol.*, vol. 802, pp. 31–47, 2014.

[99] S. Dufour, J. L. Duband, and J. P. Thiéry, “Role of a major cell-substratum adhesion system in cell behavior and morphogenesis,” *Biol. Cell*, vol. 58, no. 1, pp. 1–13, 1986.

[100] E. Ruoslahti, “RGD and other recognition sequences for integrins,” *Annu. Rev. Cell Dev. Biol.*, vol. 12, pp. 697–715, 1996.

[101] J. Elric and S. Etienne-Manneville, “Centrosome positioning in polarized cells: common themes and variations,” *Exp. Cell Res.*, vol. 328, no. 2, pp. 240–248, Nov. 2014.

[102] C. M. Hale, W.-C. Chen, S. B. Khatau, B. R. Daniels, J. S. H. Lee, and D. Wirtz, “SMRT analysis of MTOC and nuclear positioning reveals the role of EB1 and LIC1 in single-cell polarization,” *J Cell Sci*, vol. 124, no. 24, pp. 4267–4285, Dec. 2011.

[103] T. Tanaka, F. F. Serneo, C. Higgins, M. J. Gambello, A. Wynshaw-Boris, and J. G. Gleeson, “Lis1 and doublecortin function with dynein to mediate coupling of the nucleus to the centrosome in neuronal migration,” *J. Cell Biol.*, vol. 165, no. 5, pp. 709–721, Jun. 2004.

[104] R. J. Vasquez, B. Howell, A. M. Yvon, P. Wadsworth, and L. Cassimeris, “Nanomolar concentrations of nocodazole alter microtubule dynamic instability in vivo and in vitro.,” *Mol. Biol. Cell*, vol. 8, no. 6, pp. 973–985, Jun. 1997.

[105] A. J. Firestone *et al.*, “Small-molecule inhibitors of the AAA+ ATPase motor cytoplasmic dynein,” *Nature*, vol. 484, no. 7392, pp. 125–129, Mar. 2012.

[106] M. Théry and M. Piel, “Adhesive micropatterns for cells: A microcontact printing protocol,” *Cold Spring Harb. Protoc.*, vol. 2009, no. 7, p. pdb.prot5255, Jul. 2009.

[107] T. Sakamoto, J. Limouze, C. A. Combs, A. F. Straight, and J. R. Sellers, "Blebbistatin, a myosin II inhibitor, is photoinactivated by blue light," *Biochemistry (Mosc.)*, vol. 44, no. 2, pp. 584–588, Jan. 2005.

[108] M. Raab and D. E. Discher, "Matrix rigidity regulates microtubule network polarization in migration," *Cytoskeleton*, Jan. 2017.

[109] M. Raab, J. Swift, P. C. D. P. Dingal, P. Shah, J.-W. Shin, and D. E. Discher, "Crawling from soft to stiff matrix polarizes the cytoskeleton and phosphoregulates myosin-II heavy chain," *J Cell Biol*, vol. 199, no. 4, pp. 669–683, Nov. 2012.

[110] J. R. Levy and E. L. F. Holzbaur, "Dynein drives nuclear rotation during forward progression of motile fibroblasts," *J. Cell Sci.*, vol. 121, no. 19, pp. 3187–3195, Oct. 2008.

[111] F. Farina *et al.*, "The centrosome is an actin-organizing centre," *Nat. Cell Biol.*, vol. 18, no. 1, pp. 65–75, Jan. 2016.

[112] D. A. Starr and H. N. Fridolfsson, "Interactions between nuclei and the cytoskeleton are mediated by SUN-KASH nuclear-envelope bridges," *Annu. Rev. Cell Dev. Biol.*, vol. 26, pp. 421–444, 2010.

[113] E. C. Tapley and D. A. Starr, "Connecting the nucleus to the cytoskeleton by SUN–KASH bridges across the nuclear envelope," *Curr. Opin. Cell Biol.*, vol. 25, no. 1, pp. 57–62, Feb. 2013.

[114] D. Razafsky and D. Hodzic, "Bringing KASH under the SUN: the many faces of nucleo-cytoskeletal connections," *J. Cell Biol.*, vol. 186, no. 4, pp. 461–472, Aug. 2009.

[115] A. V. Burakov and E. S. Nadezhdina, “Association of nucleus and centrosome: magnet or velcro?,” *Cell Biol. Int.*, vol. 37, no. 2, pp. 95–104, Feb. 2013.

[116] J. Wu, K. C. Lee, R. B. Dickinson, and T. P. Lele, “How dynein and microtubules rotate the nucleus,” *J. Cell. Physiol.*, vol. 226, no. 10, pp. 2666–2674, Oct. 2011.

[117] J. Yi, X. Wu, A. H. Chung, J. K. Chen, T. M. Kapoor, and J. A. Hammer, “Centrosome repositioning in T cells is biphasic and driven by microtubule end-on capture-shrinkage,” *J Cell Biol*, vol. 202, no. 5, pp. 779–792, Sep. 2013.

[118] J. Y. Chan, “A clinical overview of centrosome amplification in human cancers,” *Int. J. Biol. Sci.*, vol. 7, no. 8, pp. 1122–1144, Oct. 2011.

[119] F. Bordeleau, T. A. Alcoser, and C. A. Reinhart-King, “Physical Biology in Cancer. 5. The rocky road of metastasis: the role of cytoskeletal mechanics in cell migratory response to 3D matrix topography,” *Am. J. Physiol. - Cell Physiol.*, vol. 306, no. 2, pp. C110–C120, Jan. 2014.

[120] Z. Tong, E. M. Balzer, M. R. Dallas, W.-C. Hung, K. J. Stebe, and K. Konstantopoulos, “Chemotaxis of Cell Populations through Confined Spaces at Single-Cell Resolution,” *PLoS ONE*, vol. 7, no. 1, p. e29211, Jan. 2012.

[121] S. Alexander, B. Weigelin, F. Winkler, and P. Friedl, “Preclinical intravital microscopy of the tumour-stroma interface: invasion, metastasis, and therapy response,” *Curr. Opin. Cell Biol.*, vol. 25, no. 5, pp. 659–671, Oct. 2013.

[122] S. P. Carey *et al.*, “Comparative mechanisms of cancer cell migration through 3D matrix and physiological microtracks,” *Am. J. Physiol. - Cell Physiol.*, vol. 308, no. 6, pp. C436–C447, Mar. 2015.

[123] E. T. Roussos, J. S. Condeelis, and A. Patsialou, “Chemotaxis in cancer,” *Nat. Rev. Cancer*, vol. 11, no. 8, pp. 573–587, Aug. 2011.

[124] M. Mak, C. A. Reinhart-King, and D. Erickson, “Microfabricated Physical Spatial Gradients for Investigating Cell Migration and Invasion Dynamics,” *PLoS ONE*, vol. 6, no. 6, pp. 1–8, Jun. 2011.

[125] D. Irimia and M. Toner, “Spontaneous migration of cancer cells under conditions of mechanical confinement,” *Integr. Biol.*, vol. 1, no. 8–9, pp. 506–512, 2009.

[126] Y. Fu *et al.*, “A study of cancer cell metastasis using microfluidic transmigration device,” presented at the 2012 IEEE 25th International Conference on Micro Electro Mechanical Systems (MEMS), 2012, pp. 773–776.

[127] J. Wu *et al.*, “Actomyosin Pulls to Advance the Nucleus in a Migrating Tissue Cell,” *Biophys. J.*, vol. 106, no. 1, pp. 7–15, Jan. 2014.

[128] S. S. Chang, W. Guo, Y. Kim, and Y. Wang, “Guidance of Cell Migration by Substrate Dimension,” *Biophys. J.*, vol. 104, no. 2, pp. 313–321, Jan. 2013.

[129] D. E. Discher, P. Janmey, and Y.-L. Wang, “Tissue cells feel and respond to the stiffness of their substrate,” *Science*, vol. 310, no. 5751, pp. 1139–1143, Nov. 2005.

[130] A. Sica and A. Mantovani, “Macrophage plasticity and polarization: in vivo veritas,” *J. Clin. Invest.*, vol. 122, no. 3, pp. 787–795, Mar. 2012.

[131] J. Shalhoub, M. A. Falck-Hansen, A. H. Davies, and C. Monaco, “Innate immunity and monocyte-macrophage activation in atherosclerosis,” *J. Inflamm.*, vol. 8, p. 9, 2011.

[132] F. Y. McWhorter, T. Wang, P. Nguyen, T. Chung, and W. F. Liu, “Modulation of macrophage phenotype by cell shape,” *Proc. Natl. Acad. Sci.*, vol. 110, no. 43, pp. 17253–17258, 2013.

[133] Y. Fu, L. K. Chin, T. Bourouina, A. Q. Liu, and A. M. J. VanDongen, “Nuclear deformation during breast cancer cell transmigration,” *Lab. Chip*, vol. 12, no. 19, pp. 3774–3778, Oct. 2012.

[134] M. Mak and D. Erickson, “A serial micropipette microfluidic device with applications to cancer cell repeated deformation studies,” *Integr. Biol.*, vol. 5, no. 11, pp. 1374–1384, Oct. 2013.

[135] M. Zwerger, C. Y. Ho, and J. Lammerding, “Nuclear Mechanics in Disease,” *Annu. Rev. Biomed. Eng.*, vol. 13, no. 1, pp. 397–428, 2011.

[136] A. Matsumoto *et al.*, “Global loss of a nuclear lamina component, lamin A/C, and LINC complex components SUN1, SUN2, and nesprin-2 in breast cancer,” *Cancer Med.*, vol. 4, no. 10, pp. 1547–1557, Oct. 2015.

[137] A. Ogden, P. C. G. Rida, and R. Aneja, “Heading off with the herd: how cancer cells might maneuver supernumerary centrosomes for directional migration,” *Cancer Metastasis Rev.*, vol. 32, no. 1–2, pp. 269–287, Jun. 2013.

[138] D. Zyss and F. Gergely, “Centrosome function in cancer: guilty or innocent?,” *Trends Cell Biol.*, vol. 19, no. 7, pp. 334–346, Jul. 2009.

[139] E. Scallan *et al.*, “Foodborne illness acquired in the United States--major pathogens,” *Emerg. Infect. Dis.*, vol. 17, no. 1, pp. 7–15, Jan. 2011.

[140] L. Mughini-Gras and W. van Pelt, “Salmonella source attribution based on microbial subtyping: Does including data on food consumption matter?,” *Int. J. Food Microbiol.*, vol. 191, pp. 109–115, Nov. 2014.

[141] C. T. Parker and J. Guard-Petter, “Contribution of flagella and invasion proteins to pathogenesis of Salmonella enterica serovar enteritidis in chicks,” *FEMS Microbiol. Lett.*, vol. 204, no. 2, pp. 287–291, Nov. 2001.

[142] S. Saran, M. S. Bisht, and K. Singh, “Comparing adhesion attributes of two isolates of Lactobacillus Acidophilus for assessment of prebiotics, honey and inulin,” *Int. J. Sci. Res. Publ.*, vol. 2, pp. 2–8, 2012.

[143] I. Hautefort *et al.*, “During infection of epithelial cells Salmonella enterica serovar Typhimurium undergoes a time-dependent transcriptional adaptation that results in simultaneous expression of three type 3 secretion systems,” *Cell. Microbiol.*, vol. 10, no. 4, pp. 958–984, Apr. 2008.

[144] T. S. Wallis and E. E. Galyov, “Molecular basis of Salmonella-induced enteritis,” *Mol. Microbiol.*, vol. 36, no. 5, pp. 997–1005, Jun. 2000.

[145] C. Johnston, D. A. Pegues, C. J. Hueck, C. A. Lee, and S. I. Miller, “Transcriptional activation of Salmonella typhimurium invasion genes by a member of the phosphorylated response-regulator superfamily,” *Mol. Microbiol.*, vol. 22, no. 4, pp. 715–727, 1996.

[146] J. L. Rakeman, H. R. Bonifield, and S. I. Miller, “A hila-independent pathway to salmonella typhimurium invasion gene transcription,” *J. Bacteriol.*, vol. 181, no. 10, pp. 3096–3104, 1999.

[147] B. M. Kuehn, “FDA Moves to Curb Antibiotic Use in Livestock,” *JAMA*, vol. 311, no. 4, pp. 347–348, Jan. 2014.

[148] D. Biswas *et al.*, “Pasteurized Blueberry (vaccinium Corymbosum) Juice Inhibits Growth of Bacterial Pathogens in Milk but Allows Survival of Probiotic Bacteria,” *J. Food Saf.*, vol. 32, no. 2, pp. 204–209, May 2012.

[149] R. Puupponen-Pimiä, L. Nohynek, H.-L. Alakomi, and K.-M. Oksman-Caldentey, “Bioactive berry compounds—novel tools against human pathogens,” *Appl. Microbiol. Biotechnol.*, vol. 67, no. 1, pp. 8–18, Apr. 2005.

[150] S. Salaheen, C. Nguyen, D. Hewes, and D. Biswas, “Cheap extraction of antibacterial compounds of berry pomace and their mode of action against the pathogen Campylobacter jejuni,” *Food Control*, vol. 46, pp. 174–181, Dec. 2014.

[151] H. Yang, D. Hewes, S. Salaheen, C. Federman, and D. Biswas, “Effects of blackberry juice on growth inhibition of foodborne pathogens and growth promotion of Lactobacillus,” *Food Control*, vol. 37, pp. 15–20, Mar. 2014.

[152] S. Salaheen, J. A. Almario, and D. Biswas, “Inhibition of growth and alteration of host cell interactions of Pasteurella multocida with natural byproducts,” *Poult. Sci.*, vol. 93, no. 6, pp. 1375–1382, Jun. 2014.

[153] S. Salaheen, C. Nguyen, C. Mui, and D. Biswas, “Bioactive berry juice byproducts as alternative and natural inhibitors for Salmonella Gallinarum and

Salmonella Pullorum," *J. Appl. Poult. Res.*, vol. 24, no. 2, pp. 186–197, Jun. 2015.

[154] A. Lacombe, S. Tadepalli, C.-A. Hwang, and V. C. H. Wu, "Phytochemicals in Lowbush Wild Blueberry Inactivate Escherichia coli O157:H7 by Damaging Its Cell Membrane," *Foodborne Pathog. Dis.*, vol. 10, no. 11, pp. 944–950, Aug. 2013.

[155] A. Scalbert, "Antimicrobial properties of tannins," *Phytochemistry*, vol. 30, no. 12, pp. 3875–3883, 1991.

[156] V. L. Singleton, R. Orthofer, and R. M. Lamuela-Raventós, "[14] Analysis of total phenols and other oxidation substrates and antioxidants by means of folin-ciocalteu reagent," vol. 299, B.-M. in Enzymology, Ed. Academic Press, 1999, pp. 152–178.

[157] M. Peng, U. Aryal, B. Cooper, and D. Biswas, "Metabolites produced during the growth of probiotics in cocoa supplementation and the limited role of cocoa in host-enteric bacterial pathogen interactions," *Food Control*, vol. 53, pp. 124–133, Jul. 2015.

[158] K. Konaté *et al.*, "Anti-nociceptive properties in rodents and the possibility of using polyphenol-rich fractions from sida urens L. (Malvaceae) against of dental caries bacteria," *Ann. Clin. Microbiol. Antimicrob.*, vol. 12, p. 14, 2013.

[159] J. May, K. Shannon, A. King, and G. French, "Glycopeptide tolerance in Staphylococcus aureus.," *J. Antimicrob. Chemother.*, vol. 42, no. 2, pp. 189–197, Aug. 1998.

[160] J. Ahn, J. A. Almario, S. Salaheen, and D. Biswas, “Physicochemical, Mechanical, and Molecular Properties of Nonlysogenic and P22-Lysogenic Salmonella Typhimurium Treated with Citrus Oil,” *J. Food Prot.*, vol. 77, no. 5, pp. 758–764, May 2014.

[161] M. Rosenberg, “Bacterial adherence to hydrocarbons: a useful technique for studying cell surface hydrophobicity,” *FEMS Microbiol. Lett.*, vol. 22, no. 3, pp. 289–295, May 1984.

[162] B. Del Re, B. Sgorbati, M. Miglioli, and D. Palenzona, “Adhesion, autoaggregation and hydrophobicity of 13 strains of Bifidobacterium longum,” *Lett. Appl. Microbiol.*, vol. 31, no. 6, pp. 438–442, Dec. 2000.

[163] K. J. Livak and T. D. Schmittgen, “Analysis of Relative Gene Expression Data Using Real-Time Quantitative PCR and the 2−ΔΔCT Method,” *Methods*, vol. 25, no. 4, pp. 402–408, Dec. 2001.

[164] L. J. Nohynek *et al.*, “Berry Phenolics: Antimicrobial Properties and Mechanisms of Action Against Severe Human Pathogens,” *Nutr. Cancer*, vol. 54, no. 1, pp. 18–32, Jan. 2006.

[165] C. Mertz, V. Cheynier, Z. Günata, and P. Brat, “Analysis of Phenolic Compounds in Two Blackberry Species (Rubus glaucus and Rubus adenotrichus) by High-Performance Liquid Chromatography with Diode Array Detection and Electrospray Ion Trap Mass Spectrometry,” *J. Agric. Food Chem.*, vol. 55, no. 21, pp. 8616–8624, Oct. 2007.

[166] V. K. Bajpai, K.-H. Baek, and S. C. Kang, “Control of Salmonella in foods by using essential oils: A review,” *Food Res. Int.*, vol. 45, no. 2, pp. 722–734, Mar. 2012.

[167] ICMSF, “Salmonellae. Ch 14,” *Microorg. Food 5 Microbiol. Specif. Food Pathog.*, pp. 217–264, 1996.

[168] S. L. Chiang, R. K. Taylor, M. Koomey, and J. J. Mekalanos, “Single amino acid substitutions in the N-terminus of Vibrio cholerae TcpA affect colonization, autoagglutination, and serum resistance,” *Mol. Microbiol.*, vol. 17, no. 6, pp. 1133–1142, 1995.

[169] F. D. Menozzi, P. E. Boucher, G. Riveau, C. Gantiez, and C. Locht, “Surface-associated filamentous hemagglutinin induces autoagglutination of Bordetella pertussis,” *Infect. Immun.*, vol. 62, no. 10, pp. 4261–4269, 1994.

[170] M. Schachtsiek, W. P. Hammes, and C. Hertel, “Characterization of Lactobacillus coryniformis DSM 20001T Surface Protein Cpf Mediating Coaggregation with and Aggregation among Pathogens,” *Appl. Environ. Microbiol.*, vol. 70, no. 12, pp. 7078–7085, Dec. 2004.

[171] H. Wang, S. Ding, Y. Dong, K. Ye, X. Xu, and G. Zhou, “Biofilm Formation of Salmonella Serotypes in Simulated Meat Processing Environments and Its Relationship to Cell Characteristics,” *J. Food Prot.*, vol. 76, no. 10, pp. 1784–1789, Oct. 2013.

[172] S. Chow, K. Gu, L. Jiang, and A. Nassour, “Salicylic acid affects swimming, twitching and swarming motility in Pseudomonas aeruginosa, resulting in

decreased biofilm formation," *J Exp Microbiol Immunol*, vol. 15, pp. 22–29, 2011.

[173] C. O'May and N. Tufenkji, "The Swarming Motility of Pseudomonas aeruginosa Is Blocked by Cranberry Proanthocyanidins and Other Tannin-Containing Materials," *Appl. Environ. Microbiol.*, vol. 77, no. 9, pp. 3061–3067, May 2011.

[174] K. Oliveira, T. Oliveira, P. Teixeira, J. Azeredo, and R. Oliveira, "Adhesion of Salmonella Enteritidis to stainless steel surfaces," *Braz. J. Microbiol.*, vol. 38, no. 2, pp. 318–323, Jun. 2007.

[175] N. J. Golden and D. W. K. Acheson, "Identification of Motility and Autoagglutination Campylobacter jejuni Mutants by Random Transposon Mutagenesis," *Infect. Immun.*, vol. 70, no. 4, pp. 1761–1771, Apr. 2002.

[176] Y. A. Golubeva, A. Y. Sadik, J. R. Ellermeier, and J. M. Slauch, "Integrating Global Regulatory Input Into the Salmonella Pathogenicity Island 1 Type III Secretion System," *Genetics*, vol. 190, no. 1, pp. 79–90, Jan. 2012.

[177] S. Lim *et al.*, "Analysis of HilC/D-dependent invF promoter expression under different culture conditions," *Microb. Pathog.*, vol. 52, no. 6, pp. 359–366, Jun. 2012.

[178] C. D. Ellermeier, J. R. Ellermeier, and J. M. Slauch, "HilD, HilC and RtsA constitute a feed forward loop that controls expression of the SPI1 type three secretion system regulator hilA in Salmonella enterica serovar Typhimurium," *Mol. Microbiol.*, vol. 57, no. 3, pp. 691–705, Aug. 2005.

[179] R. L. Lucas and C. A. Lee, “Roles of hilC and hilD in Regulation of hilA Expression in Salmonella enterica Serovar Typhimurium,” *J. Bacteriol.*, vol. 183, no. 9, pp. 2733–2745, May 2001.

[180] J. E. C. Chubiz, Y. A. Golubeva, D. Lin, L. D. Miller, and J. M. Slauch, “FliZ Regulates Expression of the Salmonella Pathogenicity Island 1 Invasion Locus by Controlling HilD Protein Activity in Salmonella enterica Serovar Typhimurium,” *J. Bacteriol.*, vol. 192, no. 23, pp. 6261–6270, Dec. 2010.

[181] M. Teplitski, R. I. Goodier, and B. M. M. Ahmer, “Catabolite repression of the SirA regulatory cascade in Salmonella enterica,” *Int. J. Med. Microbiol.*, vol. 296, no. 7, pp. 449–466, Nov. 2006.

[182] J. K. Salazar, K. Deng, M. L. Tortorello, M. T. Brandl, H. Wang, and W. Zhang, “Genes ycfR, sirA and yigG Contribute to the Surface Attachment of Salmonella enterica Typhimurium and Saintpaul to Fresh Produce,” *PLOS ONE*, vol. 8, no. 2, p. e57272, Feb. 2013.

[183] A. M. Prouty and J. S. Gunn, “Comparative Analysis of Salmonella enterica Serovar Typhimurium Biofilm Formation on Gallstones and on Glass,” *Infect. Immun.*, vol. 71, no. 12, pp. 7154–7158, Dec. 2003.

[184] J. B. Kaplan, “Antibiotic-induced biofilm formation,” *Int. J. Artif. Organs*, vol. 34, no. 9, pp. 737–751, Sep. 2011.

[185] Y. Zou, J. Woo, and J. Ahn, “Cellular and molecular responses of Salmonella Typhimurium to antimicrobial-induced stresses during the planktonic-to-biofilm transition,” *Lett. Appl. Microbiol.*, vol. 55, no. 4, pp. 274–282, Oct. 2012.

[186] M. N. Clifford, “Diet-Derived Phenols in Plasma and Tissues and their Implications for Health,” *Planta Med.*, vol. 70, no. 12, pp. 1103–1114, Dec. 2004.